Newsletter n°3

24 October 2022

Participants to the
2nd ACCORD ASW

ACCORD
A Consortium for COnvection-scale modelling
Research and Development

CONTACT US

Claude Fischer, ACCORD Programme Manager
@ pm@accord-nwp.org
Patricia Pottier, Consortium Scientific Secretariat
@ css@accord-nwp.org
http://www.accord-nwp.org/

Contents

Edito

Claude Fischer, ACCORD Programme Manager

Since the publication of NL2 (on 1st March 2022), we from the ACCORD community have experienced the increasing possibilities to meet in-person in fairly large-scale events. After two online venues in 2020 and 2021, the 2022 All Staff Workshop could be organized in hybrid mode with almost about 70 participants present in Ljubljana, on the invitation of our Slovenian colleagues, and 85 to 120 remote participants. Another, recent workshop of similar size was the EWGLAM/C-SRNWP one, which also could be organized in hybrid mode with a large number of colleagues meeting in-person in Brussels on the invitation of the team from RMI.

Many of you have been expressing their satisfaction that physical meetings could again take place, in fairly normal conditions. Along the same lines, ACCORD scientific visits and working weeks usually have taken place in hybrid mode. And this is probably one longer lasting outcome of the two years of COVID-related questioning regarding organization, communication, traveling and meeting: meetings of various sizes will very usually require a hybrid mode organization, and thus the relevant facility (in-person and online).

Focussing now on the ACCORD activity per se, the outcome of some of the scientific visits and working weeks organized in our consortium is reflected in the material presented in this NL3. When looking at the content of NL3, you will discover progress on new facilities in data assimilation like the operational implementation of a SEKF scheme (in Hungary) or the studies on the assimilation of microwave cellphone tower links and Sentinel-1 InSAR data (Austria). On the modeling side, you will be updated on the use of Stochastic Parameter Perturbations in Harmonie-Arome EPS (Norway and Sweden) and on the technical work carried out recently in order to clean up the data flow for aerosols in our common codes (contribution by the Algerian and French teams in this NL). While the mainstream R&D in ACCORD clearly goes towards km-scale and sub-km scale modeling, the contribution by the team of Morocco reminds us that we have a few larger-scale configurations still in use throughout our community. A constant aspect in the NLs so far has been that several teams use to propose contributions about verification methodologies, codes for MQA or results from daily monitoring. NL3 thus includes several such papers, from methods (update on SLX for monitoring extremes, or a new post-processing method for wind intensity over complex orography) to codes (report about the “harp” WW) and verification routine evaluation.

The final words of these editorial lines are an opportunity to remember our colleague Andrey Bogatchev (Bulgaria) who has left us very recently. Many of the ACCORD scientists did know him, some of us have been meeting and working with him on many occasions, such as on his regular phasing visits to Toulouse. His continued, reliable engagement in our NWP activity, as well as his kind personal relationships, will stay inspirational to a number of us in ACCORD.

Claude Fischer

Post Scriptum.

A few words about the elaboration of our ACCORD newsletters. For the concrete writing of an article, please refer to the editorial guidelines, accessible at:
http://www.accord-nwp.org/?Recommendations-templates

The newsletter content is based on voluntary contributions by the scientists and the teams in the consortium. We want it to be a useful tool for sharing both “practical” information and experience (code engineering, quality assurance, system aspects) and “more fundamental” results (advances in research work, outcome of specific meetings or working days etc.).

NL4 is expected for early 2023, however contributors can uploadtheir material at any time during the year on this shared folder. Do also not hesitate to encourage scientific contributions by young scientists (PhDs, post-docs etc.) or technical contributions (codes, porting, optimization etc.).

ACCORD events in 2022

Patricia Pottier, ACCORD Consortium Scientific Secretary

1 Introduction

The outcomes of the ACCORD events such as governance bodies meetings (Assembly, PAC, STAC, LMT), Management Group (MG) meetings, Working Days, Working Weeks, thematic WG meetings can be found on the ACCORD "Events" webpages: slides, minutes, summary, photos, videos, … (when available). The material and conclusions of the thematic meetings (WD) organised by the MG with the team or WG in their area are available on the relevant part of the ACCORD wiki.

2 ACCORD governance meetings in 2022

Committees, Assembly and Bureau

- 28 March 2022: Bureau meeting (analysis of the bid proposal for DestinE and questions for PAC)
- 25 April 2022: 2nd PACvideo-meeting (DestinE proposal and link with ACCORD, Latvia)
- 6 May 2022: Bureau meeting (analysis of PAC recommendations, voting procedure)
- 9 - 23 May 2022: remote vote by Assembly Members for the delivery of the common codes to DestinE
- 10 June 2022: STAC video-meeting (review progress on modernisation of working practice and on code adaptation, proposal for a rolling reporting per area)
- 20 June 2022: Bureau meeting (preparation of the Assembly, incl. result of the vote, PAC & STAC recommendations, …)
- 7 July 2022: 4th Assembly video-meeting
- 22 August 2022: DestinE dedicated Bureau meeting
- 5 October 2022: Bureau meeting (MG positions)
- 11 October 2022: PAC convened by the 4th Assembly to make recommendations on
- 3 afternoon - 4 morning November 2022, Copenhagen (hybrid): STAC (RWP2022 report, RWP2023, impact of DestinE on ACCORD RWP, …)
- 16 November 2022: Bureau meeting (governance positions)
- 17 November 2022: Bureau meeting (preparation of the Assembly)
- 7 afternoon - 8 morning December 2022: 5th Assembly, Darmstadt (hybrid)

Management Group

- The Management Group resumed their every other Friday morning meetings at the beginning of January and on 19 August after the summer break.
- **First in-person MG meeting** on 30 September 2022 in Brussels (after EWGLAM meeting)
- Additional meetings are dedicated to the preparation of the DAP2022, the preparation of the RWP2023, the reporting of RWP2022, …

LTM meetings

- 3rd LTM video-meeting (DAP2022, changes in CMR) on 31 January 2022
- 4th LTM video-meeting (ASW, RWP2023, CMR, cycles, ..) on 28 March 2022

- 29 June 2022: LTM video-meeting dedicated to ARPEGE LBC production changes
- 5th LTM meeting on 27 September 2022 in Brussels, besides EWGLAM, **the first in-person LTM (short) meeting** on 27 September at 17:30, continued on-line on 5 October

3 Scientific and technical meetings

With the end of the COVID travel restrictions, many events can now take place in-situ, or in hybrid format.

Thematic regular video-meetings

- Transversal activities on future software infrastructure, more information on ACCORD wiki SPTR dedicated page
- WG on Very High Resolution Modeling (VHR-MOD): meetings information
- WG on Machine Learning (ML): meetings information
- WG on Physics Interoperability, currently in strong link with SPTR
- DA Research Teams and Support Teams meetings, more information on the ACCORD wiki dedicated pages
- Surface monthly meetings, more details on the ACCORD wiki pages
- O2R WG: WG on Operation to Research, on-line meetings from October 2022 through February 2023

All Staff Workshop

The ACCORD big event in 2022 was the **2nd All Staff Workshop on 4-8 April in Ljubljana.** It was organised as an hybrid meeting, with participants in Ljubljana hotel and remote participants. For this first edition in an hybrid format, it did run smoothly: WARM CONGRATULATIONS to the Slovenian hosts. Ffuture ASWs will be hybrid as well: 3rd ASW on 27-31 March 2023 (place t.b.c.). A few figures of the ASW2022:

- 66 among the 212 registered participants attended on site and between 85 to 120 remote participants joined the sessions (about 45 - 55 the side-meetings), via bluejeans virtual rooms.
- 7 sessions + opening/closing sessions + 3 side-meetings
- 75 speakers (presentations) + 18 posters: BIG THANK to the participants, in-situ or remote
- video-recording: 30 hours

All the material is available on the ASW2022 page on the ACCORD website.

EWGLAM

The 44th European Working Group on Limited-Area Modelling (EWGLAM) and 29th Short Range NWP (SRNWP) EUMETNET meetings, hosted by the Royal Meteorological Institute of Belgium (RMI), took place from 26-29 September 2022 in Brussels, Belgium (in the Royal Library of Belgium, Mont des Arts 28, 1000 Brussels). The meeting was organized in a hybrid form, thus remote participation was possible. However, all participants, especially presenters were encouraged to participate in-person.

Although not an ACCORD event, but with the participation of many ACCORD colleagues, the meeting offered the opportunity to the LTMs and the MG to held their first in-person meetings (as a

side-meeting on Tuesday for the LTM meeting, as an additional meeting after EWGLAM on Friday for the MG meeting, hosted at RMI).

Working Days and Working Weeks

- harp training course, 16-18 February 2022, on-line: up-to-date information about the event on the ACCORD MQA wiki
- EPS Working Week, 25-29 April 2022, Innsbruck (Austria), more information on the ACCORD wiki dedicated page
- DA WW on high resolution data assimilation and nowcasting and 4D-Var, 25-29 April 2022, Budapest (Hungary): more information on the ACCORD wiki dedicated page
- NWP SURFEX training week, 9-13 May 2022, Budapest (Hungary): more information on the ACCORD wiki dedicated page
- Working week on harp standard verification set, 6-10 June, Helsinki (Finland): more information on the ACCORD wiki dedicated page
- ALARO WD Prague, 13-15 June 2022, Prague (Czech Rep.) more information on the ACCORD wiki
- DA WW dedicated to Support Teams and OOPS, 20-24 June 2022, Barcelona (Spain): more information on the ACCORD wiki dedicated page
- ACCORD DA WW & RC-LACE/DAsKIT working days 2022, 19-22 September 2022, Romania: more information on the ACCORD wiki dedicated page
- Cloud-radiation-aerosol WW, CHMI, Prague, 11-13 October 2022: more information on the ACCORD wiki dedicated page
- 3D Turbulence working week 2022, Vienna, ZAMG, 12-14 October 2022: more information on the ACCORD wiki dedicated page
- Harmonie-Arome CSC code re-factoring WW(integrated with the HARMONIE physics WW), 24-28 October 2022, Kilkenny, Ireland.
- 4th ACCORD DA working week (new observations and OOPS), DMI, Copenhagen, Denmark, 7-11 November 2022: more information on the ACCORD wiki dedicated page
- ALARO WW / code adaptation, refactoring, data structures, 7-11 November 2022, CHMI, Prague
- Autumn surface video working week, 21-25 November 2022, online only: more information on the ACCORD wiki dedicated page.
- DAVAÏ contributors-developers WW, DMI, Copenhagen, 21-25 November 2022
- Tech support visits for GIT transfer of knowledge, autumn

ACCORD resources

Patricia Pottier, ACCORD Consortium Scientific Secretary

1 Yearly documents

The ACCORD MoU-1 (article 7: resources) describes two categories of resources provided by Members: membership fees and human resources provided in-kind by Members. These resources are approved by the Assembly, monitored by the PM, with the help of the CSS and the MG, reported to the Assembly. Dedicated documents are produced.
During the 5 years of MoU-1, these documents will be yearly prepared and approved, and their actions assessed:

- The Rolling Work Plan (RWP) is a document updated every year that describes with a high level of detail the activities of the Consortium.
- The costed Detailed Action Plan (DAP) is a document drawn up each year that describes the expenses compensated by the ACCORD budget: (i) compensation for the salary of the PM, (ii) compensation for the expenses of the management and meetings of committees (PAC and STAC meetings, LTM missions, MG meetings, PM and CSS missions, All Staff Workshop organisation), (iii) travel money for scientific visits and WWs considered with highest priority by the Management Group, (iv) other types of expenses of general interest for the Consortium and agreed by the Assembly.

The life cycle of these annual documents includes an initial development phase, followed by a phase of implementation of the planned actions, and an evaluation phase. The MG, the PM and the CSS have a leading role in all these phases. The Assembly and the Committees (PAC, STAC) are presented with these documents, make recommendations and/or assess their realisation. The actions are realised by the Partners teams and under the responsibility of the LTMs.
Although they are annual documents, they have a lifespan of 2 years, between their preparation and completion.

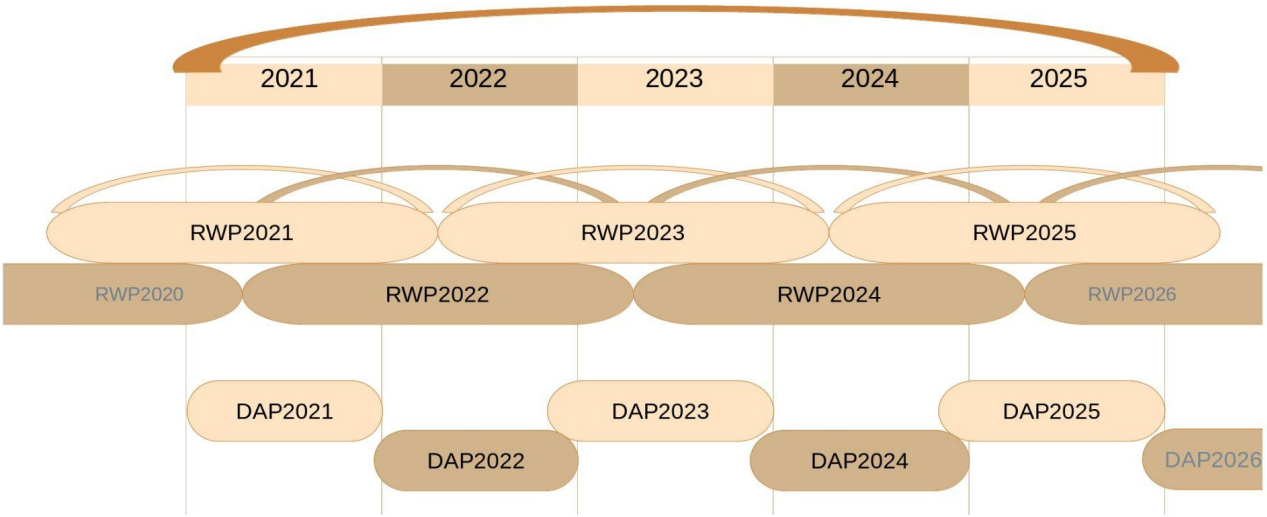

Figure 1: RWPs and DAPs over the 5-year term of the ACCORD MoU-1

1. ACCORD Rolling Work Plan YYYY

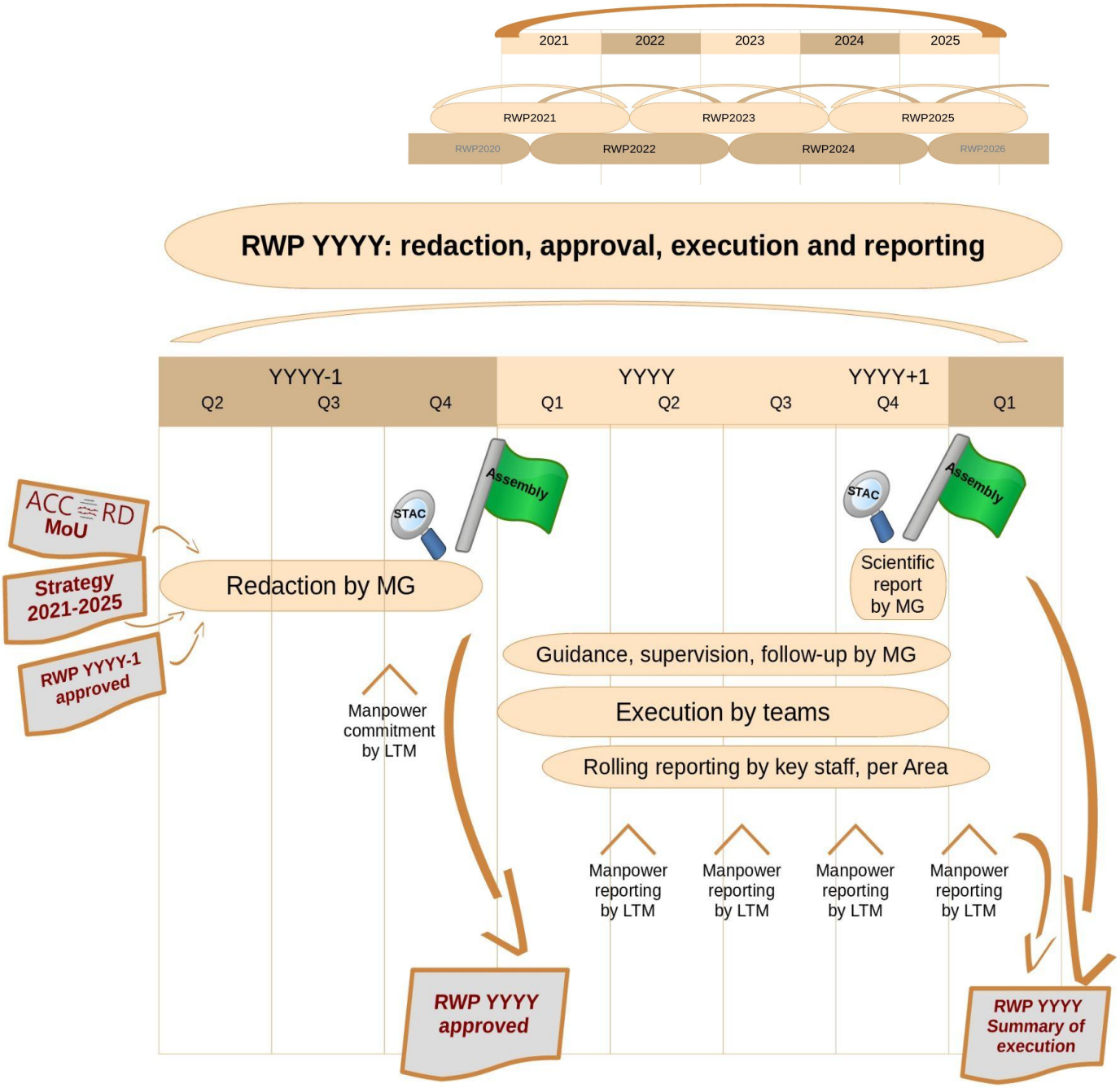

Figure 2: Detailed life cycle of a Rolling Work Plan

2. ACCORD Detailed Actions Plan

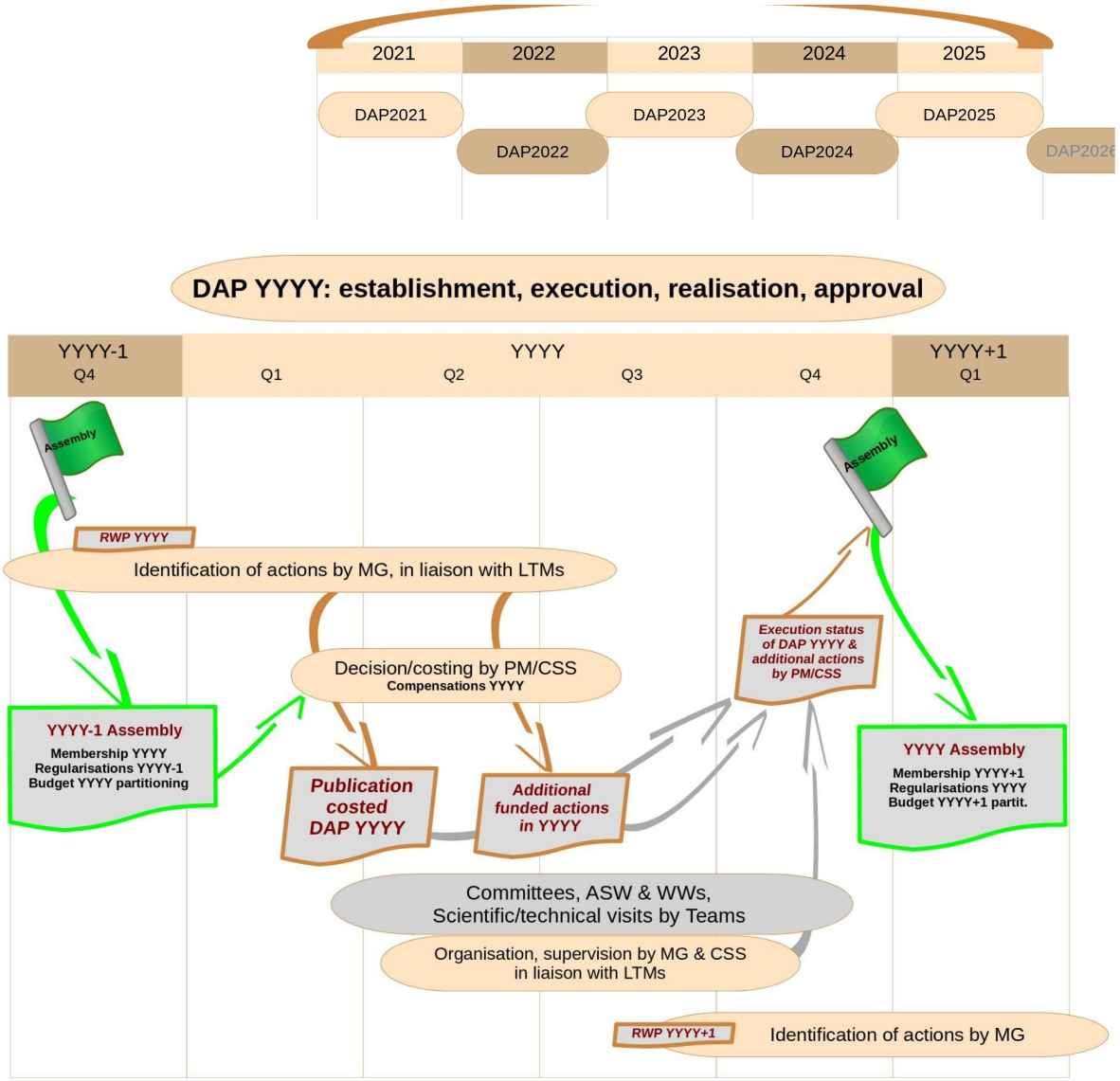

Figure 3: Life cycle of a Detailed Action Plan (not taking into account the financial procedures)

2 ACCORD budget

1. The mechanism

The financial procedures were approved by the ACCORD kick-off Assembly on the 27th of November 2022: Météo-France manages the ACCORD budget via a dedicated specific account (ACCORD 3rd party account) according to the following procedure:

- At the beginning of each year, Météo-France issues bills to collect the membership fees (amount decided by the Assembly);
- the PM and the Consortium Scientific Secretary (CSS) finalize the costed Detailed Action Plan (DAP) based on the RWP and the partitioned budget (partitioning among the possible expenses, see MoU items 121-127) adopted by the Assembly, including proposals by the AL and LTM, and in agreement with the full MG;
- As soon as the ACCORD 3rd party account has been provisioned, Météo-France starts payments to Members according to the DAP (reimbursements of the DAP actions, on a compensatory basis);
- Should a Member not be able to complete a given task for which it has received a payment, this is resolved by a budget adjustment in the following year (to avoid too many financial transfers).

The Assembly also approved the compensation rates that are used for reimbursement to the Members of the actions in the DAP.

The Directors of HIRLAM, respectively LACE, Members confirmed KNMI, respectively ZAMG, to realize all financial actions on behalf of the HIRLAM countries.

Bilateral agreements have been signed between KNMI, ZAMG and the NMSs of Algeria, Belgium, Bulgaria, France, Morocco, Portugal, Tunisia and Turkey and are valid for the MoU duration.

At the end of each year (YYYY), the Assembly formally approves of the reimbursement figures for non-executed actions during the year YYYY and of the membership fee and the partitioning of the budget for YYYY+1.

In order of maximise the rate of realisation of the DAP as requested by the 3rd Assembly , the MG and the CSS added a more flexible mechanism: with respect to the published DAP-YYYY some additional actions are discussed and approved by the MG to be ACCORD-funded in YYYY (although the reimbursement to the Members will be done with reimbursements of the DAP-YYYY+1 actions).

A document "Wiki-budget.pdf" was prepared for the LTMs and the teams with the aim of explaining the rules of the ACCORD budget, the procedure used by the MG to prepare the DAP, and proposes a F.A.Q. for travellers/hosts/LTMs.

2. Illustration of the financial procedures

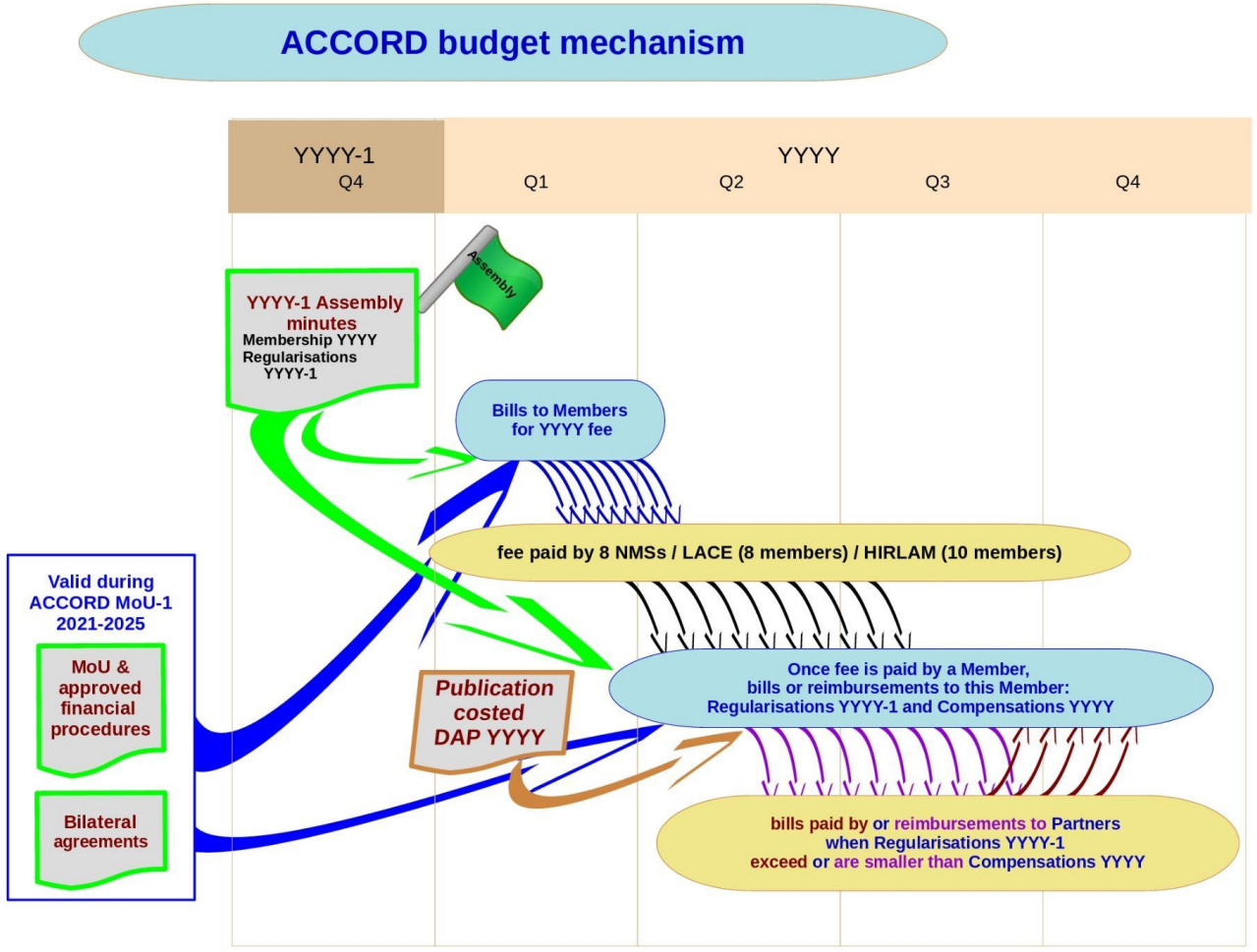

Figure 4: Realisation of the financial procedures

ACCORD-funded scientific visits and Working Weeks during the first half of 2022

Patricia Pottier, ACCORD Consortium Scientific Secretary

1 Introduction

As explained in the article "ACCORD resources", the costed Detailed Action Plan 2022 includes travel money for scientific visits and WWs considered with highest priority by the Management Group.
A scientific visit is a visit from one scientist in another institute to work on some priority tasks of the Rolling Work Plan (1-4 week visits). A Working Week is a gathering of different specialists in one place during 1 week, to work together on a priority topic. Travels to a WW are compensated as a 1 week visit.

Information of the scientific visits (including reports) can be found on the ACCORD dedicated webpage. Material for the Working Weeks or the Working Days is generally available on the ACCORD wiki (link to the wiki pages for each WW/WD).

2 Scientific visits

Below are listed the scientific visits compensated by the ACCORD budget during the first half of 2022 (click on the proposed link for the report of the visit):

- Alina Lerner (ESTEA) hosted by Roger Randriamampianina (MeT Norway), 09–27.05.2022 : Set up a high resolution NWP system with DA: report
- Mohamed Mokhtari hosted by MF (Toulouse) Yann : Coupling LIMA-Aerosols-CAMS, 7-21 June 2022, report
- Harold McInnes (Met Norway) hosted by SMHI/Ulf Andrae, Patrick, Daniel Yazgi, 13-17 June 2022 : EPS E11.2 - Extend SPP to surface parameters: report.
- Carlos Geijo (AEMET) hosted by Magnus Lindskog (SMHI), 27 June - 1 July : Meteorological Radar Doppler Wind Data Assimilation in HARMONIE-AROME using the Field-Alignment Algorithm: report
- Mats Dahlbom (DMI) and Jana Sanchez (AEMET) hosted by Martin Ridal (SMHI), 9-13 May 2022: Radar assimilation (common quality control/monitoring/status update, Doppler winds Data Assimilation, preprocessing radar data, ...): report
- Kristian Pagh Nielsen hosted by Quentin Libois & Yann Seity / Toulouse : Discuss evolution of radiation physics: report
- Ana Šljivić hosted by Eric Bazile (Toulouse) : Develop a simplified version of ISBA, in order to implement a Surfex-independent test case in DAVAÏ for the 3 CSCs): first part of the visit 30 May - 10 June; report after the second part in October.
- Ana Šljivić hosted by Alena Trojakova (CHMI), 25.07-19.08.202: report to be published later on the ACCORD webpage

3 Working Weeks

Below are listed the WWs compensated by the ACCORD budget during the first half of 2022.

- DA WW dedicated to Support Teams and OOPS, 20-24 June 2022, Barcelona (Spain): more information on the ACCORD wiki dedicated page
- Working week on harp standard verification set, 6-10 June, Helsinki (Finland): more information on the ACCORD wiki dedicated page
- NWP SURFEX training week, 9-13 May 2022, Budapest (Hungary): more information on the ACCORD wiki dedicated page
- EPS Working Week, 25-29 April 2022, Innsbruck (Austria), more information on the ACCORD wiki dedicated page
- DA WW on high resolution data assimilation and nowcasting and 4D-Var, 25-29 April 2022, Budapest (Hungary): more information on the ACCORD wiki dedicated page

Some WWs/WDs have been organised outside the DAP2022 (see the article with “ACCORD events in 2022”).

Implementation of Simplified Extended Kalman Filter in the operational AROME/HU

Helga Tóth and Boglárka Tóth
Hungarian Meteorological Service

1 Introduction

In the operational AROME/HU model, during the surface data assimilation, the soil temperature and moisture fields are statically generated from the near-surface variables, using the optimum interpolation (OI-main) method (Giard and Bazile, 2000). This is a simple, computationally efficient method, but it has limitations.
In the AROME-TEST version, we use the Simplified Extended Kalman Filter (SEKF) (Mahfouf, 2009, Tóth et al., 2022), which enables a more dynamic description depending on the weather situation as well as to use of satellite data during the surface assimilation. With this method, we expect a more accurate near-surface analysis and a forecast as well.
AROME-TEST was run in parallel to the operational forecasts 3 times a day (at 0, 6 and 12 UTC) since November 2021. The results were investigated over two selected periods in detail. Objective and subjective evaluations were carried out. The forecasters were also involved in the evaluation and they focused on the difference between the forecasts of the operational AROME and AROME-TEST runs. They recorded daily their comments. At the same time, subjective verification was done by the model developer in interesting weather situations and they ranked the model performance from 1 to 5 (where 5 is the best). The objective pointwise verification was completed by using the in-house, Perl-based OVISYS verification system. RMSE (Root Mean Square Error) and bias scores were computed for some surface parameters: mean sea level pressure, total cloudiness, temperature, dewpoint and relative humidity at 2 m, 10 m wind speed, and wind gust, and for some upper-level parameters: temperature at 850 hPa, relative humidity at 700 and 925 hPa, geopotential height at 500 hPa. Frequency bias and another scores were calculated based on the contingency table of 12- and 24-hour precipitation amounts as well. In addition, SAL verification (Wernli et al., 2008) was also made to evaluate the location, amplitude, and structure of the precipitation patterns in comparison with radar data for the nearly 1-month convective test period. This short paper mainly focusses on the results of the forecasts at 0 UTC.

2 Validation and testing

Two test periods were chosen:

1. winter period: 2021. 11. 19 – 2021. 12. 18
2. summer period: 2022. 05. 04 – 2022. 06. 01

The assimilation settings of SEKF are crucial and tuned as follows:

XERROBS (T2M, HU2M) = 1.0, 0.07
XSIGMA (WG2, WG1, TG2, TG1) = 0.15, 0.1, 2.0, 2.0
XTPRT (WG2, WG1, TG2, TG1) = 10^{-4}, 10^{-4}, 10^{-5}, 10^{-5}

Apart from the SEKF-related settings, the experimental setups were the same as in the operational AROME/HU. The model configurations are listed in Table 1 and the integration domain is presented in Fig. 1.

Table 1. Model configurations.

	AROME-OPER	AROME-TEST
Model cycle	cy43t2_bf11+SURFEX 8.0	cy43t2_bf11+SURFEX 8.0
Resolution	2.5kmL60	2.5kmL60
LBC	IFS 1h (lagged)	IFS 1h (lagged)
Method	3D-Var + OI-MAIN	3D-Var + **SEKF**
B matrix	Static EDA	Static EDA
Initialization	No	No
Observations	SYNOP + AS GNSS ZTD AMDAR TEMP, Mode-S/MRAR (SI, CZ)	SYNOP + AS GNSS ZTD AMDAR TEMP, Mode-S/MRAR (SI, CZ)

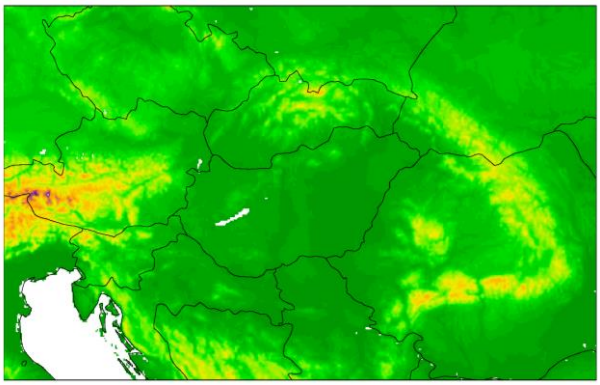

Fig. 1: Integration domain of AROME/HU model

2.1 Winter period

In the first part of the period, the models faced the challenges of forecasting of fog and low-level cloud in an anticyclonic situation which also led to near-surface temperature problems. In the rest of the period, several fronts passed Hungary, often with mixed phased precipitation.
Considerable difference between the forecasts produced by the model versions was found mainly in the anticyclonic situations.

A systematic underestimation for both 2 m temperature (Fig. 2, left) and dewpoint (Fig. 2, right) was experienced during the test period, with slightly larger extent for AROME-TEST.

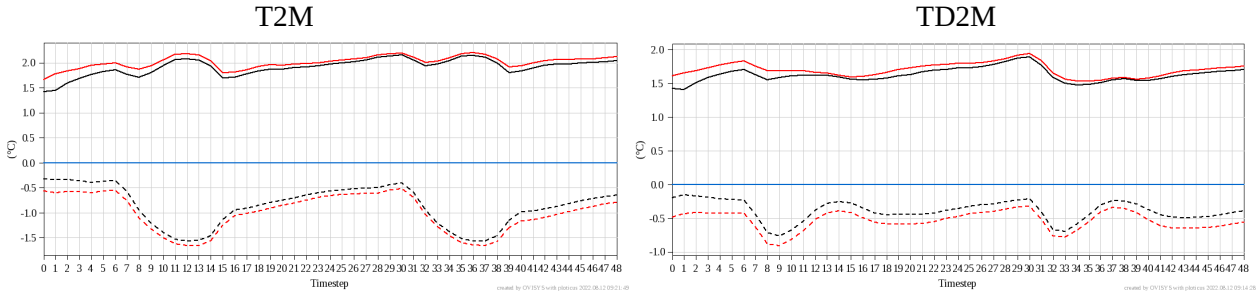

Fig. 2: Bias (dashed line) and RMSE (solid line) of 2 m temperature (left) and 2 m dewpoint (right) forecasts for the 0 UTC runs from 19 November to 18 December 2021. Curves represent: AROME-OPER, AROME-TEST.

Fig 3 shows the mean diurnal cycle in Hungary for the entire period. Both model versions underestimated the daily temperature (with around 0,5-2 °C), especially the maximum values, which was even greater when using Kalman filter. The reasons behind the temperature underestimation are

related to overestimation of low-level cloud existence in some weather situations, while it is linked to some fake snow persistence in December.

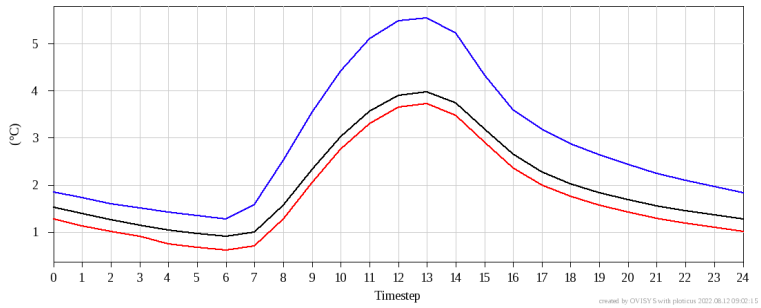

Fig. 3: 2 m temperature mean diurnal cycle from 19 November to 18 December 2021, for 0 UTC runs. Curves represent: AROME-OPER, AROME-TEST, SYNOP observations.

There was no significant difference between the two forecasts in case of 10 m wind speed and gust, precipitation during the test period. The small differences concluded for the near-surface parameters continued to decrease at higher levels for wind, temperature, and relative humidity.

2.2 Summer period

During the test period, less than average precipitation fell, which appeared in the form of showers and thunderstorms thanks to the convective period. In some events related to the front passing, intense hail also occurred in addition to stormy winds. Typically, however, local precipitation events dominated during the examined period.

At the first forecast hours, the two models performed similarly for 2 m temperature, then the biggest difference usually appeared at night (Fig. 4). In the case of forecasts beyond 24 hours, the difference between the two models decreased and AROME-TEST mostly performed better.
In the case of dewpoint, the operational run had a smaller error during the daytime hours, but the SEKF reduced the underestimation at night (Fig. 4, right).

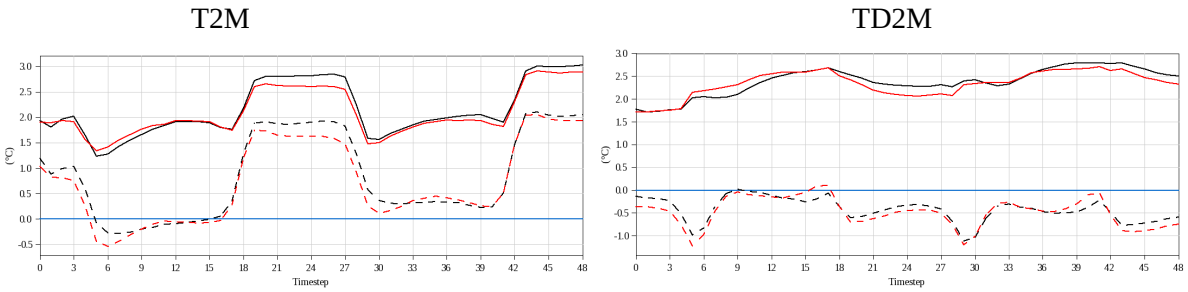

Fig. 4: Bias (dashed line) and RMSE (solid line) of 2 m temperature (left) and 2 m dewpoint (right) forecasts for the 0 UTC runs from 4 May to 1 June 2022. Curves represent: AROME-OPER, AROME-TEST.

Figure 5 shows the mean diurnal cycle in Hungary for the entire period. Both model versions predicted very good and exact daytime temperatures, however, the models made fairly large errors in predicting sunset and nighttime temperatures.

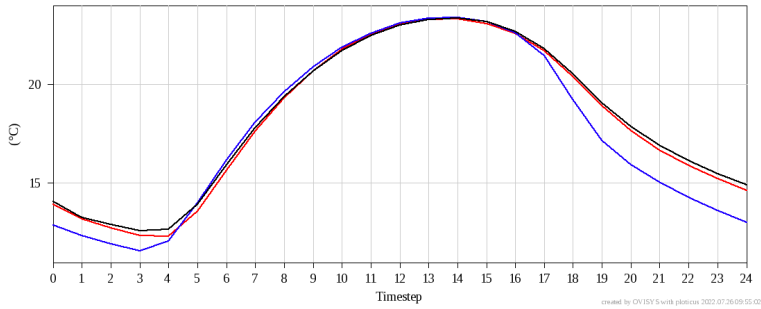

Fig. 5: 2 m temperature mean diurnal cycle from 4 May to 1 June 2022, for 0 UTC runs. Curves represent: AROME-OPER, AROME-TEST, SYNOP observations.

In the case of the minimum temperature, the model run with the new surface assimilation provided much better predictions, sometimes an improvement of nearly 1 °C occurred in RMSE and bias (Fig. 6).

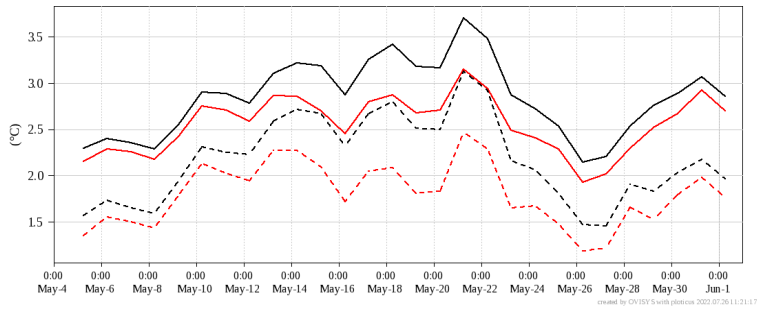

Fig. 6: RMSE (solid line) and bias (dashed line) of the 12-hour minimum temperature forecasts for the 0 UTC runs at 30-hour lead-time from 4 May to 1 June 2022. Curves represent: AROME-OPER, AROME-TEST.

During the examined period, a larger daily temperature cycle was observed in the AROME-TEST run, with more intense daytime warming, and nighttime cooling, which mostly affected the central part of the domain. This sometimes led to improvement (mostly in clear, dry, anticyclonic weather situations, like on 19 May, Fig. 7) and sometimes to deterioration.

T2M AROME-OPER T2M AROME-TEST T2M SYNOP

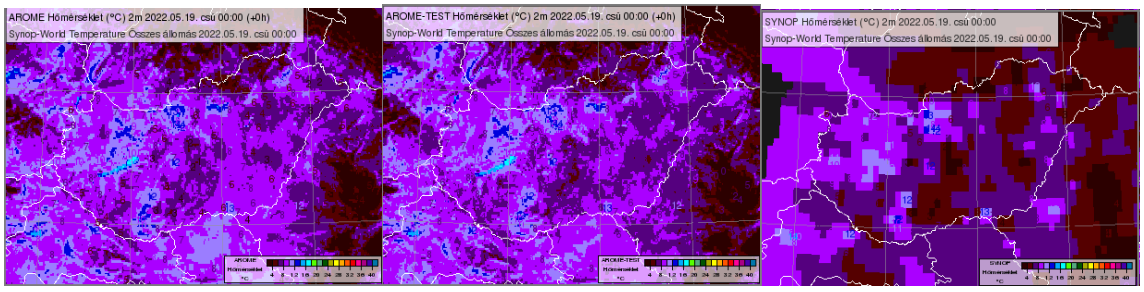

Fig. 7: 2 m temperature analysis of AROME-OPER (left), AROME-TEST (middle) and SYNOP observations (right) at 0 UTC on 19 May 2022.

Events with a precipitation amount of less than 6-7 mm were underpredicted by the models, and events exceeded this threshold were overpredicted. For high precipitation events (>10 mm), AROME-TEST performed better and the difference between the two models increased proportionally as the threshold increased (Fig. 8). The occurrence of false alarms was lower in AROME-TEST than in the operational model for almost all thresholds, and overestimation of the intensity was reduced (not shown).

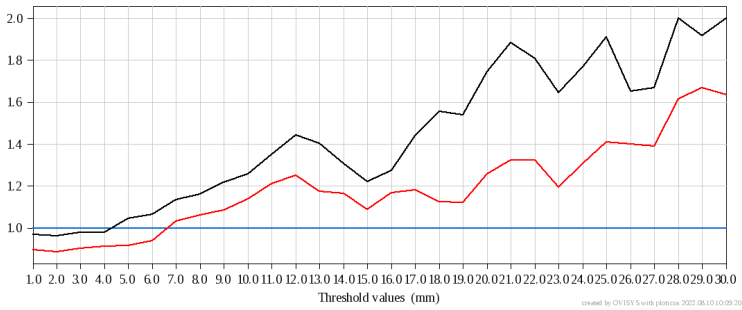

Fig. 8: Frequency bias (FBI) of the 24-hour precipitation forecast for the 0 UTC runs at 30-hour lead-time depending on different rainfall thresholds from 4 May to 1 June 2022. Curves represent: AROME-OPER, AROME-TEST. The ideal value of FBI is 1, for values greater/lower than 1, the event corresponding to the given threshold is too frequent/rare in the forecasts.

Regarding the structure of precipitation objects, AROME-TEST predicted precipitation fields with a much finer structure than the operational model and also reduced the underestimation of the number of objects. The error of the displacement of the precipitation fields has also decreased (more green and blue dots), especially for convective events (Fig. 9).

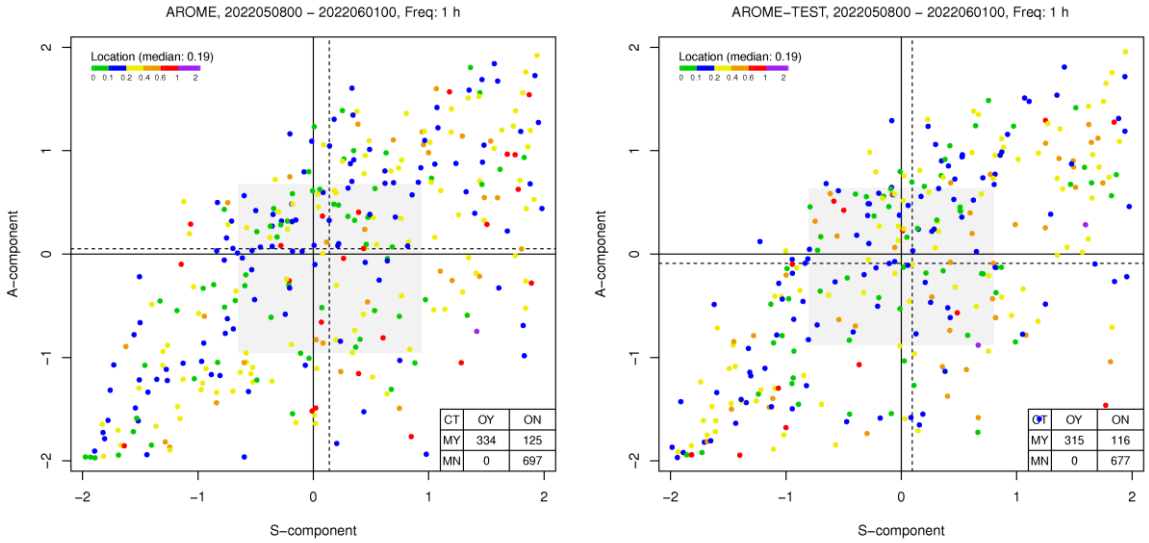

Fig. 9: SAL verification of the precipitation forecast over 1 mm threshold for the 0 UTC runs from 8 May to 1 June 2022. Left: AROME-OPER, right: AROME-TEST.

Higher than reality precipitation intensity was characterized by both AROME models, but the AROME-TEST forecasts were mostly closer to the intensity calculated from the radar data. The most intense objects were generated a bit earlier by the models and kept the intense rain longer during the day, but AROME-TEST was closer to reality in the critical period (not shown). Based on the radius of the sphere in SAL, better results were obtained with SEKF (Table 2)

Table 2: Radius of sphere in SAL statistics for 0, 6 and 12 UTC AROME-OPER and AROME-TEST runs from 4 May to 1 June 2022. The lower the value, the better.

	5%		10%		20%		50%	
	OPER	TEST	OPER	TEST	OPER	TEST	OPER	TEST
00 UTC	0.44	0.36	0.56	0.49	0.74	0.68	1.32	1.20
06 UTC	0.44	0.39	0.60	0.54	0.82	0.71	1.45	1.29
12 UTC	0.44	0.38	0.57	0.52	0.81	0.74	1.32	1.36

3 Operational implementation

The advantage of the model run with SEKF was shown in different weather situations. One of the most positive results occurred in the summer precipitation forecast, which receives special attention during the convective period: more structured, less overestimated, and better positioned forecasts in space were made by AROME-TEST.
The larger daily temperature cycle of AROME-TEST provided a more accurate forecast in dry, anticyclonic weather conditions.
A neutral or weak negative effect was observed for several parameters during the day, but the AROME-TEST run was characterized by a forecast with a smaller error at night.
After its careful evaluation, SEKF was introduced in the operational AROME deterministic suite on 29th June 2022.

4 Acknowledgements

The authors would like to thank all colleagues in OMSZ who participated in the testing of SEKF.

5 References

Giard, D. and Bazile, E.: Implementation of a New Assimilation Scheme for Soil and Surface Variables in a Global NWP Model. Mon. Weather Rev. 128, 997–1015, **2000**.
https://doi.org/10.1175/1520-0493(2000)128<0997:IOANAS>2.0.CO;2
Mahfouf, J.-F., K. Bergaoui, C. Draper, F. Bouyssel, F. Taillefer, and L. Taseva,: A comparison of two off-line soil analysis schemes for assimilation of screen level observations, J. Geophys. Res., 114, D08105, **2009**. http://dx.doi.org/10.1029/2008JD011077 .
Tóth, H., Homonnai, V., Mile, M., Várkonyi, A., Kocsis, Zs., Szanyi, K., Tóth, G., Szintai, B., and Szépszó, G.: Recent developments in the data assimilation of AROME/HU numerical weather prediction model. Időjárás, 125(4), 521–553, **2021**. https://doi.org/10.28974/idojaras.2021.4.1
Wernli, H., Paulat, M., Hagen, M. and Frei, Ch.: SAL – A novel quality measure for the verification of Quantitative Precipitation Forecast. Mon. Wea. Rev., 136, 4470–4487, **2008**.

Assimilation of new observations in AROME over Austria

Phillip Scheffknecht, Florian Meier, Christoph Wittmann

1 Assimilation of Microwave Link Data from Austrian Cell Phone Towers

Introduction

Cell phone towers are connected to each other using microwave links of various frequencies (from approximately 13 – 80 GHz) to exchange data and forward calls. These links are affected by rainfall between the towers via attenuation of the microwave signal due to rain drops. In the framework of the LINK project, ZAMG is exploring the possibility to use these microwave links for the determination of rain rates together with the project partners FH St. Pölten and Drei Hutchison.
The amount of attenuation is – simply speaking - a function of the length of the link, the frequency of the link, and the rain rate between the towers. The data set for Austria contains approximately 5000 links, however, about 75% of them are 80 GHz links, for which known methods of estimating rainfall from microwave links (see e.g. Overeem et al., 2016) do not work, because cloud droplets also affect the signal strength of high frequency links. This type of links is becoming increasingly common. Assuming the presence of rainfall can be reliably determined, this data could also open up possibilities of detecting clouds or fog between the links in the future.

Initial Results: Conversion from Attenuation to Rain Rates

For the project, the conversion from microwave link attenuation to rain data is being handled by FH St. Pölten. They use a machine learning appraoch to extract the rain information from a data set of microwave links provided by Drei Hutchison Austria and the INCA Precipitation Analysis at the corresponding points (Kovac et al., 2022). The first experiments were restricted to binary data, i.e. rain or no rain, with the results shown in Fig. 1. Ongoing work is extracting quantitative rain data from the microwave links, which will be tested this autumn.

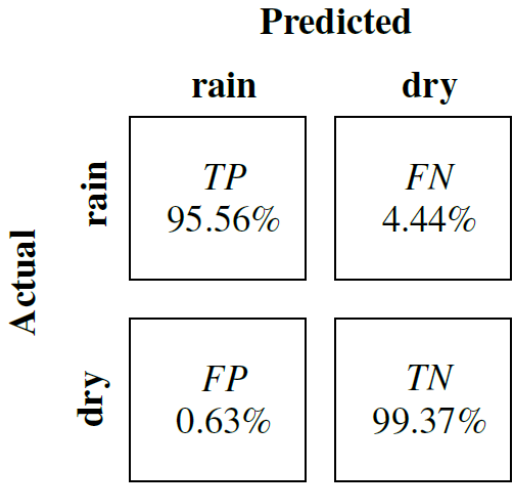

Figure 1: Confusion matrix for the binary results when converting the microwave links to precipitation data.

First Assimilation Experiment

An initial experiment was performed using AROME and binary rain data. The observations were converted to profiler data consisting of a single 100% relative humidity observation located at the longitude, latitude, and altitude of the link midpoint. Links with no rain were ignored, resulting in a data set with points of 100% RH.

A total of 2076 humidity points were assimilated for 2021-07-17 00 UTC, the results are shown below. Figure 2a and b shows that the model adjusts the moisture heavily toward the new observations, which is to be expected due to a lack of other relative humidty observations other than surface stations. Figure 2 also shows the first guess departures (c) and analysis departures (d) overlaid on a map, to illustrate where the departures are the largest. Over the south of Austria, a large number of links reported rain while the relative humidty was around 75 – 80%, thus the observations increased relative humidty in this area significantly.

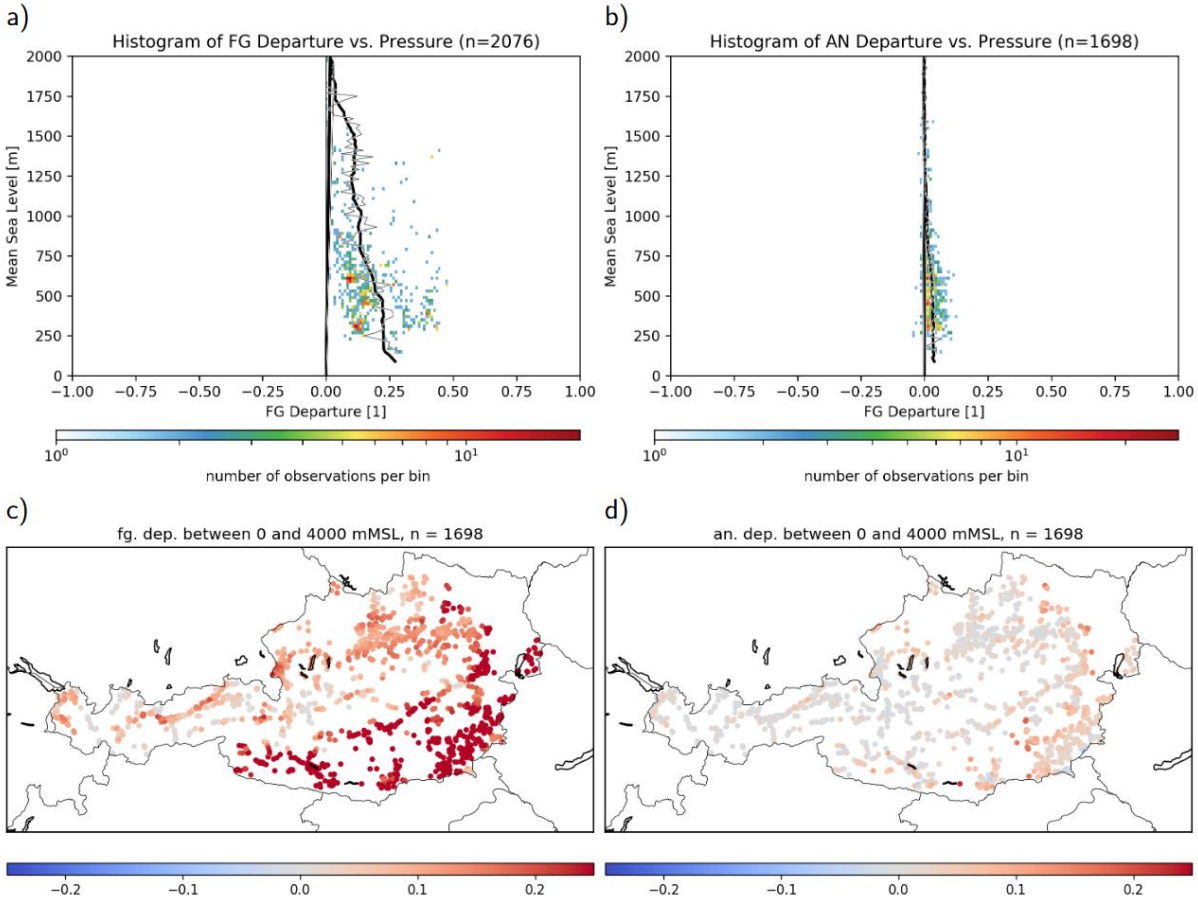

Figure 2: 2D height-departure histogram of the link measurements assimilated during the init01 experiment. The color indicates the amount of observations for the given altitude and with the given first guess departure. The total amount of observations is 1690 (out of 2084 screened observations). The thin black line shows the average departure for each altitude level, the thick black line shows five point running mean over multiple levels.

Figure 3 shows the impact of the observations on two of the model fields, specific humidty *q* (a-c) and temperature *T* (d-f). The model adjusts specific humidty toward the observations, introducing a large amount of additional water vapor into the atmosphere. To correct for the inrease in instability, the temperature is lowered in turn (Fig. 3 d-f).

Unsurprisingly, this appraoch results in higher precipitation and a general overestimation of humidity and rainfall. However, it is a usefull proof of concept which could possibly be refined using observation error and thinning. Since the observation type used here (PILOT) is generally rare, no automatic thinning is applied, resulting in a large number of observation within a small area.

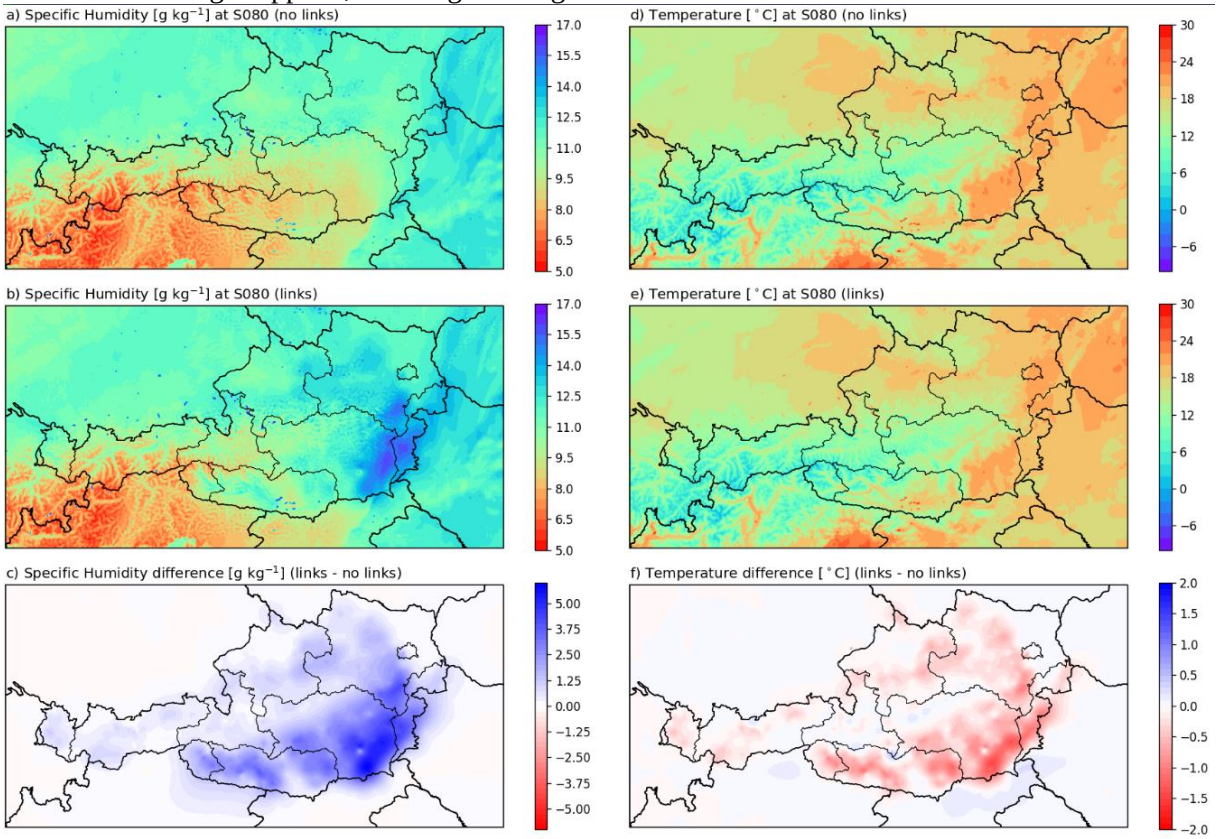

Figure 3: Specific humidity (a, b) and temperature (d, e) fields with their respective differences (c, f). The fields without (a-c) and with link data (d-e) are shown.

Outlook

Our project partner FH St. Pölten has been working on quantitative rain data and has provided an initial data set extracted from 80 GHz links exclusively. This novel data will be assimilated into AROME using the 1D + 3DVAR approach used in Lopez et al. (2007) and Sahlaoui et al. (2019). They used the method to assimilate TRMM data and surface rain gauge data, respectively, but an equivalent approach can be used to assimilate rain data obtained from microwave links. This more sophisticated approach is expected to yield better results than the crude inital test with only saturated points. The use of 80 Ghz links will also make it easier to precisely locate the rain observations, as their average length of 1.6 km is on the same scale as the model resolution of the AROME RUC model (1.2 km).

2 Assimilation of Sentinel-1 InSAR data

ZAMG is currently working on the assimilation of Interferometric Synthetic Aperture Radar (InSAR) data from Sentinel-1 A/B within two scientific projects in cooperation with Joanneum Research Graz and EOG GmbH Vienna respectively. Similar to ground based GNSS data the satellite radar beam is delayed by atmospheric moisture and temperature stratification on its way through the atmosphere. So far, only relative delay changes between two overflights were provided by the project partners. If the atmospheric signal is removed slow movement of the ground and landslides can be detected. For this purpose ZAMG provides AROME model data to Joanneum Research institute to do the correction.

Vice versa, if non-moving soil is assumed the delay can be related to atmospheric effects and assimilated like GNSS delays. The slant delay operator from de Haan and Imrisek in cy43t2 was installed and technically tested at ZAMG. An interface to convert Sentinel-1 netcdf to GNSS obsoul data was written in Python, which also allows a basic thinning of the data. To derive absolute delays the relative delay is assimilated at the time of the first overflight and the first guess departures and observed values extracted from ODB via mandalay. The difference between the latter two values delivers the simulated first guess values at that time. The interface also allows to add these derived absolute first guess values to the original difference observations to get absolute observations at the time of the second overflight with the same geometry. Typically the time between two such satellite overflights is 6 to 12 days depending if two or one Sentinel-1 satellite is available. Even if the temporal resolution of the observations is rather coarse, the high spatial resolution (few meters) makes the data interesting and complementary to the temporally highly but spatially coarser resolved GNSS ground data especially in high resolution NWP simulations. The derived absolute values at time of the second overflight can be finally assimilated like slant GNSS observations into AROME. However, first assimilation experiment from 15th August 2021 shows a rather large scale increment indicating that the data are still strongly biased (Figure 4). This can be related to the significant difference between real and model orography in the Alpine region, low AROME model top (around 20hPa) not covering all the atmosphere, sensor bias, time delay between analysis and observation values in 3D-Var and other sources. Next challenge will be therefore a proper bias correction where we will try to minimize the time and domain averaged increment by AI and conventional techniques keeping the spatial variability. Then we can expect a gain by the data for the model analysis especially in case of small scale moisture linked weather phenomena like convection or fog (see Mateus et al. 2018). It is also planned to derive absolute observation values directly based on calibration of Sentinel-1 with nearby GNSS stations such that no dependence on model performance at the previous overflight occurs.

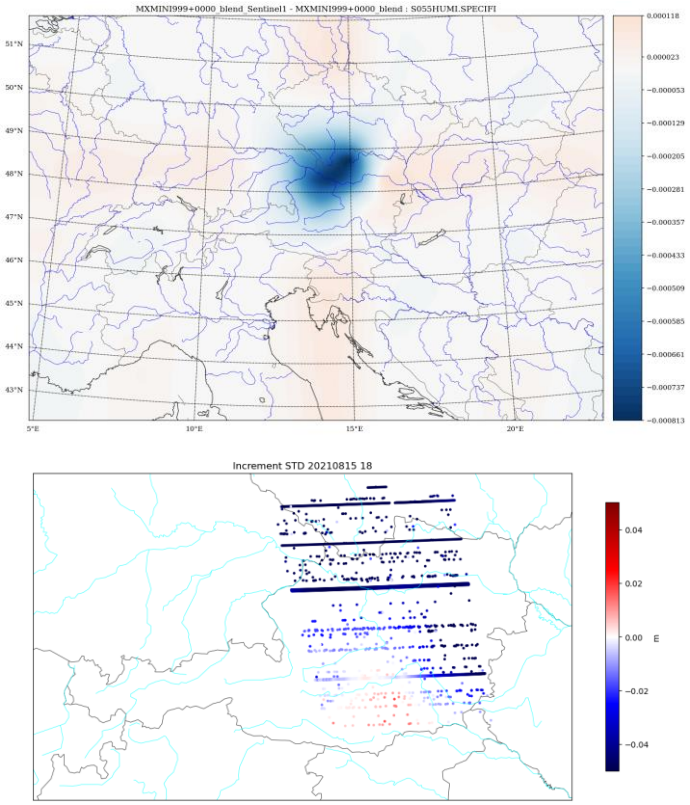

Figure 4: Difference in AROME specific humidity kg/kg level 55 (about 850hPa) with and without assimilation of Sentinel-1 InSAR (top) and InSAR increment at observation points (bottom) 20210815 18UTC.

3 References

De Haan, Siebren and Martin Imrišek, 2019: GNSS slant total delays in the ALADIN NWP system: Phasing of the source code from cy40h1 to cy43t2 – KNMI stay report available at: https://www.rclace.eu/media/files/Data_Assimilation/2019/repStay_MImrisek_STDphasing_2019.pdf

F. Kovac, O. Eigner, A. Adrowitzer, H. Scholnast and A. Buchelt, "Classification of rain events using directional radio data of commercial microwave links," in 2022 IEEE International Conference on Omni-layer Intelligent Systems (COINS), Barcelona, Spain, 2022 pp. 1-6.

Lopez, P., & Bauer, P. (2007). "1D+4DVAR" Assimilation of NCEP Stage-IV Radar and Gauge Hourly Precipitation Data at ECMWF, Monthly Weather Review, 135(7), 2506-2524.

Mateus, P., Pedro M. Miranda, Giovanni Nico, Joao Catalao, Paulo Pinto and Ricardo Tomé, 2018: Assimilating InSAR Maps of Water Vapor to Improve Heavy Rainfall Forecasts: A Case Study With Two Successive Storms. Journal of Geophysical Research Atmospheres 123, 7, 3341-3355. DOI: https://doi.org/10.1002/2017JD027472

Overeem, A., Leijnse, H., and Uijlenhoet, R.: Retrieval algorithm for rainfall mapping from microwave links in a cellular communication network, Atmos. Meas. Tech., 9, 2425–2444, https://doi.org/10.5194/amt-9-2425-2016, 2016.

Sahlaoui, Zahra & Mordane, Soumia & Wattrelot, Eric & Mahfouf, Jean-Francois. (2019). Improving heavy rainfall forecasts by assimilating surface precipitation in the convective scale model AROME: A case study of the Mediterranean event of November 4, 2017. Meteorological Applications. 27. 10.1002/met.1860.

Fa mt-2019-412.

Assimilation of clear-sky SEVIRI radiances in AEMET HARMONIE-AROME model

Joan Campins, María Díez, Alberto Jiménez and Beatriz Navascués

1 Introduction

Radiance data from geostationary satellites have been assimilated in global numerical weather prediction models since a long time (Köpken et al., 2003; Szyndel et al., 2004). Their high spatial and temporal coverage are particularly beneficial on global scales and in regions with a lack of ground-based measurements. As an example, the assimilation of radiance data from Meteosat-8 and Meteosat-11 continues to be of value to the ECMWF system (Burrows, 2020). Similarly, limited area models can benefit from these radiances. In fact, some operational centres assimilate radiance data from geostationary satellites in their convective-scale numerical weather prediction models (Gustafsson et al. 2018).

The present contribution describes the implementation and evaluation of the radiances assimilation of two water vapour channels (WV6.2 and WV7.3) and an infrared channel (IR13.4) of SEVIRI instrument, in the AEMET HARMONIE-AROME system. The impact of using clear-sky radiances from the geostationary satellite Meteosat-11 has been assessed separately through different parallel experiments covering two geographical domains (Iberian Peninsula and Canary Islands) over two study periods.

The main features of the data processing are described. Special care has been devoted to bias correction, in particular to the number of variational bias correction predictors. After the control and experimental suites are presented, the impact studies carried out are introduced and some aspects of the analysis performance are shown. An objective verification of all the experiments has allowed to assess the impact on forecasts, with emphasis on the shorter lead times to better understand the influence of the assimilation of these SEVIRI channels.

2 Experimental framework

Control suite

The setup of the AEMET HARMONIE_AROME suite is based on cycle 43h.2.1.1 on the local HPC. The model runs at 2.5 km horizontal resolution and 65 vertical model levels extending up to 10 hPa, and over two domains: one centred on the Iberian Peninsula that includes the Balearic Islands (called AIB), and other centred on the Canary Islands (called AIC).

The upper-air assimilation uses a 3DVar scheme with a 3-hr cycle using 70 minutes cut-off time for the observations. Many types of observations are assimilated, including conventional measurements (radiosonde, aircraft, buoy, ship, and synop, 2-meter temperature and relative humidity), Global Navigation Satellite System (GNSS) Zenith Total Delay (ZTD) data, weather radar reflectivity information, as well as scatterometer data and passive microwave and infrared (IR) clear-sky radiances from various satellite platforms. Scatterometer data are provided by Metop-B and C satellites. Passive microwave radiances are provided by the Advanced TIROS Operational Vertical Sounder (ATOVS) from AMSU-A and MHS instruments on board of NOAA-18 and 19, and Metop-B and C satellites.

And finally, the IR radiances are sensed by the Infrared Atmospheric Sounding Interferometer (IASI) placed on board the Metop-B satellite.

For the surface analysis, CANARI optimal interpolation with conventional observations (snow depth, 2-meter temperature and relative humidity) is used. The large scale from the host model is included in the analysis through a scale selection method (LSMIX) for temperature and wind, but not for humidity.

As lateral boundary conditions, Global forecasts provided by the European Centre for Medium-Range Weather Forecasts (ECMWF) are used. These forecasts are launched every 6 h with a 1 h output frequency.

SEVIRI radiances: Instrument, channels, and pre-processing

The Spinning Enhanced Visible and InfraRed Imager (SEVIRI) is the Meteosat Second Generation primary instrument. It has twelve spectral channels, eight of them take measurements in the infrared band of the spectra, the rest for the visible channels (one of them in high resolution). The horizontal resolution is 3 km, except for the high resolution visible channel that is 1 km. Time resolution is one image every 15 minutes.

Table 1: Infra-red SEVIRI channels and their main characteristics.

SEVIRI Channels	**Main characteristics**
IR 3.9	It is used at night to detect fog and very low clouds Window channel of CO_2
WV 6.2	Water Vapour Channels
WV 7.3	
IR 8.7	Window channel of H_20
IR 9.7	Ozone absorption channel. Not suitable to data assimilation
IR 10.8	Window channel of H_20
IR 12.0	
IR 13.4	CO_2 absorption band

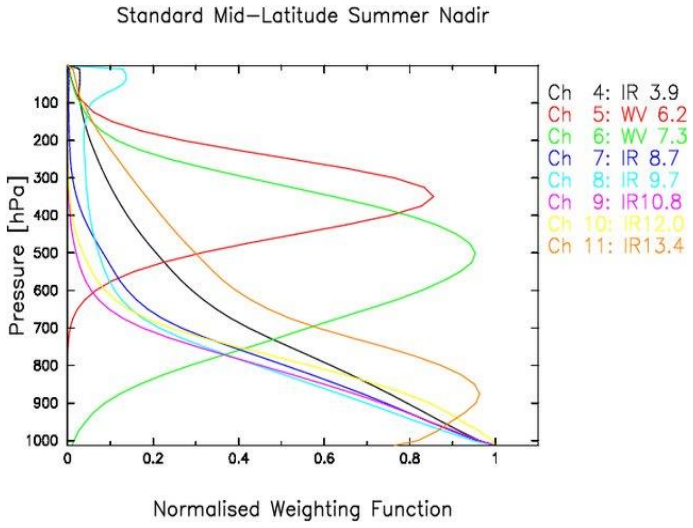

Figure 1: Normalised Weighting Function of SEVIRI Infrared channels. Source EUMETSAT.

The Figure 1 shows the normalised Weighting Function for the Infrared channels for SEVIRI. According that, Channels IR3.9 and IR9.7 are not suitable for data assimilation purposes, IR3.9 has a contribution of solar radiation during the day time and IR 9.7 gives information of stratospheric ozone. Channels IR8.7, IR10.8, IR12.0 are low–peak channels and have a strong influence of surface, so even in some meteorological services are assimilated them over sea (Montmerle et al, 2007 and Kelly 2008) we decided not using for the time being. The WV channels give information about humidity at high and mid-levels and the sensitivity of surface is minimum, so they are the most valuable channels for us. Also IR13.4 even it has a strong relation with surface, the maximum value of the normalised weighting function is over 850 hPa so we decided to take it into account.

The radiances assimilated must be over clear sky. The method employed to discriminate cloudy pixels from non-cloudy pixels use the Nowcasting SAF (NWCSAF) products Cloud Type (CT) and Cloud Top Temperature and Height (CTTH).

The SEVIRI pre-processing software reduces the resolution of the files, only takes one pixel out of 5, changes the format of the original files from NetCDF to GRIB and generates a single file ready to be read by HARMONIE-AROME. This single file includes the brightness temperature for all infrared channel, CT and CTTH products from NWCSAF.

The observations used in this study are taken in the SEVIRI instrument on board of Meteosat-11 (MSG-4), located on the longitude 0º over the Ecuador.

Bias correction of SEVIRI radiances

Background departures for radiance observations present biases that can be due to systematic errors in the satellite instrument itself, deficiencies in the radiative transfer model, or bias in the first guess. In HARMONIE-AROME, bias correction for radiances is carried out using the Variational Bias Correction scheme (VarBC), which is a particular adaptive scheme that is embedded inside the assimilation system. Bias is estimated by means of a multivariate linear regression implemented into the assimilation cycle (Auligné et al., 2007). While the number of bias predictors is fixed, the bias coefficients are updated in each assimilation cycle. In the reference system, a set of 5 predictors (p0, p1, p2, p3 and p4) are used for SEVIRI WV channels, where p0 = 1 to allow a constant component for the bias, p1 and p2 depend on the atmospheric state at the observed location (that is 1000-300 hPa and 200-50 hPa thickness), p3 is the skin temperature, and p4 is the total column water at the observed location.

The convergence of the bias coefficients to a certain timescale is set by means of the stiffness parameter (NBG_MSG_HR in this case), which depends on the number of assimilated observations and the cycling strategy. In the reference system NBG_MSG_HR is set to 5000, but in our initial tests, as the mean number of assimilated observations is large, NBG_MSG_HR was reduced to 2000. For radiances, the cycling strategy is set to 24 hours.

The VarBC method itself cannot distinguish the origin of the bias, and so, it can convert any model error into an observational bias. As the analysis process uses redundant information given by other observing systems to decide what is the most probable error source, the use of not biased observations like TEMP and AMDAR reports (called ‘anchoring data’) acts as a constraint on the assessment of the control variable and, in particular, of the VarBC bias predictors. In those cycles where there are not anchoring observations (or only a few), bias correction can be affected by the presence of model errors. Moreover, taking into account that some bias predictors are related to the model temperature and that this variable is biased (especially at low levels), the use of 5 bias predictors can be questioned. For this reason, the reference set of 5 bias predictors was compared with the simplest approach consisting in only 1 bias predictor (a constant bias-offset).

Experimental design

To evaluate the impact of SEVIRI radiances in the AEMET HARMONIE-AROME limited-area NWP system a set of parallel data assimilation and forecast experiments were designed. The aim was both to find the best set of predictors in VarBC when only the two WV channels were assimilated and to study the impact of assimilating together the two water vapour channels and the IR13.4 channel. Different experiments were run for AIB and AIC domains. In all suites, SEVIRI observations were only assimilated over the sea. In the first tests, radiances over land were also assimilated for WV channels, but despite the major contribution of these channels comes from mid and upper troposphere, the bias correction was negatively affected and the impact on the forecast was clearly detrimental. For this reason, we decided in both areas to use only radiances over sea.

- Testing the set of predictors for VarBC

The following experiments were run:

CONTROL: Data assimilation settings as the reference system and observation usage as described previously. The SEVIRI WV channels were passively assimilated.

SEV_WV_5p: Like in CONTROL. In addition to the observations assimilated in CONTROL, radiances of SEVIRI WV-channels were also actively assimilated. As in the reference system, a set of 5 predictors were used. This experiment started with initial state and VarBC predictor coefficients from CONTROL.

SEV_WV_1p: Like in CONTROL. In addition to the observations assimilated in CONTROL, radiances of SEVIRI WV-channels were also actively assimilated. Only one VarBC predictor used (predictor 0, i.e. constant). This experiment started from cold-start with passive assimilation during a month. Later, WV channels were assimilated in active mode.

The set of parallel experiments was performed for a summer period, during a month. To allow for minor adjustments to the VarBC between newly introduced and existing assimilated radiances in SEV_WV_1p and SEV_WV_ 5p, the first nine days were excluded from the verification. During the study period forecasts up to a range of 24 h were launched four times a day, at 0000, 0600, 1200 and 1800 UTC.

- Active assimilation of IR13.4 channel

The following experiments were run:

CONTROL: Data assimilation settings as the reference system and observation usage as described previously.

SEV_WV_1p: As described previously.

SEV_WV_IR_1p: Like in SEV_WV_1p. In addition to the channels assimilated in SEV_WV_1p, radiances of SEVIRI IR13.4 channel was also actively assimilated. This experiment started with both initial state and VarBC predictor coefficient from SEV_WV_1p.

This set of parallel experiments was run for the same summer period as the previous one. Additionally, a second period was also evaluated, only for CONTROL and SEV_WV_IR_1p. This second period was a wet period, which extended along one month. For this experiment, VarBC predictor coefficients

were extracted from CONTROL. To adjust the VarBC predictor coefficients to the new period, all SEVIRI channels were assimilated as passive during the previous fifteen days. Then, WV6.2, WV7.3 and IR13.4 channels were actively assimilated. Again, to allow for minor adjustments the first nine days were excluded from the verification. During this period, forecasts up to a range of 24 h were launched four times a day, at 0000, 0600, 1200 and 1800 UTC.

3 Analysis performance

When SEVIRI radiances are actively assimilated, the fit of the model first guess to observations can change compared to when they are not assimilated (or they are passively assimilated). To analyse this effect, the bias and the standard deviation of brightness temperature observation minus first guess (ob-fg) values are calculated for: SEVIRI radiances, microwave radiances (AMSU-A and MHS), and infrared radiances from IASI, for different experiment runs over AIB domain.

The active assimilation of observations of SEVIRI channels seems to reduce the standard deviation of first guess departures for these channels compared with CONTROL, where observations of these channels are assimilated as passive. Table 2 shows that standard deviation of brightness temperature innovations is smaller when channels WV6.2 and WV7.3 are actively assimilated (SEV_WV_1p and SEV_WV_5p). However if IR13.4 channel is also assimilated as active (SEV_WV_IR_1p), standard deviation is practically the same as in the other experiments. In all channels and experiments the bias is close to zero, indicating in all cases the good performance of the variational bias correction.

Table 2: Bias and standard deviation (sd) of ob-fg for different SEVIRI channels for AIB and summer period. Analysis time: 00 UTC.

Channel	WV6.2		WV7.3		IR13.4	
Experiment	Bias	Sd	bias	sd	bias	sd
CONTROL	-0.05	1.15	-0.04	1.07	-0.02	0.54
SEV_WV_1p	-0.01	0.99	-0.01	0.94	-0.09	0.53
SEV_WV_5p	-0.02	0.99	0.0	0.95	-0.02	0.53
SEV_WV_IR_1p	-0.02	0.99	-0.01	0.93	-0.01	0.52

For AMSU-A radiances, bias and standard deviation of ob-fg values are almost the same for experiments which assimilate SEVIRI observations and CONTROL (not shown). This indicates that the assimilation of SEVIRI observations has no impact on background departures for AMSU-A radiances.

Table 3: Bias and standard deviation (sd) of ob-fg for different MHS channels for AIB and summer period. Analysis time: 21 UTC.

Channel	3		4		5	
Experiment	bias	sd	bias	sd	bias	sd
CONTROL	-0.44	2.10	-0.37	1.92	-0.22	1.47
SEV_WV_1p	-0.38	1.92	-0.32	1.78	-0.19	1.34
SEV_WV_5p	-0.37	1.91	-0.313	1.77	-0.19	1.34
SEV_WV_IR_1p	-0.38	1.94	-0.32	1.78	-0.19	1.33

In Table 3, the bias and standard deviation of ob-fg of three MHS channels for different experiments in summer period at 21 UTC are displayed. Negative bias and standard deviation for all three MHS channels are reduced in SEV_WV_1p, SEV_WV_5p and SEV_WV_IR_1p compared to CONTROL.

However, negligible differences are observed in bias and standard deviation between experiments SEV_WV_1p, SEV_WV_5p and SEV_WV_IR_1p.

Observation and first guess departures are also calculated for the assimilated IASI radiances. For IR-CO2 channels results are similar to those obtained for AMSU-A, i.e. the impact of assimilating SEVIRI observations is not significant (not shown). However, some differences are obtained for IR-H_2O channels (Figure 2). In this case, bias and standard deviation of ob-fg from different experiments present a positive impact for all channels when SEVIRI radiances are assimilated, the bias and standard deviation of first guess departures are reduced. In particular, for channels ranging from 6.6 to 7.6 microns (close to WV6.2 and WV7.3), the assimilation of SEVIRI radiances allow for an un-biased first-guess departures. Like MHS, no differences are obtained between SEV_WV_1p and SEV_WV_IR_1p, reflecting the small impact of SEVIRI IR13.4 channel. Besides, negligible differences are found between variational bias correction performed with 1 or with 5 predictors (not shown).

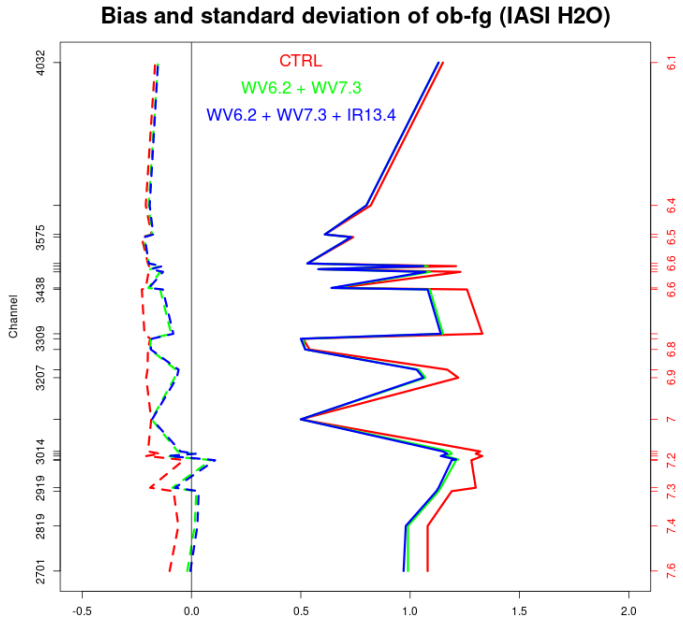

Figure 2: Vertical profile of bias (discontinued lies) and standard deviation (solid lines) of ob-fg for IASI-H_20 channels and different experiments. Analysis at 21 UTC for AIB and summer period.

DFS

The impact of observations on the analysis system can be evaluated using the degrees of freedom for signal (DFS) diagnostic. DFS is the derivative of the analysis increments in observation space with respect to the observations used in the analysis system. However, it is important to recall that DFS does not measure whether this impact is positive or negative.

Here we compare the DFS values for the experiment SEV_WV_IR_1p against CONTROL for a subset of three separated days in the wet period in AIB. All eight assimilation cycles within the three selected days are included in calculations.

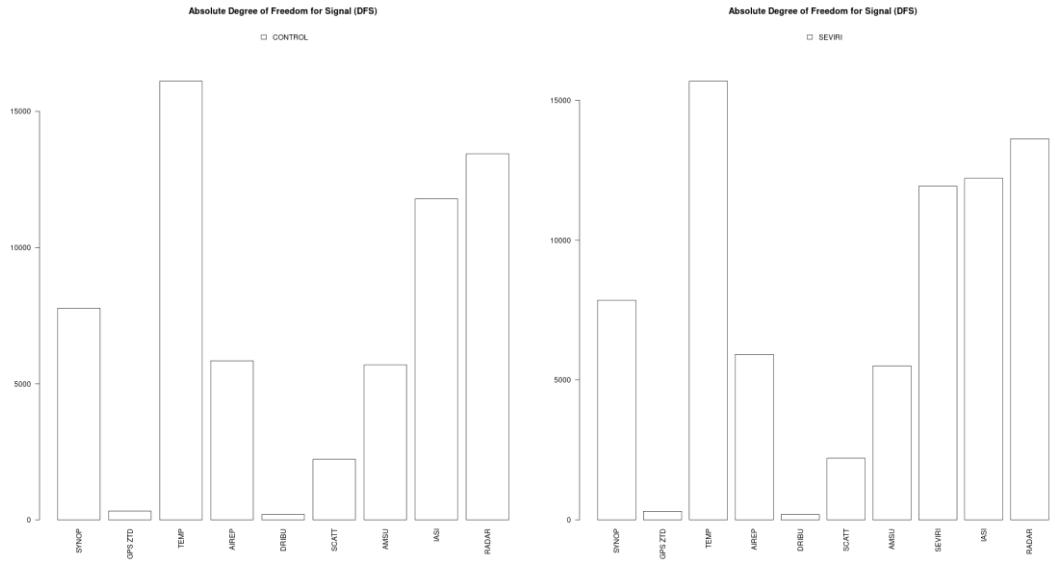

Figure 3: Absolute DFS for the experiments CONTROL (left) and SEV_WV_IR*_1p (right) subdivided for various observation types. Data for a set of cycles in the wet period in AIB.*

In Figure 3, we present the absolute DFS subdivided into various observation types for CONTROL (left panel) and for experiment SEV_WV_IR_1p (right panel). Results show very similar values for all the observation types, except for SEVIRI type in experiment SEV_WV_IR_1p. Graphics show that TEMP observations exhibit the highest impact on the analyses, but radar reflectivity and IASI radiances also influence on the analyses. For SEV_WV_IR_1p, DFS value for SEVIRI is comparable to IASI, but as the number of assimilated observations is smaller for SEVIRI than for IASI, the relative impact of SEVIRI data is larger than IASI ones (not shown). Absolute DFS value for SEVIRI data includes the contribution of WV6.2, WV7.3, and IR13.4 channels. A separated absolute DFS analysis (not shown) demonstrates that for SEVIRI type, almost all the contribution come from the WV6.2 and WV7.3 (96.7 %), and IR13.4 slightly contributes to the impact (3.3 %).

4 Observation impact on the forecasts

The impact of the SEVIRI assimilation has been assessed through the forecast objective verification of all the experiments against SYNOP and TEMP observations during two test periods and for both domains. All the experiments which assimilated SEVIRI radiances were compared with CONTROL in their corresponding study periods.

Overall, in all the experiments which assimilated SEVIRI radiances a slight positive impact was obtained. There are not noticeable differences between the scores obtained for AIB and AIC, neither between the summer and wet study periods. In more detail, for upper-level parameters, for AIB and AIC and in both study periods, the forecast impact was neutral for almost parameters and levels, except for mid-level relative humidity and wind speed where it was slightly positive (Figure 4 and Figure 5).

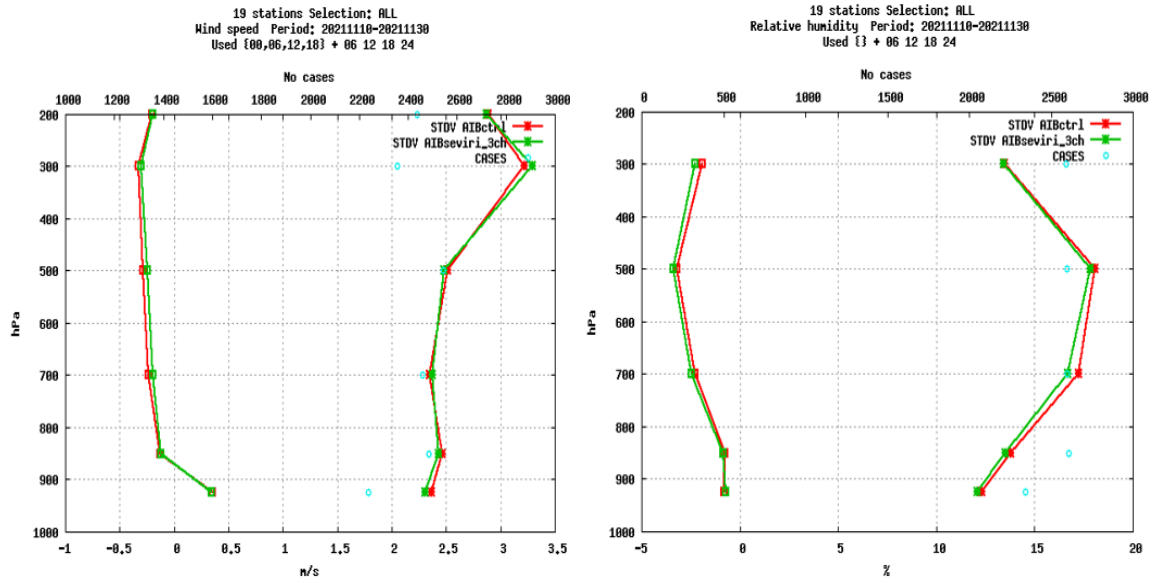

Figure 4: Bias and standard deviation of vertical profile of wind speed (left panel), and relative humidity (right panel) forecast for CONTROL (red) and SEV_WV_IR_1p (green). Scores for the AIB domain and for the wet period.

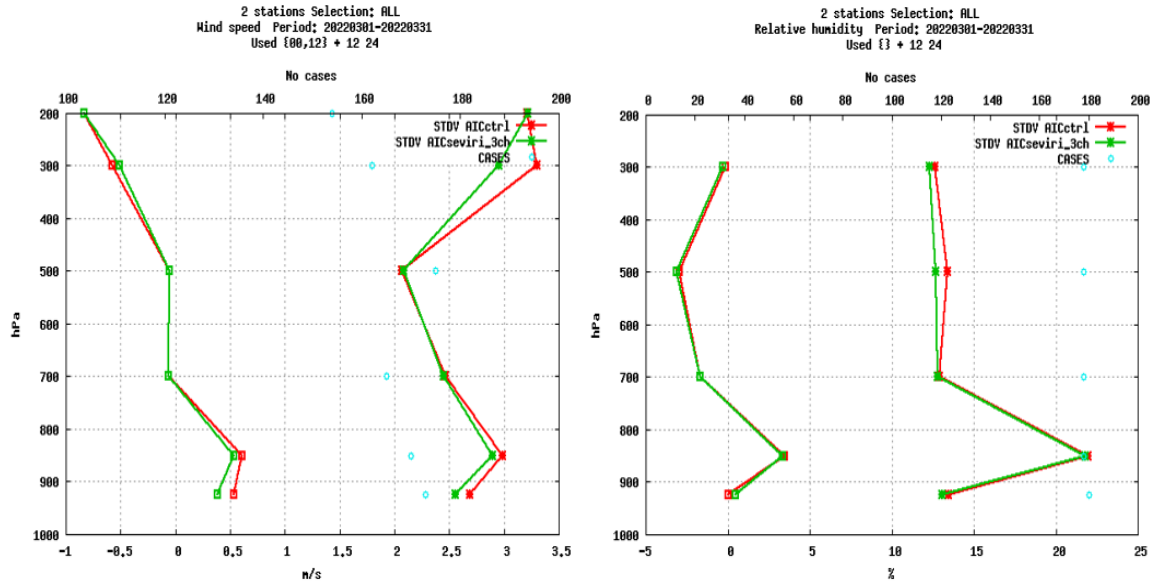

Figure 5: Bias and standard deviation of vertical profile of wind speed (left panel), and relative humidity (right panel) forecast for CONTROL (red) and SEV_WV_IR_1p (green). Scores for the AIC domain and for the wet period.

The overall impact for surface parameters was also neutral for AIB and AIC, except in AIC for the wet period, when a small reduction of the bias for mslp can be observed (not shown). For precipitation, no impact was noticed in low and moderate amounts and not conclusive results were found for larger amounts of accumulated precipitation.

5 Summary

We shortly presented the performance of assimilating a few SEVIRI channels into the AEMET HARMONIE-AROME system. First, the handling of clear-sky SEVIRI radiances was described. Radiances were pre-processed in order to reduce the size and change the format of the files using the NWCSAF products to discriminate between clear-sky and cloudy pixels. Later, the control and different parallel experiments were presented. An important issue was the set-up of the bias correction so that two particular configurations were compared: one using five VarBC predictors (the default) and the other one using only one predictor (the constant one). Besides, the approach of assimilating only the two water vapour SEVIRI channels (WV6.2 and WV7.3) or adding a third channel (IR13.4) was also evaluated. This set of parallel runs were done over the two domains used in the actual AEMET set-up.

The impact of assimilating clear-sky SEVIRI radiances was positive on the analyses and the forecasts in any all those experiments that assimilated SEVIRI radiances (compared to CONTROL). Thus, first-guess departures were reduced for other assimilated observations as for MHS channels and those IASI humidity channels. The impact on the forecast was neutral for surface and upper level parameters, except a slight positive impact on mid-level relative humidity and wind speed. Although the impact is small, it shows to be consistent for the two geographical domains over the two study periods.

When comparing the impact on the analyses and forecast of all the parallel experiments assimilating SEVIRI data, very small differences can be underlined. So, any of them could be a valid option to include in the next operational suite. However, as bias correction is an essential task in the assimilation, the simplest choice, that is one predictor (the constant offset), seems to be preferable. On whether it is better to assimilate not only the WV channels but also the IR13.4 one, again the conservative choice seems the best option. The inclusion of IR13.4 has no impact on the analyses and the forecasts, but this channel has an important contribution from the surface and low troposphere, which may not be accurately enough described by the forecast model. For these reasons, the set-up used for SEVIRI_WV_1p, based on a single VarBC predictor for SEVIRI radiances and that only assimilates data from WV6.2 and WV7.3 channels, is actually running in pre-operational mode.

6 Acknowledgements

The authors wish to acknowledge Javier Calvo, who participated in fruitful discussions and carried out the forecast objective verification of the parallel experiments against SYNOP and TEMP observations and Gema Morales for maintaining the obsmon tool in AEMET. We would like also to acknowledge the AEMET NWCSAF team for their support in this work.

7 References

Auligné, T., McNally, A. P. and Dee, D. P. 2007. Adaptive bias correction for satellite data in a numerical weather prediction system. Q. J. R. Meteorol. Soc. 133, 631–642. https://doi:10.1002/qj.56.

Burrows, C. 2020. Assimilation of radiance observations from geostationary satellites: third year report. Research report No. 52, EUMETSAT/ECMWF Fellowship programme, ECMWF, Reading, UK.

Gustafsson, N, Janjić, T, Schraff, C, et al. 2018. Survey of data assimilation methods for convective-scale numerical weather prediction at operational centres. Q. J. R. Meteorol. Soc. 144: 1218– 1256. https://doi.org/10.1002/qj.3179.

Kelly G. 2008. Preparations and experiments to assimilate satellite image data into high resolution NWP. Met Office. Technical Report No. 522.

Köpken C, Thépaut J-N, Kelly G. 2003. Assimilation of geostationary WV radiances from GOES and Meteosat at ECMWF. Research report No. 14, EUMETSAT/ECMWF Fellowship programme. ECMWF, Reading, UK.

Montmerle, T., Rabier, F. and Fischer, C. 2007. Relative impact of polar-orbiting and geostationary satellite radiances in the Aladin/France numerical weather prediction system. Q. J. R. Meteorol. Soc., 133: 655-671. https://doi.org/10.1002/qj.34.

Szyndel M, Kelly G, Thépaut J-N. 2004. Evaluation and potential for assimilation of SEVIRI radiance data from Meteosat-8. Research report No. 15, EUMETSAT/ECMWF Fellowship programme, ECMWF, Reading, UK.

Coupling LIMA-Aerosol-CAMS

Mohamed Mokhtari, Yann Seity, Abdenour Ambar

1 Introduction

The impact of aerosols on climate and the mechanism of its interactions have been widely discussed. In microphysics, aerosols could act as cloud condensation nuclei (CCN) and/or as ice freezing nuclei (IFN). LIMA (Liquid Ice Multiple Aerosols) is a two moment microphysical scheme, with several aerosols modes of cloud condensation nuclei and ice freezing nuclei that are considered individually (B. Vié et al.,2016).

The LIMA scheme is inserted into the Meso-NH model to improve the complex aerosol–cloud interactions modeling. This scheme has been implemented in AROME model since cy42t1 cycle (Viktória Homonnai, 2016). The flexibility of this scheme is illustrated by two 2-D experiments. The first highlights the sensitivity of orographic ice clouds to IFN types and IFN concentrations; the second case deals with the impacts of pure CCN and IFN pollutant plumes at the scale of the microstructure of a mixed phase squall line cloud.

In 2019, during his scientific stay at Météo France, A.Ambar has managed to achieve the offline coupling of LIMA scheme with desert dust in AROME (A.Ambar, 2019). But problems were encountered for online coupling of LIMA and desert dust schemes. He had pointed out the problem of confusion in GFL's array related to LIMA and dust variables especially in aro_turb_mnh.F90 routine.

Solving this problem was one of the objectives of my scientific stay at Météo France in June 2022. Indeed, during this stay, we managed to solve these problems related to the code. Then, we carried out two simulations:

- The first simulation is an interactive online coupling of LIMA with dust schemes. Here, the IFNs LIMA variables are provided by the coarse and medium modes of desert dust, calculated by dust scheme at each time step.

- In the second simulation, all related LIMA variables (IFN and CCN) are provided by CAMS aerosol fields every three hours.

In this article, the results of these two simulations will be compared to ICE3 scheme simulations (reference). We will mainly focus to show the hydrometeors and aerosols number concentration fields.

2 Methodology

LIMA is a two-moment scheme, its prognostic variables are mixing ratio of hydrometeors (r_C, r_R, r_I, r_S, r_G), number concentration of aerosols (N Free , N Activated) and hydrometeors (N_C, N_R, N_I) (Table 1).

LIMA predicts the number concentration of free and activated aerosols. For initialization, we already have the number concentrations of the free aerosols CCN (1,2,3) and IFN (1,2) pre-calculated from the CAMS fields for every three hours. So, our objective in this work consists to replace the two IFN modes of CAMS by the coarse and medium modes of dust aerosols calculated by the dust scheme every time step as shown in figure 1.

The size and mass distributions, geometric standard deviation, number median diameter and fraction of each mode of dust aerosols in AROME_DUST are given by table 2 according to the AMMA parameterization (Mokhtari et al., 2012). The three modes are ordered in order of importance. In our case, the default order (3, 2, 1) relative to (coarse, medium, fine) is used.

Various changes have been made in the code, especially in apl_arome.F90 routine, in order to achieve this coupling. These modifications will be detailed and documented in another separate article.

Table 1: LIMA prognostic variables, which has to be initialized

	Name of variables (number concentrations)	Short name	Initialized values
1	Cloud droplets	N_CLOUD	calculated from mixing ratio
2	Rain drops	N_RAIN	calculated from mixing ratio
3	CCN free 1	N_CCN_F1	SEA.SALT1..3
4	CCN free 2	N_CCN_F2	SULFAT+NITRAT+AMMONI
5	CCN free 3	N_CCN_F3	ORG.MAT1 + BLACK.CAR1
6	CCN activated 1	N_CCN_A1	0
7	CCN activated 2	N_CCN_A2	0
8	CCN activated 3	N_CCN_A3	0
9	Pristine ice crystals	N_ICE	calculated from mixing ratio
10	IFN free 1	N_IFN_F1	DES.DUST1..3
11	IFN free 2	N_IFN_F2	ORG.MAT2 + BLACK.CAR2
12	IFN activated 1	N_IFN_A1	0
13	IFN activated 2	N_IFN_A1	0
14	Haze homogeneous freezing	N_HHONI	0

Table 2: Dust size distribution parameters (AMMA) used in AROME-DUST (Mokhtari et al., 2012).

Dust mode	**Mode 1**	**Mode 2**	**Mode 3**
Number fraction (%)	97.52	1.95	0.52
Mass fraction (%)	0.08	0.92	99
Geometric standard deviation	1.75	1.76	1.70
Number median diameter (μm)	0.078	0.64	5.0
Mass median diameter (μm)	0.20	1.67	11.6

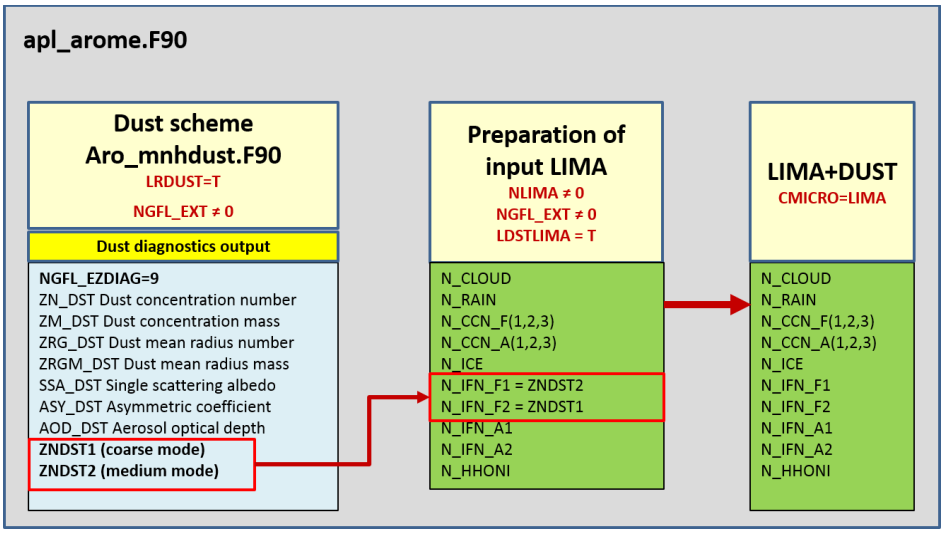

Figure 1: Simultaneous interactive activation diagram of dust aerosols and LIMA schemes in AROME. ZNDST1 and ZNDST2 are number concentration of coarse and medium modes of dust, respectively.

3 Simulations and namelists arrangement

In order to verify that our code modifications are working correctly, we carried out eight (8) simulations with several coupling options between LIMA and DUST schemes. We choose the situation of March 12th, 2021, occurred in the Algerian Sahara. We already have a CAMS coupling set with a three-hourly frequency containing the five (5) free aerosol fields of LIMA. The options tested are summarized in Table 3.

Table 3 : Summary of the tested options and the results of the proper functioning tests of code.

	LDSTLIMA	NMOD-IFN	NMOD-CCN	NLIMA	NGFL_EXT	NCOUPLING	NREQIN	RESULT
EXP1	TRUE	2	3	14	9	0	0	OK
EXP2	TRUE	2	3	14	9	1	1	OK
EXP3	TRUE	2	3	14	9	0	1	OK
EXP4	TRUE	1	3	12	9	0	1	OK
EXP5	FALSE	2	3	14	9	1	1	OK
EXP6	FALSE	2	3	14	0	1	1	OK
EXP7	FALSE	0	0	0	9	0	0	OK
EXP8	FALSE	1	1	8	9	1	1	OK
ICE3	FALSE	-----	------	0	9	-----	-----	OK

In the following, we will present the arrangements made to the main blocks of namelists allowing the simultaneous interactive activation of LIMA and dust schemes for EXP3 case.

&NAMARPHY	&NAMPARAR	&NEMELBC0B	&NAMRIP
LMPA=.TRUE., LMICRO=.TRUE., LTURB=.TRUE., LMSE=.TRUE., LKFBCONV=.FALSE., LKFBD=.FALSE., LKFBS=.FALSE., LMFSHAL=.TRUE., **LRDEPOS=.TRUE.,** **LRDUST=.TRUE.,** **LDSTLIMA=.TRUE.,**	**CMICRO='LIMA',** LOSUBG_COND=.FALSE., LOSIGMAS=.FALSE., LOSEDIC=.TRUE., CMF_CLOUD='DIRE', CSEDIM='SPLI',	NEK0=20, NEK1=30, NEFRSPCPL=1, NEN1=4, NEN2=8, SPNUDVOR=0.01, SPNUDDIV=0.01, SPNUDT=0.01, SPNUDQ=0., !TEFRCL=3600., **TEFRCL=10800.,**	CSTOP='h24', TSTEP=60.,

&NAMAFN	&NAMFPC	&NAMLIMA
…….. TFP_LIMA(1)%CLNAME='N_CLOUD', TFP_LIMA(1)%IBITS=16, TFP_LIMA(2)%CLNAME='N_RAIN', TFP_LIMA(2)%IBITS=16, TFP_LIMA(3)%CLNAME='N_CCN_F1', TFP_LIMA(3)%IBITS=16, TFP_LIMA(4)%CLNAME='N_CCN_F2', TFP_LIMA(4)%IBITS=16, TFP_LIMA(5)%CLNAME='N_CCN_F3', TFP_LIMA(5)%IBITS=16, TFP_LIMA(6)%CLNAME='N_CCN_A1', TFP_LIMA(6)%IBITS=16, TFP_LIMA(7)%CLNAME='N_CCN_A2', TFP_LIMA(7)%IBITS=16, TFP_LIMA(8)%CLNAME='N_CCN_A3', TFP_LIMA(8)%IBITS=16, TFP_LIMA(9)%CLNAME='N_ICE', TFP_LIMA(9)%IBITS=16, TFP_LIMA(10)%CLNAME='N_IFN_F1', TFP_LIMA(10)%IBITS=16, TFP_LIMA(11)%CLNAME='N_IFN_F2', TFP_LIMA(11)%IBITS=16, TFP_LIMA(12)%CLNAME='N_IFN_A1', TFP_LIMA(12)%IBITS=16, TFP_LIMA(13)%CLNAME='N_IFN_A2', TFP_LIMA(13)%IBITS=16, TFP_LIMA(14)%CLNAME='N_HHONI', TFP_LIMA(14)%IBITS=16, TFP_EZDIAG(1)%IBITS=16, TFP_EZDIAG(2)%IBITS=16, TFP_EZDIAG(3)%IBITS=16, TFP_EZDIAG(4)%IBITS=16, TFP_EZDIAG(5)%IBITS=16,	**……..** CFP3DF(13)='N_CLOUD', CFP3DF(14)='N_RAIN', CFP3DF(15)='N_CCN_F1', CFP3DF(16)='N_CCN_F2', CFP3DF(17)='N_CCN_F3', CFP3DF(18)='N_CCN_A1', CFP3DF(19)='N_CCN_A2', CFP3DF(20)='N_CCN_A3', CFP3DF(21)='N_ICE', CFP3DF(22)='N_IFN_F1', CFP3DF(23)='N_IFN_F2', CFP3DF(24)='N_IFN_A1', CFP3DF(25)='N_IFN_A2', CFP3DF(26)='N_HHONI', CFP3DF(27)='AOD_DST', CFP3DF(28)='ZN_DST', CFP3DF(29)='ZM_DST', CFP3DF(30)='ZN1_DST', CFP3DF(31)='ZN2_DST',	LWARM_LIMA = T, LACTI_LIMA = T, HINI_CCN='AER', HTYPE_CCN(1)='M', HTYPE_CCN(2)='M', HTYPE_CCN(3)='M', **NMOD_CCN = 3,** XALPHAR = 1., XNUR = 1., LACTIT_LIMA=T, LRAIN_LIMA=T, LSEDC_LIMA=T, LSCAV=F, LAERO_MASS=F, LCCN_HOM=F, CCCN_MODES='COPT', XCCN_CONC(1)=300., XCCN_CONC(2)=140., XCCN_CONC(3)=50., XCCN_CONC(4)=0.01, LCOLD_LIMA = T, LNUCL_LIMA = T, LSEDI_LIMA=F, LHHONI_LIMA=T, LSNOW_LIMA=T, LHAIL_LIMA=F, **NMOD_IFN=2,** NPHILLIPS=8, CPRISTINE_ICE_LIMA = 'PLAT', CHEVRIMED_ICE_LIMA = 'GRAU', NIND_SPECIE = 1, LMEYERS_LIMA=F, NMOD_IMM=0, LIFN_HOM=T, CIFN_SPECIES='', CINT_MIXING='DM1', XIFN_CONC(1)=1000., XIFN_CONC(2)=100.,

&NAMGFL (YEZDIAG_NL arrays)	&NAMGFL (hydro-meteor arrays)	&NAMGFL
NGFL_EZDIAG=12, YEZDIAG_NL(1)%CNAME='EZDIAG01', YEZDIAG_NL(1)%LREQOUT=.FALSE., YEZDIAG_NL(2)%CNAME='EZDIAG02', YEZDIAG_NL(2)%LREQOUT=.FALSE., YEZDIAG_NL(3)%CNAME='EZDIAG03', YEZDIAG_NL(3)%LREQOUT=.FALSE., **YEZDIAG_NL(4)%CNAME='ZN_DST',** **YEZDIAG_NL(5)%CNAME='ZM_DST',** **YEZDIAG_NL(6)%CNAME='ZN_RGDST',** **YEZDIAG_NL(7)%CNAME='ZM_RGDST',** **YEZDIAG_NL(8)%CNAME='SSA_DST',** **YEZDIAG_NL(9)%CNAME='ASY_DST',** **YEZDIAG_NL(10)%CNAME='AOD_DST',** **YEZDIAG_NL(11)%CNAME='ZN1_DST',** **YEZDIAG_NL(12)%CNAME='ZN2_DST',** **YZNDST1=11,** **NZNDST2=12,** **NDSTLIMA_LINK=0**	YQ_NL%LQM=.TRUE., YQ_NL%NREQIN=1, YQ_NL%LSLHD=.FALSE., YQ_NL%LCOMAD=.TRUE., YL_NL%NREQIN=0, YL_NL%NCOUPLING=-1, YL_NL%REFVALC=0., YL_NL%LQM=.TRUE., YL_NL%LSLHD=.FALSE., YL_NL%LCOMAD=.TRUE., YL_NL%LINTLIN=.TRUE., YI_NL%NREQIN=0, YI_NL%NCOUPLING=-1, YI_NL%REFVALC=0., YI_NL%LQM=.TRUE., YI_NL%LSLHD=.FALSE., YI_NL%LCOMAD=.TRUE., YI_NL%LINTLIN=.TRUE., YS_NL%NREQIN=0, YS_NL%NCOUPLING=-1, YS_NL%REFVALC=0., YS_NL%LQM=.TRUE., YS_NL%LSLHD=.FALSE., YS_NL%LCOMAD=.TRUE., YS_NL%LINTLIN=.TRUE.,	YR_NL%NREQIN=0, YR_NL%NCOUPLING=-1, YR_NL%REFVALC=0., YR_NL%LQM=.TRUE., YR_NL%LSLHD=.FALSE., YR_NL%LCOMAD=.TRUE., YR_NL%LINTLIN=.TRUE., YG_NL%NREQIN=0, YG_NL%NCOUPLING=-1, YG_NL%REFVALC=0., YG_NL%LQM=.TRUE., YG_NL%LSLHD=.FALSE., YG_NL%LCOMAD=.TRUE., YG_NL%LINTLIN=.TRUE., YTKE_NL%NREQIN=-1, YTKE_NL%NCOUPLING=0, YIRAD_NL%LGP=.TRUE., YLRAD_NL%LGP=.TRUE.,

&NAMGFL (YEXT_NL arrays)	&NAMGFL	&NAMGFL
NGFL_EXT=9, YEXT_NL(1)%LGP=.TRUE., YEXT_NL(2)%LGP=.TRUE., YEXT_NL(3)%LGP=.TRUE., YEXT_NL(4)%LGP=.TRUE., YEXT_NL(5)%LGP=.TRUE., YEXT_NL(6)%LGP=.TRUE., YEXT_NL(7)%LGP=.TRUE., YEXT_NL(8)%LGP=.TRUE., YEXT_NL(9)%LGP=.TRUE., YEXT_NL(1)%LADV=.TRUE., YEXT_NL(2)%LADV=.TRUE., YEXT_NL(3)%LADV=.TRUE., YEXT_NL(4)%LADV=.TRUE., YEXT_NL(5)%LADV=.TRUE., YEXT_NL(6)%LADV=.TRUE., YEXT_NL(7)%LADV=.TRUE., YEXT_NL(8)%LADV=.TRUE., YEXT_NL(9)%LADV=.TRUE., YEXT_NL(1)%LQM=.TRUE., YEXT_NL(2)%LQM=.TRUE., YEXT_NL(3)%LQM=.TRUE., YEXT_NL(4)%LQM=.TRUE., YEXT_NL(5)%LQM=.TRUE., YEXT_NL(6)%LQM=.TRUE., YEXT_NL(7)%LQM=.TRUE., YEXT_NL(8)%LQM=.TRUE., YEXT_NL(9)%LQM=.TRUE.,	YEXT_NL(1)%LREQOUT=.TRUE., YEXT_NL(2)%LREQOUT=.TRUE., YEXT_NL(3)%LREQOUT=.TRUE., YEXT_NL(4)%LREQOUT=.TRUE., YEXT_NL(5)%LREQOUT=.TRUE., YEXT_NL(6)%LREQOUT=.TRUE., YEXT_NL(7)%LREQOUT=.TRUE., YEXT_NL(8)%LREQOUT=.TRUE., YEXT_NL(9)%LREQOUT=.TRUE., YEXT_NL(1)%LGPINGP= .TRUE., YEXT_NL(2)%LGPINGP= .TRUE., YEXT_NL(3)%LGPINGP= .TRUE., YEXT_NL(4)%LGPINGP= .TRUE., YEXT_NL(5)%LGPINGP= .TRUE., YEXT_NL(6)%LGPINGP= .TRUE., YEXT_NL(7)%LGPINGP= .TRUE., YEXT_NL(8)%LGPINGP= .TRUE., YEXT_NL(9)%LGPINGP= .TRUE., YEXT_NL(1)%LPC= .TRUE., YEXT_NL(2)%LPC= .TRUE., YEXT_NL(3)%LPC= .TRUE., YEXT_NL(4)%LPC= .TRUE., YEXT_NL(5)%LPC= .TRUE., YEXT_NL(6)%LPC= .TRUE., YEXT_NL(7)%LPC= .TRUE., YEXT_NL(8)%LPC= .TRUE., YEXT_NL(9)%LPC= .TRUE., YEXT_NL(1)%LSLHD=.FALSE., YEXT_NL(2)%LSLHD=.FALSE., YEXT_NL(3)%LSLHD=.FALSE., YEXT_NL(4)%LSLHD=.FALSE., YEXT_NL(5)%LSLHD=.FALSE., YEXT_NL(6)%LSLHD=.FALSE., YEXT_NL(7)%LSLHD=.FALSE., YEXT_NL(8)%LSLHD=.FALSE., YEXT_NL(9)%LSLHD=.FALSE.,	YEXT_NL(1)%LPT= .TRUE., YEXT_NL(2)%LPT= .TRUE., YEXT_NL(3)%LPT= .TRUE., YEXT_NL(4)%LPT= .TRUE., YEXT_NL(5)%LPT= .TRUE., YEXT_NL(6)%LPT= .TRUE., YEXT_NL(7)%LPT= .TRUE., YEXT_NL(8)%LPT= .TRUE., YEXT_NL(9)%LPT= .TRUE., YEXT_NL(1)%NREQIN=1, YEXT_NL(2)%NREQIN=1, YEXT_NL(3)%NREQIN=1, YEXT_NL(4)%NREQIN=1, YEXT_NL(5)%NREQIN=1, YEXT_NL(6)%NREQIN=1, YEXT_NL(7)%NREQIN=1, YEXT_NL(8)%NREQIN=1, YEXT_NL(9)%NREQIN=1, YEXT_NL(1)%LCOMAD=.TRUE., YEXT_NL(2)%LCOMAD=.TRUE., YEXT_NL(3)%LCOMAD=.TRUE., YEXT_NL(4)%LCOMAD=.TRUE., YEXT_NL(5)%LCOMAD=.TRUE., YEXT_NL(6)%LCOMAD=.TRUE., YEXT_NL(7)%LCOMAD=.TRUE., YEXT_NL(8)%LCOMAD=.TRUE., YEXT_NL(9)%LCOMAD=.TRUE., YEXT_NL(1)%LINTLIN=.TRUE., YEXT_NL(2)%LINTLIN=.TRUE., YEXT_NL(3)%LINTLIN=.TRUE., YEXT_NL(4)%LINTLIN=.TRUE., YEXT_NL(5)%LINTLIN=.TRUE., YEXT_NL(6)%LINTLIN=.TRUE., YEXT_NL(7)%LINTLIN=.TRUE., YEXT_NL(8)%LINTLIN=.TRUE., YEXT_NL(9)%LINTLIN=.TRUE.,

&NAMGFL (YLIMA_NL arrays)	&NAMGFL	&NAMGFL
NLIMA=14, YLIMA_NL(1)%CNAME='N_CLOUD', YLIMA_NL(1)%LPT=.TRUE., YLIMA_NL(1)%NREQIN=0, YLIMA_NL(1)%REFVALI=0., YLIMA_NL(1)%NCOUPLING=0, YLIMA_NL(1)%REFVALC=0., YLIMA_NL(1)%LQM=.TRUE., YLIMA_NL(1)%LSLHD=.FALSE., YLIMA_NL(1)%LCOMAD=.TRUE., YLIMA_NL(1)%LINTLIN=.TRUE., YLIMA_NL(2)%CNAME='N_RAIN', YLIMA_NL(2)%LPT=.TRUE., YLIMA_NL(2)%NREQIN=0, YLIMA_NL(2)%REFVALI=0., YLIMA_NL(2)%NCOUPLING=0, YLIMA_NL(2)%REFVALC=0., YLIMA_NL(2)%LQM=.TRUE., YLIMA_NL(2)%LSLHD=.FALSE., YLIMA_NL(2)%LCOMAD=.TRUE., YLIMA_NL(2)%LINTLIN=.TRUE., YLIMA_NL(3)%CNAME='N_CCN_F1', YLIMA_NL(3)%LPT=.TRUE., YLIMA_NL(3)%NREQIN=1, YLIMA_NL(3)%NCOUPLING=1, YLIMA_NL(3)%LQM=.TRUE., YLIMA_NL(3)%LSLHD=.FALSE., YLIMA_NL(3)%LCOMAD=.TRUE., YLIMA_NL(3)%LINTLIN=.TRUE., YLIMA_NL(4)%CNAME='N_CCN_F2', YLIMA_NL(4)%LPT=.TRUE., YLIMA_NL(4)%NREQIN=1, YLIMA_NL(4)%NCOUPLING=1, YLIMA_NL(4)%LQM=.TRUE., YLIMA_NL(4)%LSLHD=.FALSE., YLIMA_NL(4)%LCOMAD=.TRUE., YLIMA_NL(4)%LINTLIN=.TRUE., YLIMA_NL(5)%CNAME='N_CCN_F3', YLIMA_NL(5)%LPT=.TRUE., YLIMA_NL(5)%NREQIN=1, YLIMA_NL(5)%NCOUPLING=1, YLIMA_NL(5)%LQM=.TRUE., YLIMA_NL(5)%LSLHD=.FALSE., YLIMA_NL(5)%LCOMAD=.TRUE., YLIMA_NL(5)%LINTLIN=.TRUE.,	YLIMA_NL(6)%CNAME='N_CCN_A1', YLIMA_NL(6)%LPT=.TRUE., YLIMA_NL(6)%NREQIN=0, YLIMA_NL(6)%REFVALI=0., YLIMA_NL(6)%NCOUPLING=0, YLIMA_NL(6)%REFVALC=0., YLIMA_NL(6)%LQM=.TRUE., YLIMA_NL(6)%LSLHD=.FALSE., YLIMA_NL(6)%LCOMAD=.TRUE., YLIMA_NL(6)%LINTLIN=.TRUE., YLIMA_NL(7)%CNAME='N_CCN_A2', YLIMA_NL(7)%LPT=.TRUE., YLIMA_NL(7)%NREQIN=0, YLIMA_NL(7)%REFVALI=0., YLIMA_NL(7)%NCOUPLING=0, YLIMA_NL(7)%REFVALC=0., YLIMA_NL(7)%LQM=.TRUE., YLIMA_NL(7)%LSLHD=.FALSE., YLIMA_NL(7)%LCOMAD=.TRUE., YLIMA_NL(7)%LINTLIN=.TRUE., YLIMA_NL(8)%CNAME='N_CCN_A3', YLIMA_NL(8)%LPT=.TRUE., YLIMA_NL(8)%NREQIN=0, YLIMA_NL(8)%REFVALI=0., YLIMA_NL(8)%NCOUPLING=0, YLIMA_NL(8)%REFVALC=0., YLIMA_NL(8)%LQM=.TRUE., YLIMA_NL(8)%LCOMAD=.TRUE., YLIMA_NL(8)%LINTLIN=.TRUE., YLIMA_NL(8)%LSLHD=.FALSE., YLIMA_NL(9)%CNAME='N_ICE', YLIMA_NL(9)%LPT=.TRUE., YLIMA_NL(9)%NREQIN=0, YLIMA_NL(9)%REFVALI=0., YLIMA_NL(9)%NCOUPLING=0, YLIMA_NL(9)%REFVALC=0., YLIMA_NL(9)%LQM=.TRUE., YLIMA_NL(9)%LSLHD=.FALSE., YLIMA_NL(9)%LCOMAD=.TRUE., YLIMA_NL(9)%LINTLIN=.TRUE., YLIMA_NL(10)%CNAME='N_IFN_F1', YLIMA_NL(10)%LPT=.TRUE., **YLIMA_NL(10)%NREQIN=1,** **YLIMA_NL(10)%NCOUPLING=0,** YLIMA_NL(10)%LQM=.TRUE., YLIMA_NL(10)%LSLHD=.FALSE., YLIMA_NL(10)%LCOMAD=.TRUE., YLIMA_NL(10)%LINTLIN=.TRUE.,	YLIMA_NL(11)%CNAME='N_IFN_F2', YLIMA_NL(11)%LPT=.TRUE., **YLIMA_NL(11)%NREQIN=1,** **YLIMA_NL(11)%NCOUPLING=0,** YLIMA_NL(11)%LQM=.TRUE., YLIMA_NL(11)%LSLHD=.FALSE., YLIMA_NL(11)%LCOMAD=.TRUE., YLIMA_NL(11)%LINTLIN=.TRUE., YLIMA_NL(12)%CNAME='N_IFN_A1', YLIMA_NL(12)%LPT=.TRUE., YLIMA_NL(12)%NREQIN=0, YLIMA_NL(12)%REFVALI=0., YLIMA_NL(12)%NCOUPLING=0, YLIMA_NL(12)%REFVALC=0., YLIMA_NL(12)%LQM=.TRUE., YLIMA_NL(12)%LSLHD=.FALSE., YLIMA_NL(12)%LCOMAD=.TRUE., YLIMA_NL(12)%LINTLIN=.TRUE., YLIMA_NL(13)%CNAME='N_IFN_A2', YLIMA_NL(13)%LPT=.TRUE., YLIMA_NL(13)%NREQIN=0, YLIMA_NL(13)%REFVALI=0., YLIMA_NL(13)%NCOUPLING=0, YLIMA_NL(13)%REFVALC=0., YLIMA_NL(13)%LQM=.TRUE., YLIMA_NL(13)%LSLHD=.FALSE., YLIMA_NL(13)%LCOMAD=.TRUE., YLIMA_NL(13)%LINTLIN=.TRUE., YLIMA_NL(14)%CNAME='N_HHONI', YLIMA_NL(14)%LPT=.TRUE., YLIMA_NL(14)%NREQIN=0, YLIMA_NL(14)%REFVALI=0., YLIMA_NL(14)%NCOUPLING=0, YLIMA_NL(14)%REFVALC=0., YLIMA_NL(14)%LQM=.TRUE., YLIMA_NL(14)%LSLHD=.FALSE., YLIMA_NL(14)%LCOMAD=.TRUE., YLIMA_NL(14)%LINTLIN=.TRUE.,

4 Results and discussion

We have chosen a convective situation over Algerian Sahara that occurred on March 12th, 2021. It was characterized by severe dust storm and rainfall as shown by satellite image (Fig.02). The precipitations amount and the aerosol optical depth (AOD) values were nicely simulated by AROME over this region (Fig.03).

The hydrometeor fields (cloud water, rain, ice crystal and snow) obtained from two simulations experiments (LIMA_DUST and LIMA_CAMS) will be analyzed in this part. The reference for the comparison will be ICE3 simulations.

Vertical sections are calculated along the parallel 27° north, while the vertical profiles are averaged over the red area as indicated in figure 03.

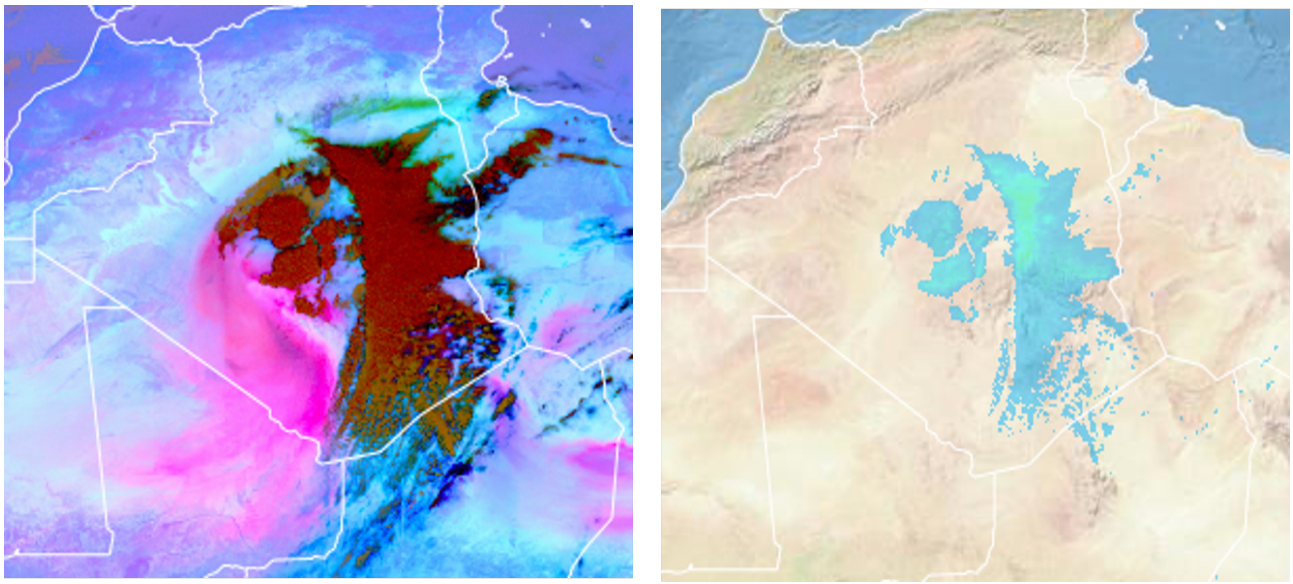

Figure 2 : Satellite image of dust plumes (left) and the instantaneous precipitation rate estimated from satellite images (right), for March 12th, 2021 at 15h UTC.

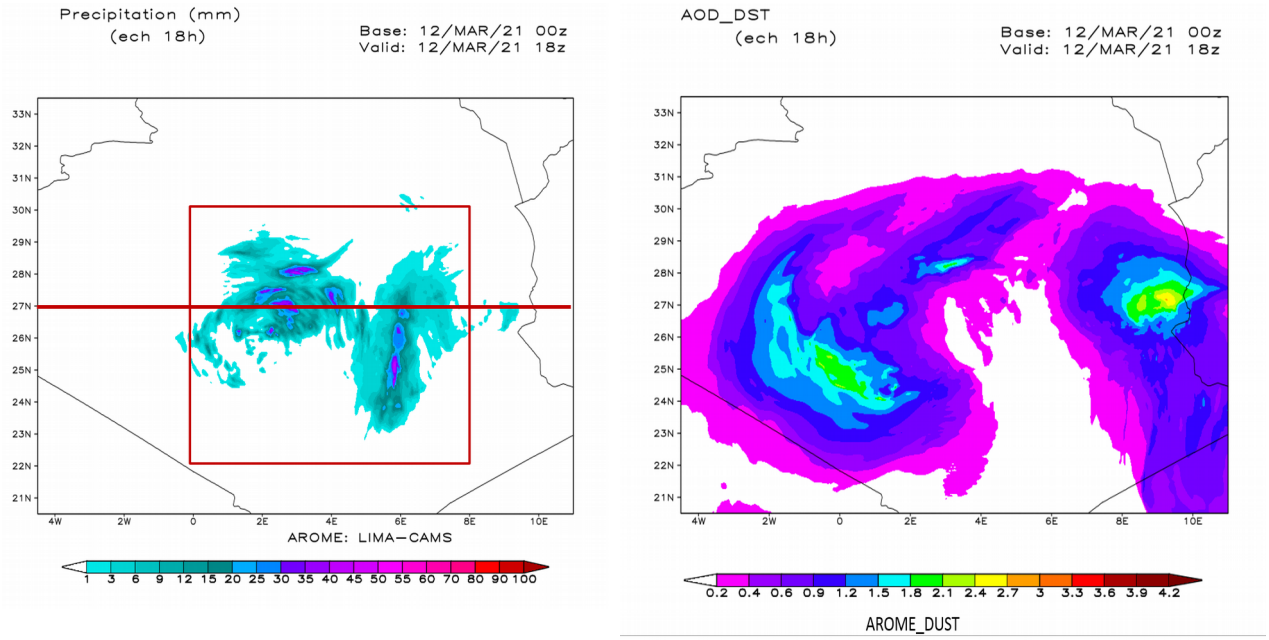

Figure 3: Total precipitations (at left) and Aerosol optical depth (at right) simulated by AROME for March 12th, 2021 at 18h UTC.

a) Hydrometeor fields:

Figure 04 and 05 show the hydrometeor fields simulated by AROME with different configurations: LIMA_Dust, ICE3, LIMA_CAMS.

As indicated previously, ICE3 will be used as reference simulation because it was validated in operational configurations of AROME. Both new configurations, LIMA_Dust and LIMA_CAMS, showed more reasonable values than ICE3 in term of spatial distribution and magnitude order. However, between the two LIMA configurations, it's hard to distinguish the differences between the outputs.

The same remarks are observed for the vertical cross sections, except for the ice crystal field, where we can easily notice that ICE3 predict higher values than LIMA's configurations.

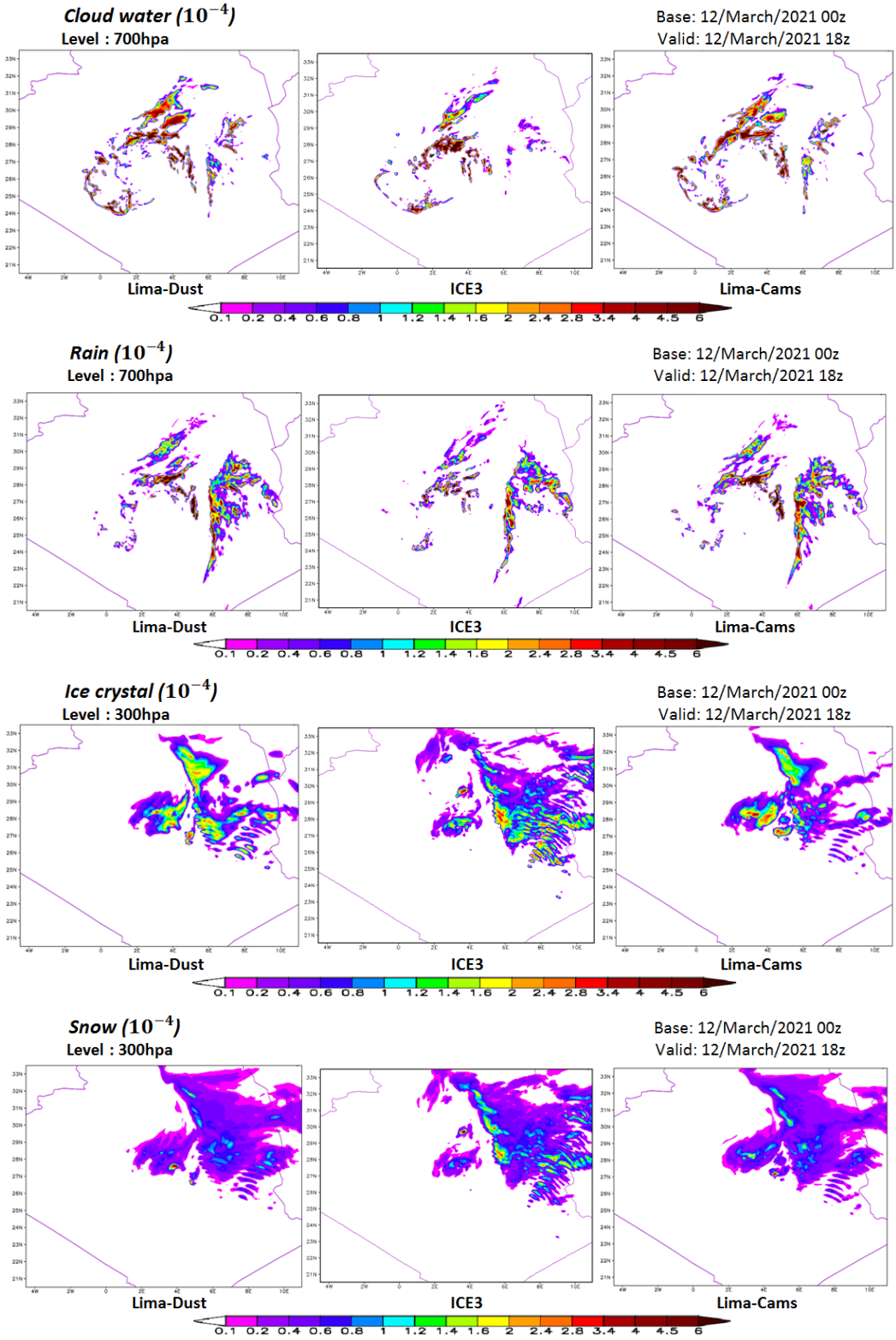

Figure 4: Hydrometeor fields simulated by AROME at 18h UT with: LIMA_Dust (at left), ICE3 (middle) and LIMA_CAMS (right).

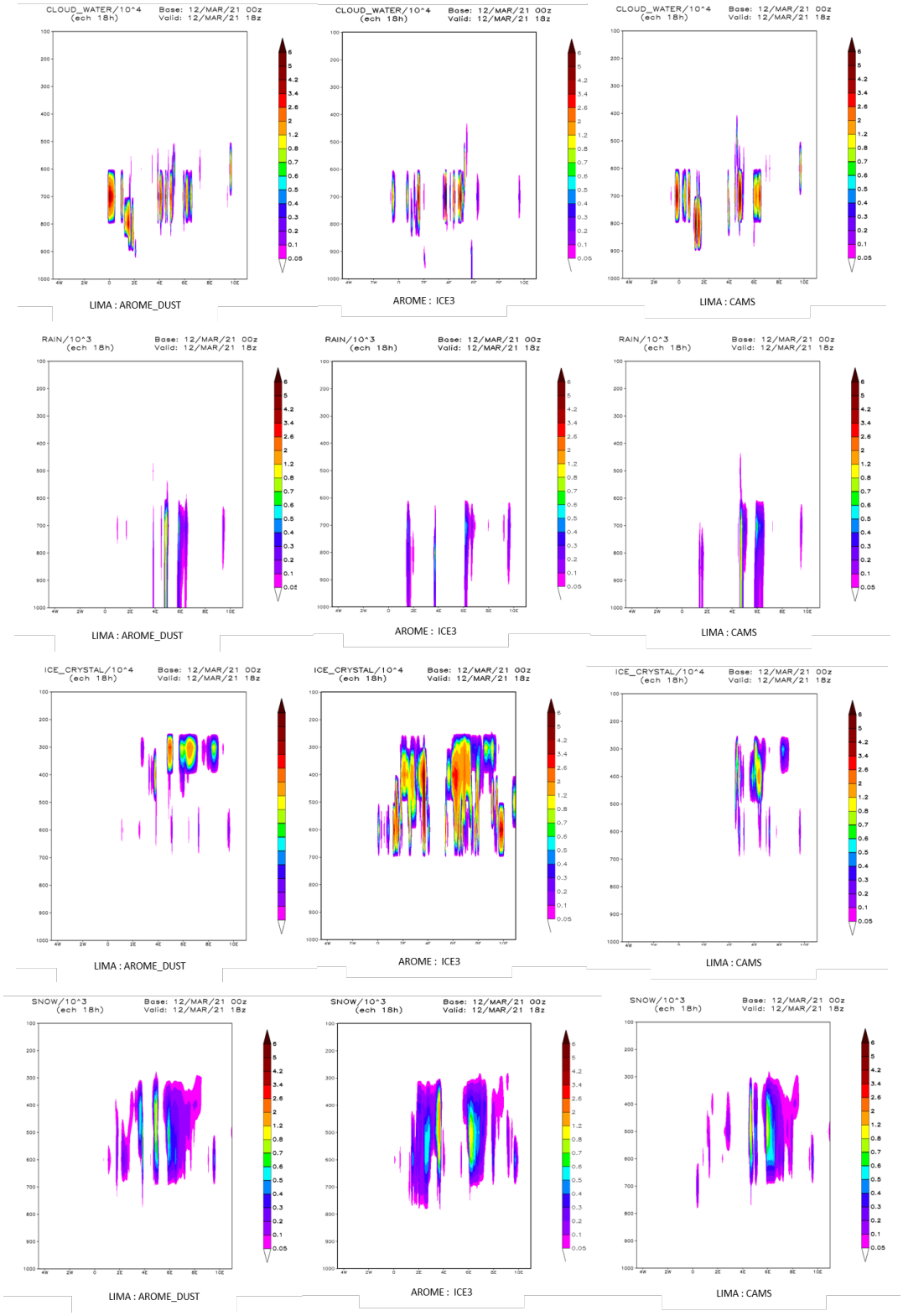

Figure 5: Vertical sections (at 27° north latitude) of hydrometeor fields simulated by AROME at 18h UT with: LIMA_Dust (at left), ICE3 (middle) and LIMA_CAMS (right).

b) LIMA fields (N_CCN, N_IFN) :

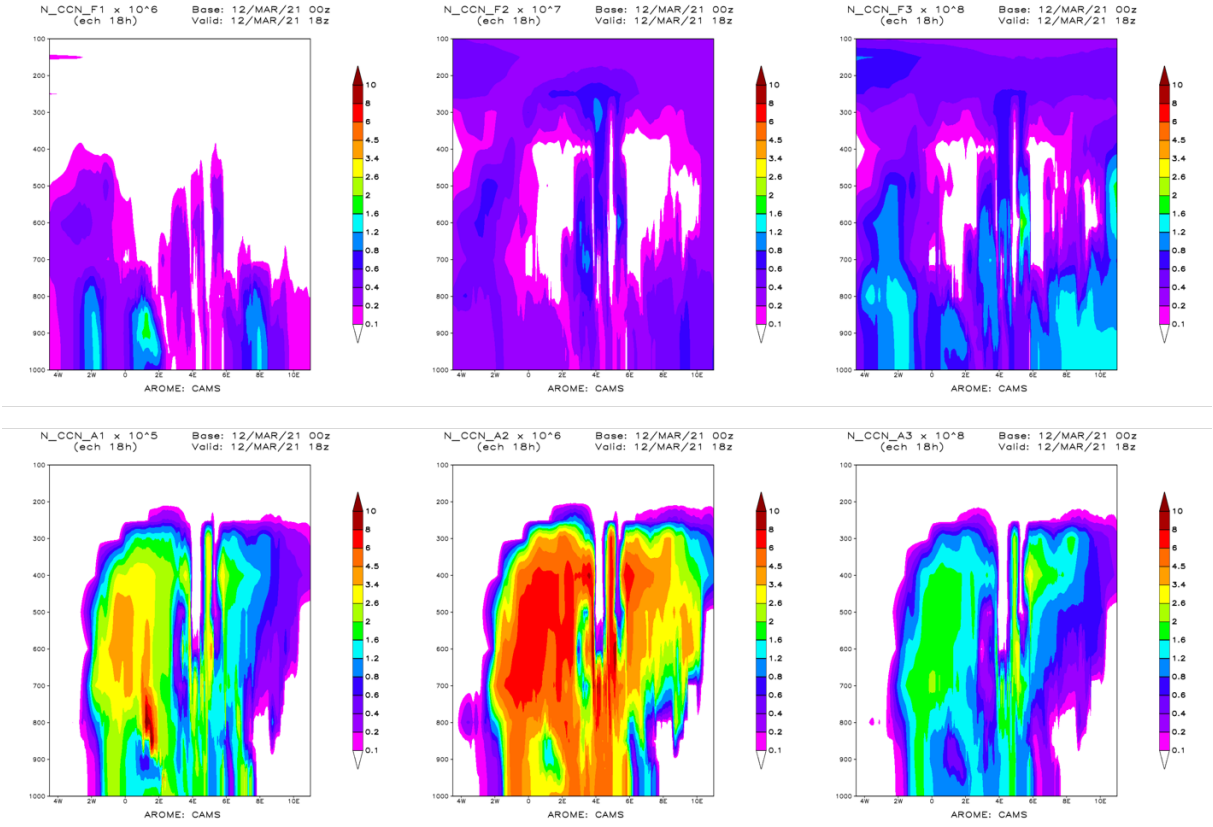

Figure 6: Vertical sections (at 27° north latitude) of cloud condensation nuclei activated (CCN_A) and free (CCN_F) simulated by AROME with LIMA-CAMS at 18h UT.

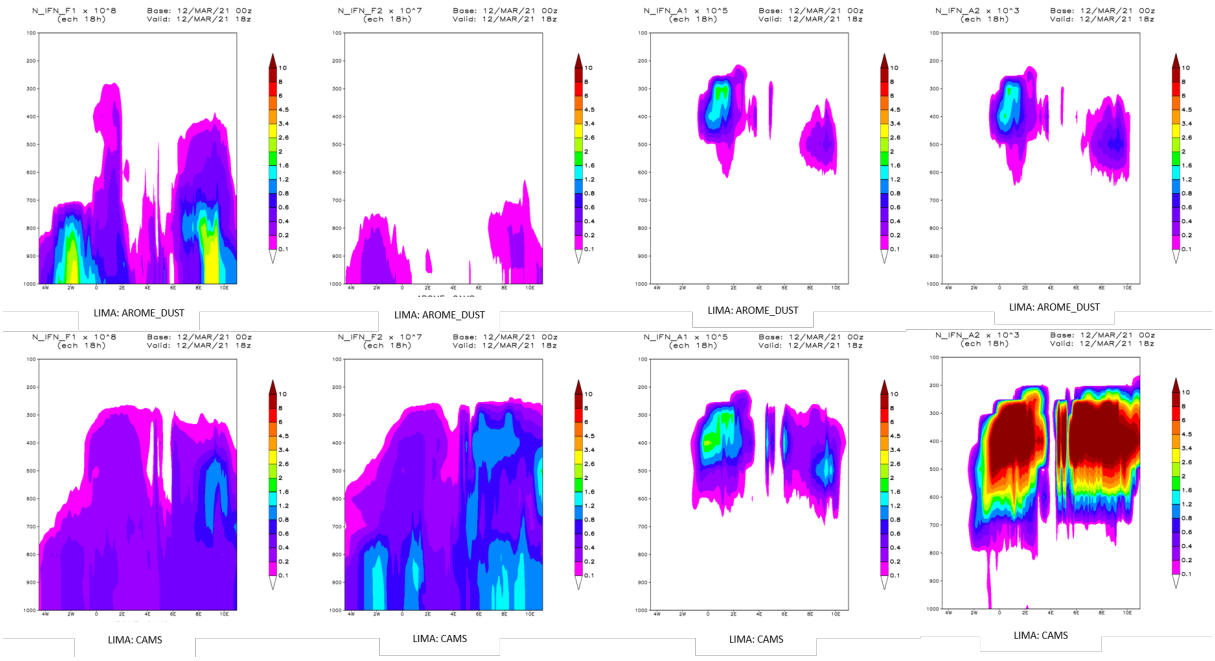

Figure 7: Vertical sections (at 27° north latitude) of ice freezing nuclei activated (IFN_A) and free (IFN_F) in case of LIMA_Dust and LIMA_CAMS, simulated by AROME at 18h UT.

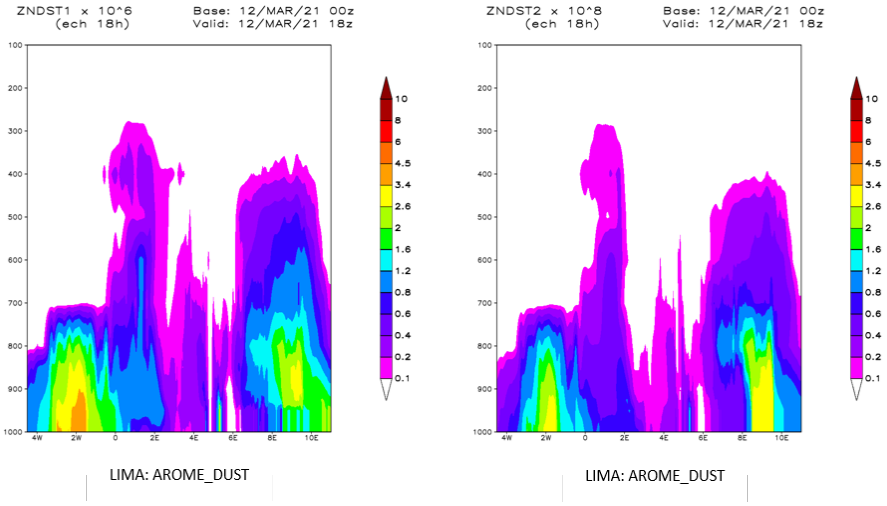

Figure 8: Vertical sections (at 27° north latitude) of dust concentration number of coarse mode (ZNDST1) and medium mode (ZNDST2), simulated by AROME at 18h UT.

5.3.3 Vertical profiles

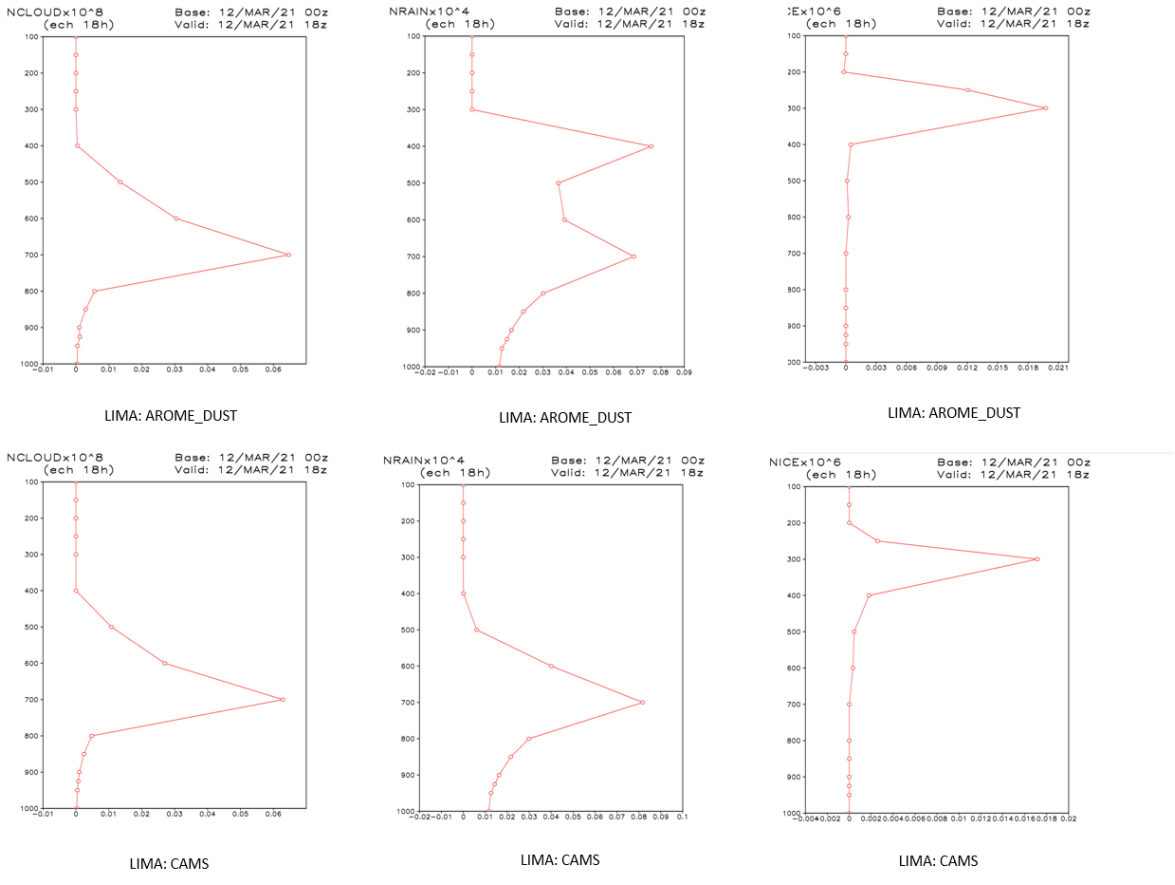

Figure 9: Vertical profile of hydrometeor fields in case of LIMA_Dust and LIMA_CAMS, simulated by AROME at 18h UT.

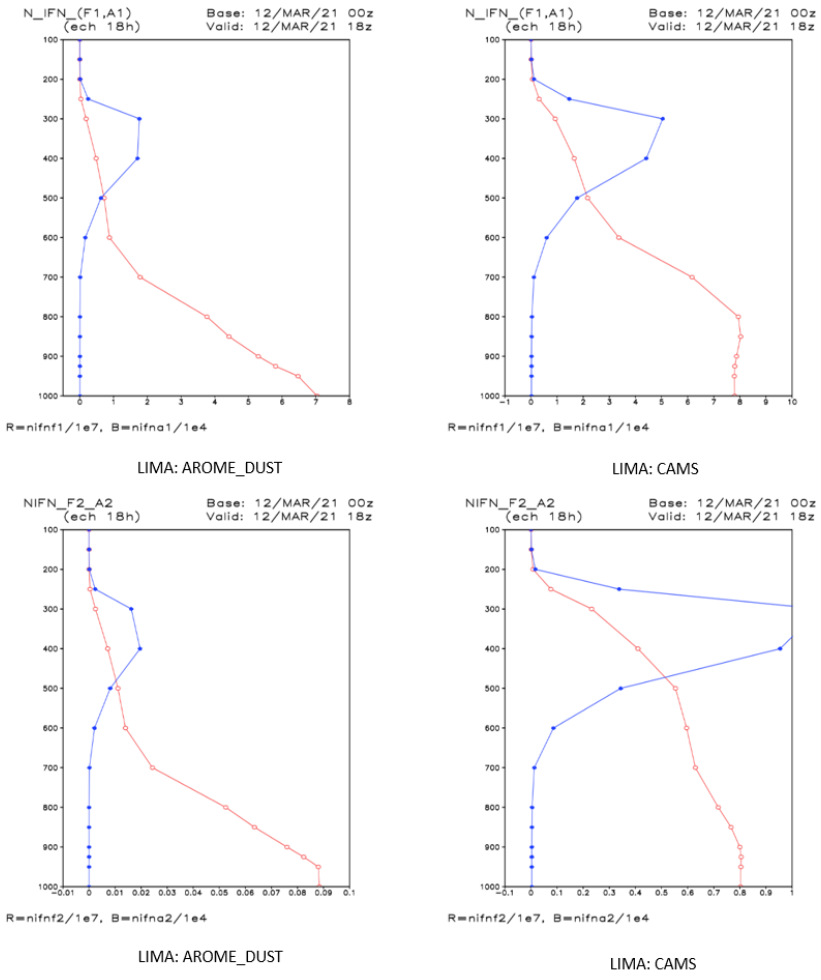

Figure 10: Vertical profile of ice freezing nuclei activated IFN_A (blue plot) and free IFN_F (red plot, values are multiplied by 10) in case of LIMA_DUST and LIMA_CAMS, simulated by AROME at 18h UT.

5 Conclusions

The confusion between LIMA fields and dust aerosols has been solved: now it is possible to perform AROME simulations by activating simultaneously the LIMA scheme with desert dust processes. Also, we succeeded to make an online post-processing of all the LIMA variables and those of the dust.

The new pack, including all the code modifications, has been tested for eight configurations during this study. All of them worked correctly: The LIMA and Dust fields are pretty much fine comparing to the reference ICE3. We have also noticed that the order of magnitude of the fields is quite reasonable and consistent. Further investigation about the inter-comparison between the LIMA simulations with DUST and LIMA with CAMS will be made later in order to better understand the impact of aerosols fields on microphysics.

6 References

Ambar, A : Desert dusts aerosols and microphysics interaction in AROME: Initialization of ice freezing nuclei in LIMA scheme, stay report, Toulouse 2019.

Mokhtari, M. et al., Importance of the surface size distribution of erodible material: an improvement on the Dust Entrainment And Deposition (DEAD) Model, Geosci. Model Dev., 5, 581–598, 2012, doi:10.5194/gmd-5-581-2012.

Vié, B., Pinty, J.P., Berthet, S., and Leriche, M. M.: LIMA (v1.0): A quasi two moment microphysical scheme driven by a multimodal population of cloud condensation and ice freezing nuclei, Geosci. Model Dev., 9, 567 586, doi:10.5194/gmd 9 567 2016, 2016.

Viktória Homonnai, Initialization of aerosols in LIMA scheme for AROME, RC LACE stay report, Toulouse, 2 nd November − 30 th November 2016.

ACCORD visit to Météo France 2022–04

Kristian Pagh Nielsen

1 Introduction

The visit was decided following an invitation to join the jury for the evaluation and defence of the PhD of Erfan Jahangir at Météo France. Since this was planned for April 14$^{\text{th}}$ in the week following the ACCORD All Staff Week in Ljubljana, a possibility for a 3–4 day visit to Météo France was available. Planning was made with Yann Seity and Quentin Libois

- Implementing ecRad in cy46 (t/h)
- Passing aerosols optical properties to ecRad
- Using better aerosols (initialisation+advection or full online)
- Coupling microphysics and radiation (via r_e)
- Erfan's new r_e parameterization
- Thoughts on how to extend this strategy to the LW $\rightarrow$ could be a Master 2 internship
- Crocus albedo in the explicit snow scheme - adaption to Nordic and Arctic regions incl. glaciers
- Crocus-TARTES - are there any plans for using this in AROME?
  - How can other impurities be included, e.g. Icelandic volcanic dust?
- Extraction of extra solar diagnostics for solar energy applications
- Estimation of true direct radiation (not delta-Eddington)

2 New aerosols in EcRad

EcRad runs in cy46t_op1, while there has still has been no success to run it in cy46h. A substantial amount of code changes have been merged in cy46h and the use of the newest aerosol climatology from ECMWF implemented. Here Yann explained that it is necessary to set the arguments

```
'LAERODES' => '.FALSE.,',
'LAEROLAN' => '.FALSE.,',
'LAEROSEA' => '.FALSE.,',
'LAEROSOO' => '.FALSE.,',
```

...in the namelist when using the new aerosols. This enables the call to radact.F90 from apl_arome.F90 Also, the variable `PDELP` must be used rather than `PAPRSM` in the call to radheat.F90 from apl_arome.F90.

Yann further explained that tests show that advecting the aerosols does not add any substantial computation time. When using near real time aerosols in cy46, this is then an obvious choice. In particular if full 3D aerosol input is used.

3 Cloud microphysics and radiation

The cloud droplet number concentration (CDNC) in the ICE3 cloud microphysics is now used consistently in the cy43h radiation scheme. Here it is important to understand that CDNC is

Together with CDNC changes of fixed values for land and sea made by Karl-Ivar Ivarsson of SMHI, we have shown CDNC to matter greatly for the cloud forecasts in our region. The main takeaway here is that cloud microphysics impacts on the radiation, also is important for the short-term cloud forecasts.

The shortwave effect of cloud droplets is the topic of Erfan Jahangir's PhD thesis, which Quentin has supervised. The cloud droplet effective size r_e depends on three variables

$$r_e = \sqrt[3]{\frac{3L}{4\pi\rho_w k N_{\mathrm{TOT}}}}, \tag{1}$$

where L is the cloud liquid water concentration, N_{TOT} is the CDNC, and k is an empirical constant first suggested by Bower & Choularton (1992) for the linear relationship between the cube of the mean volume radius and the cube of the effective radius of cloud droplets. ρ_w is the density of liquid water.

For shortwave radiation the cloud optical thickness is proportional with the cloud water load, and approximately inversely proportional with r_e. Here it is clear from Eq. 1 that variations of both the k and N_{TOT} factors are of as large importance as variations of L for the value of r_e and thereby for the shortwave cloud optical thickness. Jahangir et al. (2021) derives k to be

$$k = \frac{\nu^2+\nu}{(\nu+2)^2} \tag{2}$$

$$k = e^{-3\sigma^2} \tag{3}$$

respectively for assumed modified gamma (Eq. 2) and log-normal (Eq. 3) distributions of the cloud droplet sizes. Here ν and σ are the shape parameters of the two distributions.

Since cloud droplet size distribution shapes are also assumed in the AROME cloud microphysics schemes ICE3 and LIMA, the k parameter can then be used consistently with these in the radiation physics. In the radiation physics, both in the older cy25r and the new cy47r ecRad scheme, it is stated that the Martin et al. (1994) parametrization is used for computing r_e (Eq. 1), however, Martin et al. recommends a k value of 0.80 for sea and 0.67 for land, while the actual values used are 0.77 for sea and 0.69 for land. For ecRad this is done in the subroutine

`.../arpifs/phys_radi/liquid_effective_radius.F90`

and k is a local hard-coded variable with the name `ZSPECTRAL_DISPERSION`. There is no explanation for this difference. Additionally, a factor (`ZWOOD_FACTOR`) is multiplied with r_e in ecRad. This accounts for the effect of drizzle on k (Wood et al. 2000; doi:10.1002/qj.49712657015).

Quentin, Yann and I discussed that k should be made consistent with the ν values of the gamma distributions used in ICE3 and LIMA. For ICE3 Yann and Quentin derived k values of 0.48 for land and 0.74 for sea. For land this is a reduction of 30% relative to the currently used value in the radiation scheme. **This again corresponds to a reduction of the liquid cloud optical thickness over land of more than 10%.**

Put into a general modelling context a relative change of $\sqrt[3]{k}$ or $\sqrt[3]{N_{\mathrm{TOT}}}$ has the approximate effect of scaling the liquid cloud optical thickness. As was presented by Laure Raynaud (2012) at the recent ACCORD ASW scaling the cloud optical thickness in the shortwave and longwave with the factors RSWINHF and RLWINHF provides 2 out the 8 most important variables for making the AROME-France ensemble prediction system have a realistic spread. More precisely, RSWINHF and RLWINHF are currently varied in the intervals 0.6–1.0.

These factors represent cloud inhomogeneity effects and are inherited from the IFS model of ECMWF when this was run at a much coarser resolution than is used for AROME today. Here a more physically based uncertainty of the cloud optical thickness can be explained by the uncertainty of the cloud microphysical variables k and N_{TOT}. At Météo France students and candidates are already looking into this.

Another obvious test of the importance of k is to adjust the current k values in the HARMONIE-AROME and AROME radiation schemes to the k values derived from ICE3.

I also presented my computations of LW cloud liquid optical properties, which have been added to cy43h2.2. Some of these computations can be seen in Figure 1. For these it would also be worth to test the sensitivity of $k_{\mathrm{gamma}}(\nu)$. This is work to be done. Quentin mentioned that a M2 internship about this could be an idea.

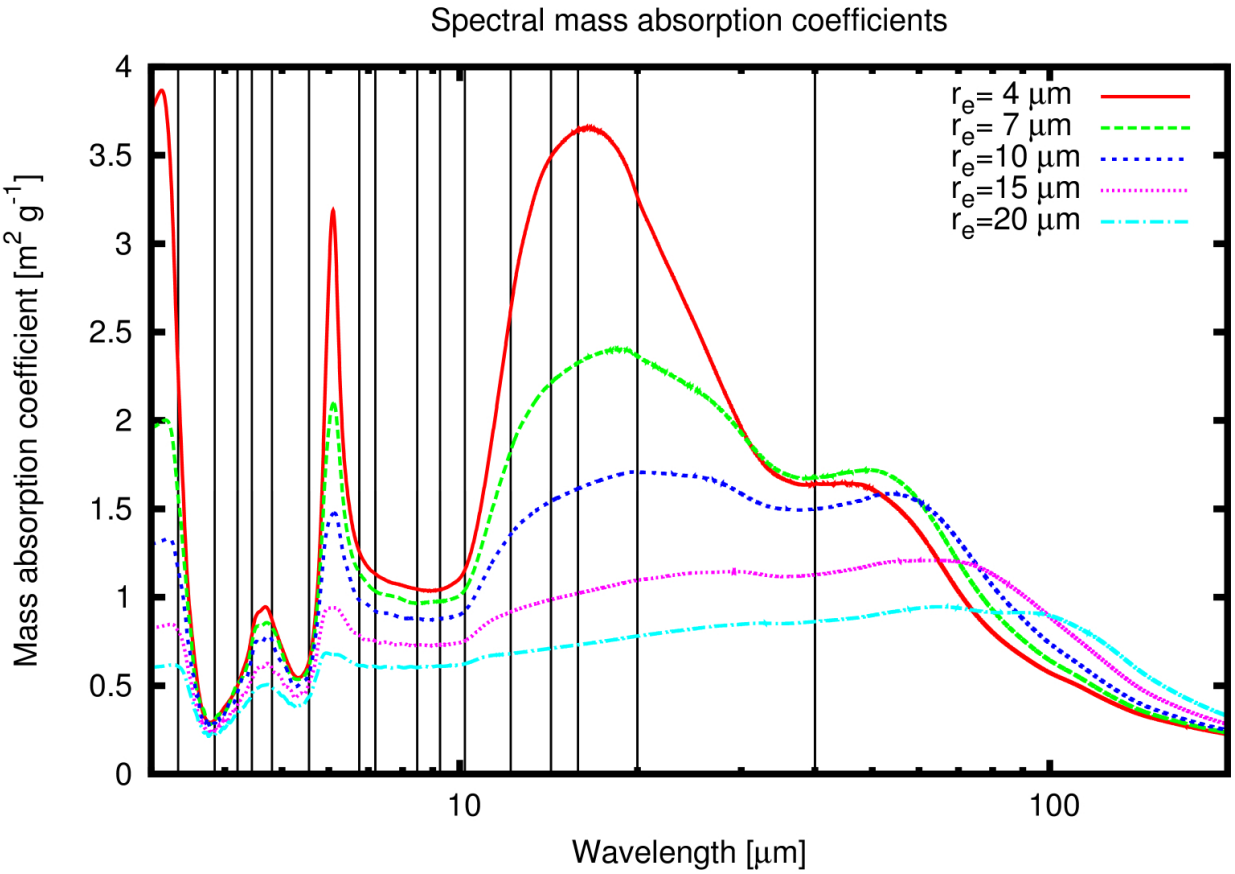

Figure 1: Mass absorption coefficients as a function of wavelengths in the thermal "LW" part of the spectrum for different values of r_e. The vertical lines mark the delimitations of the 16 LW spectral bands that are used in RRTM. The Mie computations are made with the algorithm of Wiscombe (1980)

4 Snow-radiation interactions in the AROME-SURFEX system

First I described the new method for using satellite-derived albedos for glaciers in the Arctic domains of DMI, IMO and MET Norway. This is implemented for the C3S Arctic Regional Reanalysis for use in the D95 snow scheme. We also have plans for using this in the Crocus albedo scheme, which is used also in the explicit snow scheme in SURFEX 8.1. Before the D95 snow albedo scheme was used in this.

When checking how to use satellite-derived albedos in the Crocus albedo scheme, detailed in Figure 2, I found that the spectral divisions in this appear to be wrong. Here the spectral band weights are set to be 71%, 21% & 8%, respectively, for the three bands listed in Figure 2. For the MEB patch in SURFEX, however, the first

Spectral band	Albedo α	Absorption coefficient β (m^{-1})
0.3–0.8 μm	$\max(0.6, \alpha_i - \Delta\alpha_{\text{age}})$ where: $\alpha_i = \min\left(0.92, 0.96 - 1.58\sqrt{d_{\text{opt}}}\right)$ and: $\Delta\alpha_{\text{age}} = \min\left(1., \max\left(\frac{P}{P_{\text{CDP}}}, 0.5\right)\right) \times 0.2\frac{A}{60}$	$\max\left(40, 0.00192\rho/\sqrt{d_{\text{opt}}}\right)$
0.8–1.5 μm	$\max(0.3, 0.9 - 15.4\sqrt{d_{\text{opt}}})$	$\max\left(100, 0.01098\rho/\sqrt{d_{\text{opt}}}\right)$
1.5–2.8 μm	$346.3d' - 32.31\sqrt{d'} + 0.88$ where: $d' = \min(d_{\text{opt}}, 0.0023)$	$+\infty$

Figure 2: The 3 SW spectral band CROCUS snow albedo parametrization (Vionnet et al. (2012); doi:10.5194/gmd-5-773-2012). Temporal evolution of snow albedo and absorption coefficient β (Vionnet et al. 2012). P_{CDP} = 870 hPa. This means that the darkening effect of impurities is assumed to increase at higher surface pressures, i.e. at lower altitudes. In the actual SURFEX model the relative surface pressure is allowed to vary up to 1.5 · 870 hPa and the $\beta = +\infty$ absorption coefficient is set to 2000 m^{-1}. Additionally, the aging coefficient is removed for glacier (“permanent snow") surfaces in the actual SURFEX model.

spectral band weight is set to 48% in stead, and for the MEB patch only 2 SW spectral bands are used. Since approximately half of the SW irradiance reaching the surface is in the UV-visible (0.3–0.8 μm) spectral band the MEB spectral division is more reasonable than the CROCUS spectral division.

In Figure 3 the differences due to changing the CROCUS spectral division to that from the MEB patch can be seen. Since the MEB patch only has 2 spectral bands for the snow albedo the ratio between spectral bands 2 and 3 has been kept constant in the experiment, i.e. the new spectral band weights are 48%, 38% & 14%. Since the UV-visible spectral band in which snow reflects most of the incoming SW radiation is weighted less, the obvious overall result is that the net radiation and the skin temperature both mostly increase. At times of the year without snow on the ground the differences are zero or very low. Likewise at night the differences are low. Complex feedback mechanisms are represented by occasional negative differences in the net radiation and by general increases in the positive differences during Winter and Spring. Here increased snow metamorphism is a likely culprit. The extreme temperature differences at the end of spring are due to the snow disappearing earlier in the MEB spectral division run. These results clearly show how important the spectral albedo effects are!

In CROCUS a better snow radiative transfer code is available, i.e. the spectral albedo model Two-streAm Radiative TransfEr in Snow (TARTES) (Libois et al. 2013). Quentin explained that with this the issue of thin layers of new snow increasing the snow albedo to its maximum values is resolved. We discussed how the spectral coupling can be made from the atmosphere to this multi-spectral scheme. The problem here is that the atmospheric spectral bands are different from those in TARTES - and also in the original CROCUS snow albedo scheme. Quentin mentioned that Marie Dumont has made algorithms for computing the solar spectrum from the atmospheric constituents. I will check with her about this. He wasn’t sure that she has remembered to account for the effect of the atmospheric integrated water vapour on the snow reflectance as illustrated in Figure 4. So maybe I can contribute something to this.

By setting

```
&NAM_ISBA_SNOWn
                        CSNOWRAD = 'T17'
```

... in the SURFEX namelist, a successful run with the current version of TARTES for CROCUS was made. The feasibility of using this in AROME needs to be checked further, but for offline runs, such as those made in Iceland and Poland, this option should be considered.

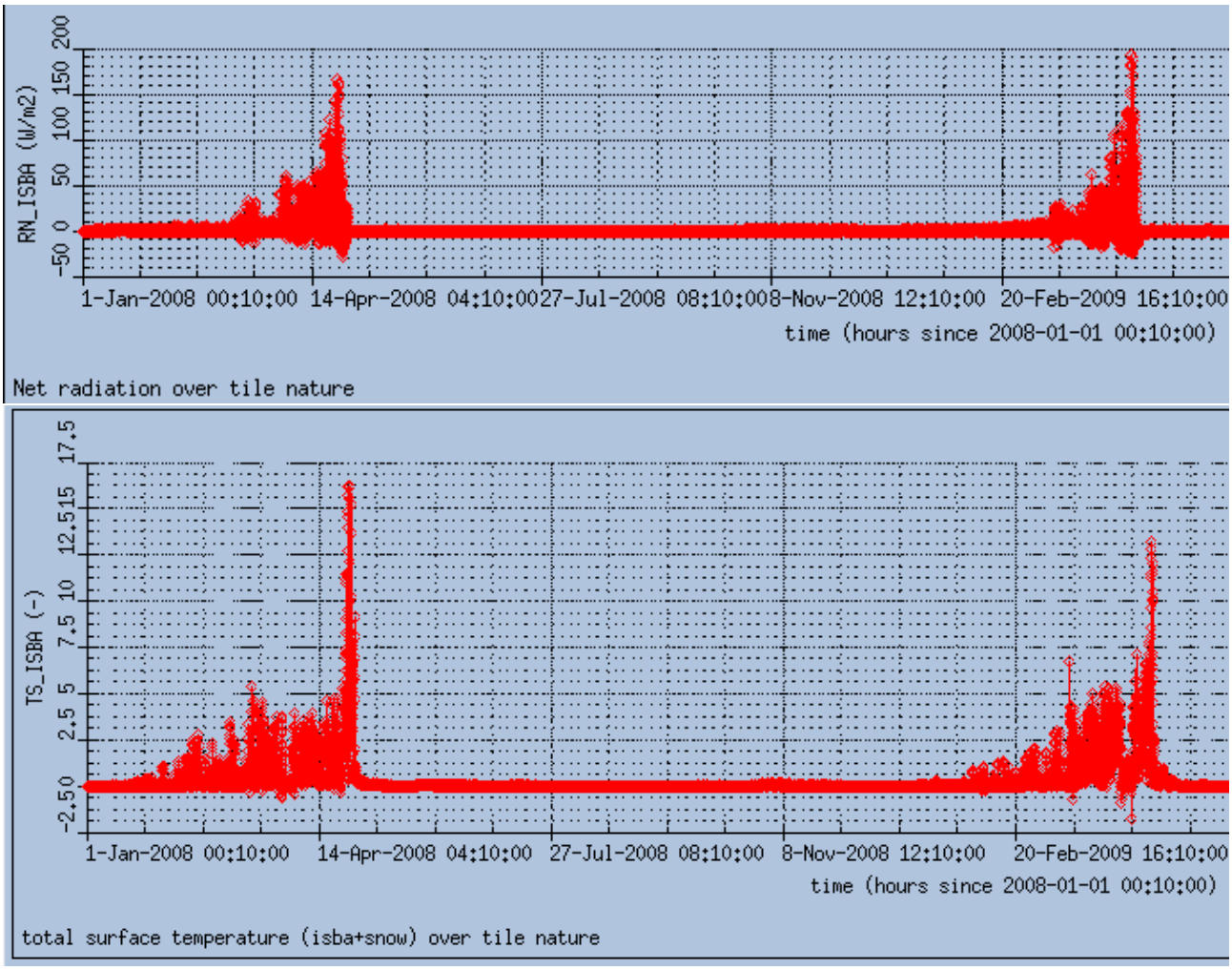

Figure 3: Results from stand-alone SURFEX runs with forcing files for Sodankylä, Finland. The runs cover 1.5 years. The top plot shows the difference in the surface net radiation, that is the sum of SW net radiation and LW net radiation, when using the MEB spectral division rather than the original CROCUS spectral division. The bottom plot shows the correcsponding difference in the skin surface temperature.

5 Other topics

In general, the coupling of the atmospheric radiation model to SURFEX needs attention. In HARMONIE-AROME with made an attempt with the code that is activated with the logical switch HLRADUPD, however, this was made before understanding what happens in SURFEX. This included the HIRLAM method for accounting for the effect of the albedo dependence on the solar zenith angle. For the ISBA (nature) tile in the current SURFEX the direct and diffuse albedos are set to be equal to each other in the subroutine `.../surfex/SURFEX/albedo_from_nir_vis.F90`.

We discussed solar energy meteorology, where I showed, what validations we run for this in UWC-West and recommended getting the clear sky SW radiation variables as standard output from AROME. These are: “Surface net solar radiation, clear sky" and “Clear-sky direct solar radiation at surface." With them the modelled clear sky index (CSI) can be accurately calculated, and the effects of aerosols and clouds on the radiation can be distinguished (Nielsen & Gleeson 2018; Gleeson & Nielsen 2021).

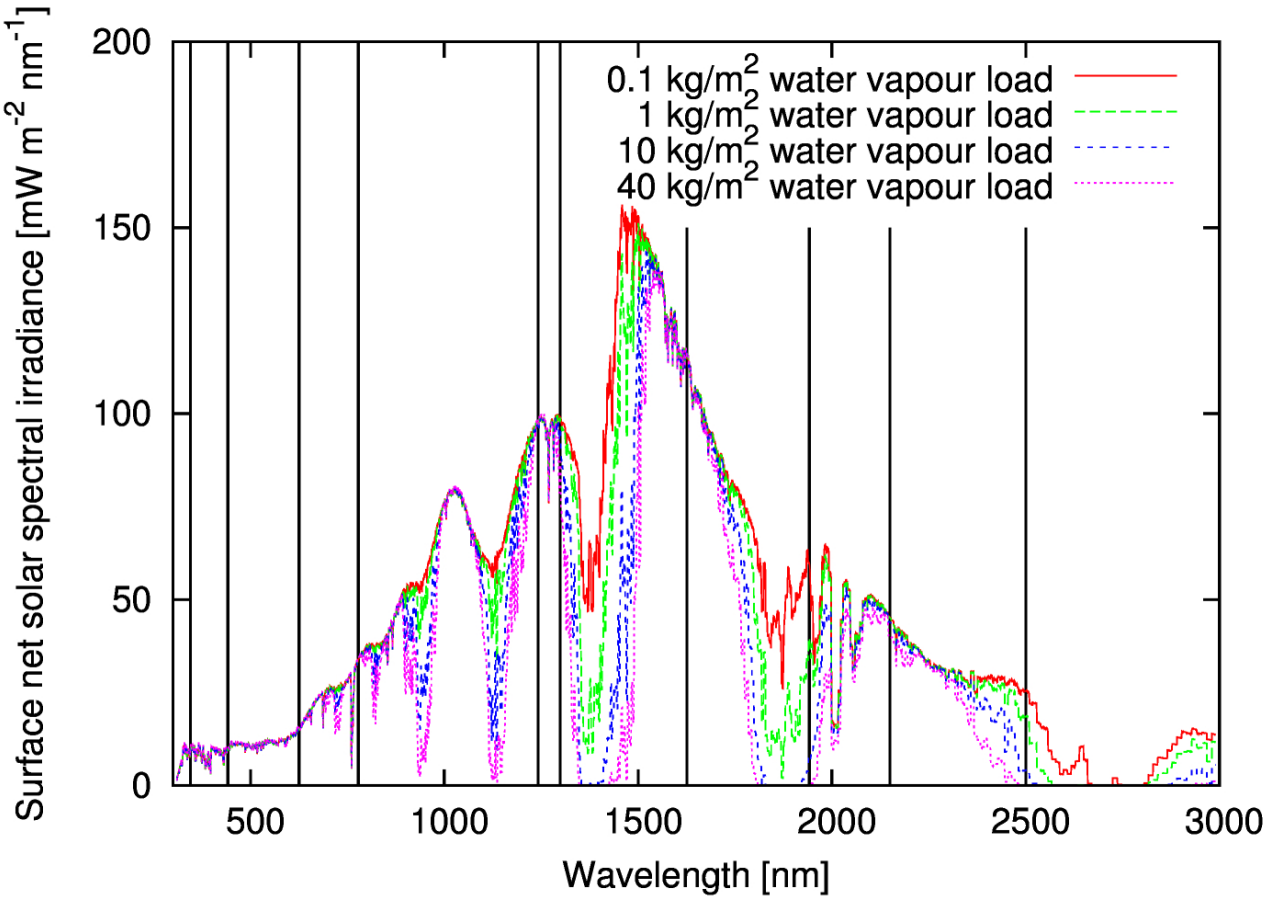

Figure 4: Net SW spectral irradiance for different atmospheric water vapour loads. The vertical bands show the limits of the RRTM SW spectral bands.

6 References

Bower K. N. and T. W. Choularton, A parameterisation of the effective radius of ice free clouds for use in global climate models, doi:10.1016/0169-8095(92)90038-C, Atmospheric Research, 27 (4), 305–339, 1992.

Gleeson, E. and K. P. Nielsen, Use of a Clear Sky Index to Evaluate Solar and Cloud NWP Forecasts, doi:10.5194/ems2021-387, EMS Annual Meeting Abstracts, 2021.

Jahangir E., Q. Libois, F. Couvreux, B. Vié, D. Saint-Martin, Uncertainty of SW Cloud Radiative Effect in Atmospheric Models Due to the Parameterization of Liquid Cloud Optical Properties, doi:10.1029/2021MS002742, Journal of Advances in Modeling Earth Systems, 13 (12), 2021.

Libois Q., G. Picard, J. L. France, L. Arnaud, M. Dumont, C. M. Carmagnola and M. D. King, Influence of grain shape on light penetration in snow, doi:10.5194/tc-7-1803-2013, The Cryosphere, 7, 1803–1818, 2013.

Martin, G. M., D. W. Johnson and A. Spice, The Measurement and Parameterization of Effective Radius of Droplets in Warm Stratocumulus Clouds, doi:10.1175/1520-0469(1994)051<1823:TMAPOE>2.0.CO;2, Journal of the Atmospheric Sciences, 51 (13), 1823–1842, 1994.

Nielsen, K. P. and E. Gleeson, Using Shortwave Radiation to Evaluate the HARMONIE-AROME Weather Model, doi:10.3390/atmos9050163, Atmosphere, 9 (5), 163, 2018.

Raynaud, L., AROME-EPS Current status and future directions, www.accord-nwp.org/IMG/pdf/raynaud_prez.pdf, ACCORD ASW 2022, Ljubljana, Slovenia, 2022.

Vionnet, V., E. Brun, S. Morin, A. Boone1, S. Faroux, P. Le Moigne, E. Martin and J.-M. Willemet, The detailed snowpack scheme Crocus and its implementation in SURFEX v7.2, doi:10.5194/gmd-5-773-2012, Geoscientific Model Development, 5, 773–791, 2012.

Wiscombe, W. J., Improved Mie scattering algorithms, doi:10.1364/AO.19.001505, Applied Optics, 19 (9), 1505–1509, 1980.

Wood, R., Parametrization of the effect of drizzle upon the droplet effective radius in stratocumulus clouds, doi:10.1002/qj.49712657015, Quarterly Journal of the Royal Meteorological Society, 126 (570), 3309–3324, 2000.

Increasing the ensemble spread by a new model uncertainty representation in MEPS

Inger-Lise Frogner MET Norway, Ulf Andrae SMHI

1. Introduction

The MetCoOp ensemble prediction system, MEPS, has been operational since late 2016 (Andae et al. 2020). On 30 August 2022 MEPS was updated with a new model uncertainty scheme. The aim of this scheme is to increase the spread of the ensemble, particularly the cloud products.

The main sources of uncertainty in NWP models originate from (i) incomplete reconstruction of the current atmospheric state (due to lack of observations, limitations in data assimilation, etc.), and (ii) errors in model construction (arising from the need to approximate and discretize the atmospheric governing equations, which then results in parameterization of unresolved processes). These are referred to as initial state uncertainty and model uncertainty, respectively. A third source of uncertainty arises from how interactions are handled between the atmosphere and other Earth system components (land, oceans, glaciers, etc.). In limited area modelling (LAM) an additional uncertainty source comes from how lateral boundary conditions from the host model are handled (see e.g., Frogner et al. 2019). By the introduction of the new model uncertainty scheme SPP, The Stochastically Perturbed Parameterizations Scheme, all these sources of uncertainty are now represented in MEPS. SPP introduces stochastic perturbations to selected uncertain parameters in the representation of sub grid physical processes (Frogner et al. 2022).

2. The SPP scheme in MEPS

In the current implementation 5 parameters are perturbed that are involved in different parts of the model physics (liquid microphysics, ice microphysics, convection and turbulence, see Table 1). The parameters perturbed are all uncertain and are varied in SPP according to our knowledge about this uncertainty and careful adjustment of the range and distribution of the perturbations. The parameters are perturbed both spatially and temporally, each parameter and each ensemble member with a unique pattern like the one shown in Figure 1. Spatial and temporal correlation length scales of 200 km and 12 h are used. See Frogner et al. (2022) for more information on the technical aspects of SPP.

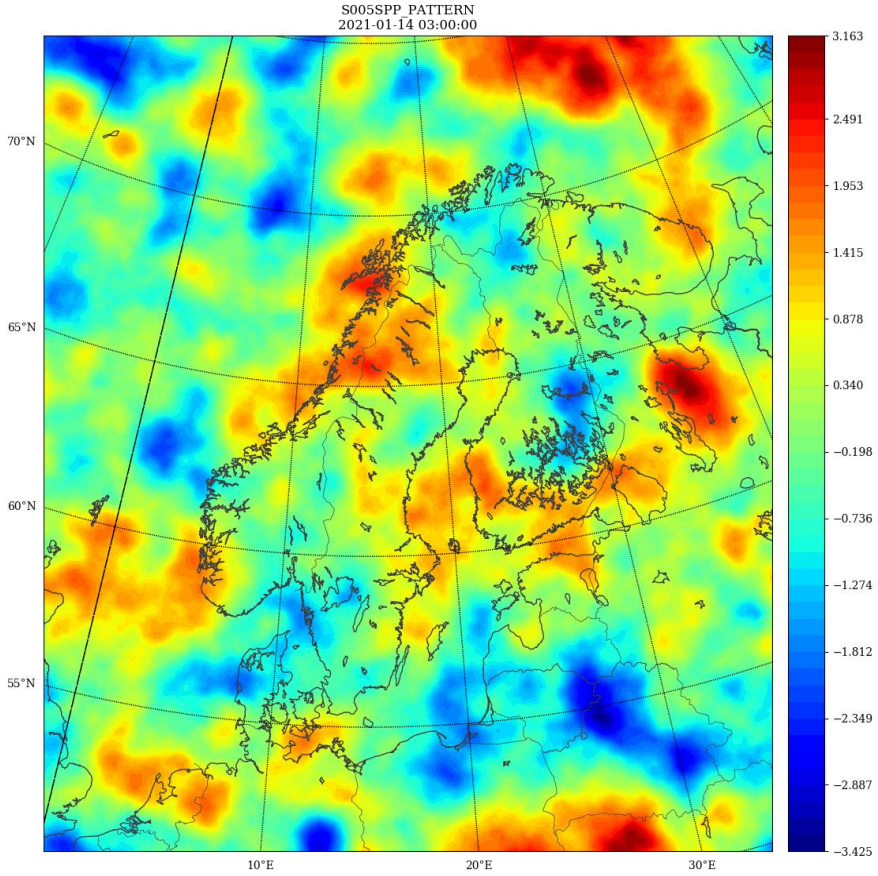

Figure 1: Example of a perturbation pattern.

Table 1: The following parameters are perturbed in MEPS

Description	**Parameter**	**Type**
Threshold for cloud thickness used in shallow/deep convection decision	CLDDPTHDP	convection
Saturation limit sensitivity for condensation	VSIGQSAT	liquid microphysics
Cloud ice content impact on cloud thickness	ICE_CLD_WGT	ice microphysics
Stable conditions length scale	RZC_H	turbulence
Asymptotic free atmospheric length scale	RZL_INF	turbulence

3. Meteorological impact

The main impact of SPP is to allow the model to develop in different directions and thereby increase the spread of the ensemble. This gives a better agreement between the spread and the root-mean-square error of the ensemble mean (referred to as “skill”). The ensemble spread is a measure of the difference between the ensemble members and is represented by the standard deviation with respect to the ensemble mean. On average, small spread indicates high forecast accuracy; larger spread corresponds to lower forecast accuracy of the ensemble mean, and of most of the ensemble members. Spread usually increases with the forecast range. The RMSE of the ensemble mean is mainly unchanged by introducing SPP, giving a better spread-skill relationship as intended. See Table 2 for a summary score card.

Table 2: Summary of the verification scores for 2 metre temperature (T2m), 2 metre relative humidity (RH2m), 10 metre wind speed (S10m), mean sea level pressure (PMSL), total cloud cover (CCtot), low cloud cover (CClow), cloud base height (Cbase) and 6 h accumulated precipitation (AccPcp6h). + means preop is better than MEPS, - means MEPS is better and empty cell means there is little difference in the scores between MEPS and preop.

	SPREAD	SKILL	MEAN BIAS
T2m	+		+
RH2m	+		+
S10m	+		+
PMSL	+		+
CCtot	+		
CClow	+		-
Cbase	+		-
AccPcp6h	+		

Prior to implementation special attention has been paid to address unwanted bias changes caused by the perturbations (as was seen in Frogner et al. 2022), and the current scheme has little impact on the bias.

In the following figures, figure 2 - figure 9, verification scores for most of the period SPP ran in MEPS preoperational is compared to MEPS (22 June 2022 - 8 August 2022). A clear increase in spread is seen for all variables, in particular for the cloud variables, while the RMSE is mainly unchanged. The mean bias changes slightly, sometimes to the better and sometimes to the worse, but the changes are small (note the scale on the y-axis in the plots).

1. Total cloud cover

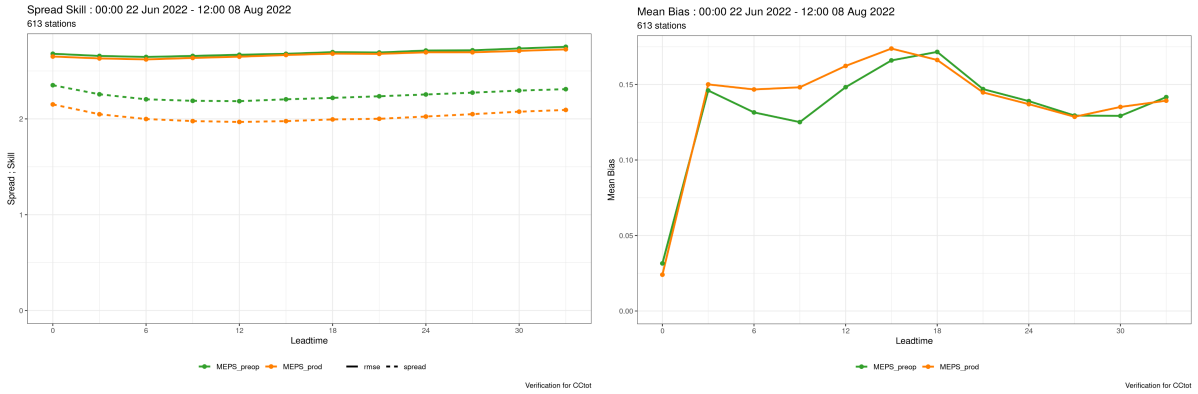

Figure 2: Left: Spread (dashed) and skill (RMSE of ensemble mean, solid). Right: mean bias. For total cloud cover. MEPS in orange and MEPS_preop in green.

2. Low cloud cover

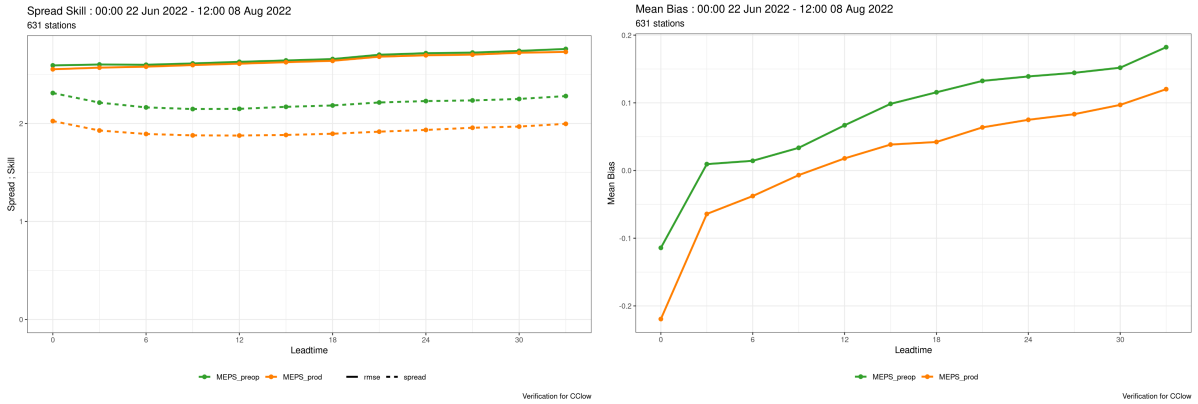

Figure 3: Left: Spread (dashed) and skill (RMSE of ensemble mean, solid). Right: mean bias. For low cloud cover. MEPS in orange and MEPS_preop in green.

3. Cloud base height

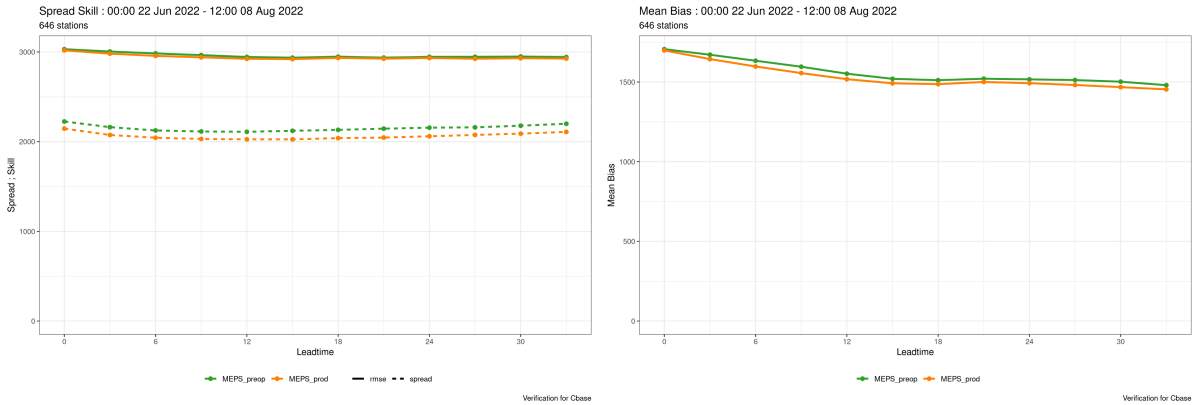

Figure 4: Left: Spread (dashed) and skill (RMSE of ensemble mean, solid). Right: mean bias. For cloud base height. MEPS in orange and MEPS_preop in green.

4. 10 m wind speed

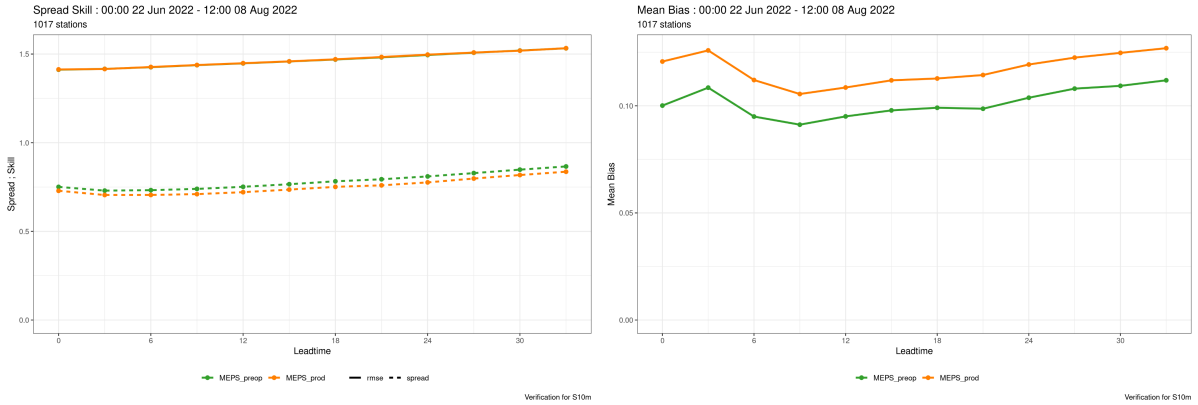

Figure 5: Left: Spread (dashed) and skill (RMSE of ensemble mean, solid). Right: mean bias. For 10 metre wind speed. MEPS in orange and MEPS_preop in green.

5. 2 m temperature

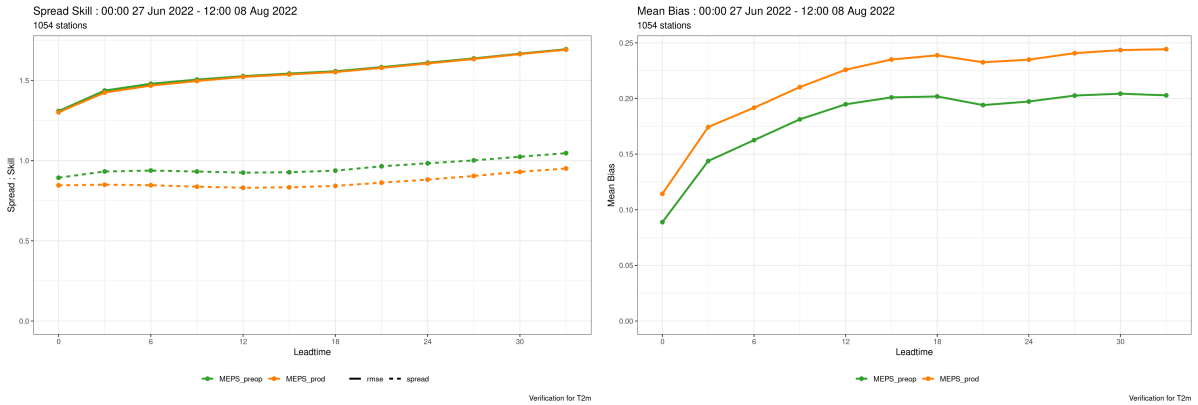

Figure 6: Left: Spread (dashed) and skill (RMSE of ensemble mean, solid). Right: mean bias. For 2 metre temperature. MEPS in orange and MEPS_preop in green.

6. 2 m relative humidity

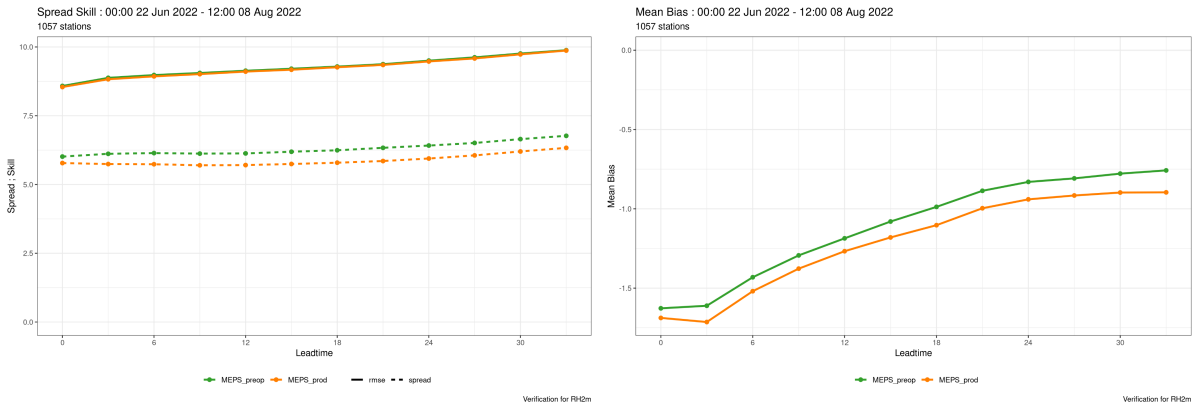

Figure 7: Left: Spread (dashed) and skill (RMSE of ensemble mean, solid). Right: mean bias. For 2 metre relative humidity. MEPS in orange and MEPS_preop in green.

7. 6 h accumulated precipitation

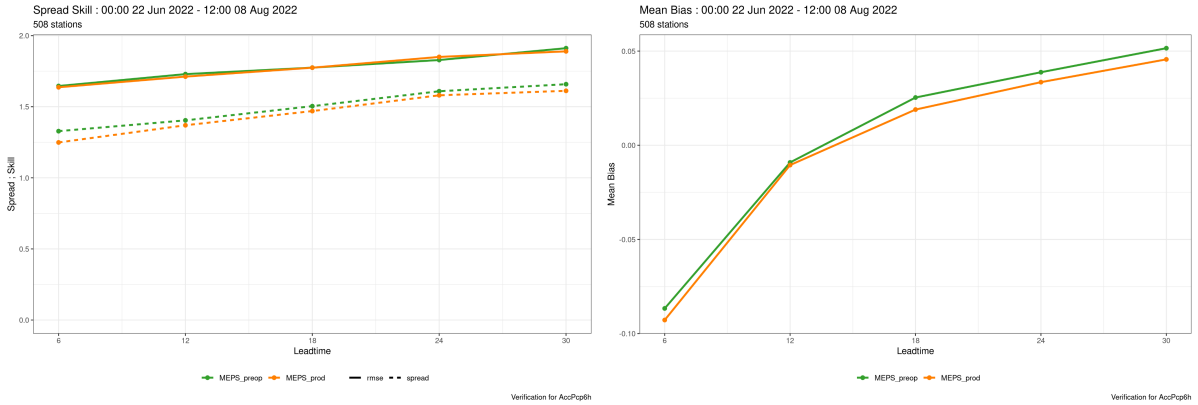

Figure 8: Left: Spread (dashed) and skill (RMSE of ensemble mean, solid). Right: mean bias. For 6 h accumulated precipitation. MEPS in orange and MEPS_preop in green.

8. Mean sea level pressure

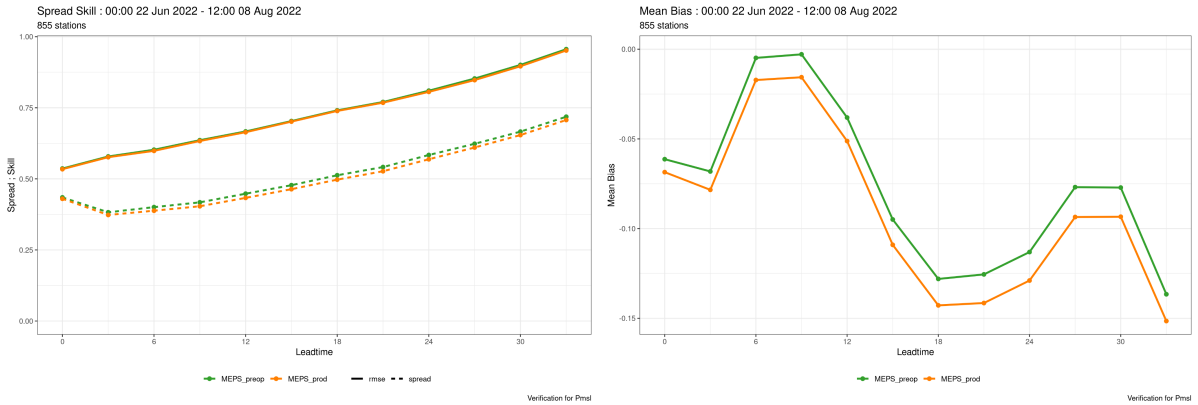

Figure 9: Left: Spread (dashed) and skill (RMSE of ensemble mean, solid). Right: mean bias. For mean sea level pressure. MEPS in orange and MEPS_preop in green.

4. References

Andrae U., Frogner I-L., Vignes O., A continuous EDA based ensemble in MetCoOp, ALADIN-HIRLAM Newsletter No. 14, 2020.

Frogner, I.-L. , and Coauthors, 2019: HarmonEPS—The HARMONIE ensemble prediction system. *Wea. Forecasting*, **34**, 1909–1937, https://doi.org/10.1175/WAF-D-19-0030.1.

Frogner, I.-L., Andrae, U., Ollinaho, P., Hally, A., Hämäläinen, K., Kauhanen, J., Ivarsson, K., & Yazgi, D. (2022). Model Uncertainty Representation in a Convection-Permitting Ensemble - SPP and SPPT in HarmonEPS, *Monthly Weather Review*, *150*(4), 775-795. https://journals.ametsoc.org/view/journals/mwre/150/4/MWR-D-21-0099.1.xml

Tiedtke-Bechtold deep convection parametrisation in ALADIN-NORAF model: Introduction of an advective moisture tendency into the CAPE closure

Siham Sbii and Noureddine Semane

1 Introduction

In this document, we present the first results of the introduction of an advective moisture tendency into the CAPE closure used in the Tiedtke-Bechtold deep convection parametrisation. The model used is ALADIN-NORAF which covers north tropical and intertropical zones. The deep and shallow convection schemes based on Tiedtke 1989 and modified by Bechtold 2008 and Bechtold 2014, were previously implemented in the "Cy43t2" version of ALADIN-NORAF moist physics package. The results have shown a better precipitation diurnal cycle in comparison with Global Precipitation Measurments over Sahel regions and over the atlantic ocean. The representation of convective cells, seen in the Infrared simulated brightness temperature, is similar to the version using the original CAPE closure.

2 Steps of the deep convection scheme modification used in this study

2.1 Tiedtke-Bechtold scheme

The first step in this study was the implementation of Tiedtke-Becthold convection scheme used in the ECMWF IFS model. It is based on Tiedtke 1989 and modified later following Bechtold et al. 2008, 2014. The scheme acts to remove a density weighted buoyancy integral of an entraining ascending air parcel $PCAPE$ over a convective adjustment timescale τ. The formulation of this $CAPE$ is given by:

$$PCAPE = -\int_{p|_{z=z_b}}^{p|_{z=z_t}} \frac{T_{\mathrm{vc}} - \overline{T_{\mathrm{v}}}}{\overline{T_{\mathrm{v}}}} dp; \quad dp = \rho g dz \tag{1}$$

where z is height, z_{b} is the cloud base, z_{t} is the cloud top, T_{v} is the virtual temperature and g is the gravity, ρ the density, the subscript c denotes convective values, and the bar denotes large-scale or grid-mean values.

Its relaxation to a reference value $PCAPE_{bl}$ is given by:

$$\left.\frac{\partial PCAPE}{\partial t}\right|_{\mathrm{c}} = -\frac{PCAPE - PCAPE_{bl}}{\tau} \tag{2}$$

and $PCAPE_{bl}$ represents the bouandary layer forcing, which is computed as follows:

$$PCAPE_{\mathrm{bl}} = -\frac{\tau_{\mathrm{bl}}}{T_\star} \int_{p|_{z=0}}^{p|_{z=z_b}} \left.\frac{\partial \overline{T_{\mathrm{v}}}}{\partial t}\right|_{\mathrm{bl}} dp \tag{3}$$

where $p|_{z=0}$ is the surface pressure, $T_\star = 1K$ is a temperature parameter, $\overline{w}_c$ is the average vertical wind speed in the cloud layer and $\overline{u}_{\rm bl}$ is the average horizontal wind speed in the boundary layer. The boundary layer adjustment time scale $\tau_{\rm bl}$ is set to $\frac{z_{\rm t}-z_{\rm b}}{\overline{w}_c}$ over the continental boundary layer and $\frac{z_{\rm b}}{\overline{u}_{\rm bl}}$ over the oceanic boundary layer.

2.2 Introduction of an advective moisture tendency into the CAPE closure

The second step of this study is about the modification of the CAPE closure that includes a dependence on the total moisture convergence as done in the ECMWF IFS moist physics parametrisation since cycle CY47r3. Indeed, as shown in Becker et al. 2021, the inclusion of moisture convergence in the CAPE closure produces a better organization of the mesoscale convective systems, especially when instability is weak and vertical and horizontal advection is strong. The aim of this part of the study is to test the sensitivity of ALADIN-NORAF forecasts to the modification of the CAPE closure. This is done as explained in Becker et al. 2021 by adding a moisture convergence term Q_{adv}.

$$\left.\frac{\partial PCAPE}{\partial t}\right|_{\rm c} = \frac{PCAPE_{bl} - Q_{adv} - PCAPE'}{\tau} \tag{4}$$

where Q_{adv} is given by :

$$Q_{adv} = -\frac{\alpha\tau_{\rm c}L}{g(z_{\rm t}-z)}\int_{p|_{z=0}}^{p|_{z=z_m}} \frac{\overline{q_v}}{\overline{q_s}}\left.\frac{\partial\overline{q}}{\partial t}\right|_{\rm adv} dp \tag{5}$$

where z_m is the model-top altitude, $\frac{\overline{q_v}}{\overline{q_s}}$ is the relative humidity and the α parameter is set to 0.8.

The $PCAPE'$ is formulated as follows:

$$PCAPE' = (1-\alpha)PCAPE + \alpha\int_{p|_{z=z_b}}^{p|_{z=z_t}} \left(\frac{T_{\rm vc} - \overline{T'_{\rm v}}}{\overline{T'_{\rm v}}} - l_{\rm c}\right) dp \tag{6}$$

$l_{\rm c}$ is cloud water/ice content in the updraught and $\overline{T'_{\rm v}}$ is computed by subtracting the advective tendency from the dynamically updated state variable $\overline{T_{\rm v}}$ to avoid double counting in line with Becker et al. 2021.

3 Model configuration and experimental results

3.1 Model configuration and experimental design

The model configuration used in the present study is based on CY43 of the north african version of ALADIN (ALADIN-NORAF) running at 10km of horizontal resolution and 70 vertical levels. The lateral boundary conditions and the initial files are provided by the global ARPEGE model. The three experiments run in this study are all based on the ALADIN Canonical Model configuration described in Termoninia et al. 2018. The fisrt one is the operational configuration (Oper) running with the Bougeault 1985 deep convection scheme, the second (B14) and the third (B21) are using respectively Bechtold et al. 2014 and Becker et al. 2021 as decribed previously in this document. The other physical proccesses are listed in table 1.

3.2 Experiments Results

To assess the impact of each modification on the rainfall diurnal cycle, we compared the 1-hour cumulated rainful from the three experiments to the Global Precipitation Measurments (GPM). The comparison is performed

Table 1: The activated subgrib processes in the operational and modified configurations

Exp name	***Oper***	***B14***	***B21***
Radiation	*RRTMG_LW, SW6: Mlawer et al. 1997, Iacono et al 2008, Fouquart and Bonnel (1980)*	*RRTMG_LW, SW6: Mlawer et al. 1997, Iacono et al 2008, Fouquart and Bonnel (1980)*	*RRTMG_LW, SW6: Mlawer et al. 1997, Iacono et al 2008, Fouquart and Bonnel (1980)*
Turbulence	*CBR Cuxart et al. 2000, Bougeault et Lacarrere (1989)*	*CBR Cuxart et al. 2000, Bougeault et Lacarrere (1989)*	*CBR Cuxart et al. 2000, Bougeault et Lacarrere (1989)*
Microphysics	*Lopez 2002, Bouteloup et al. 2005*	*Lopez 2002, Bouteloup et al. 2005*	*Lopez 2002, Bouteloup et al. 2005*
Clouds	*Smith 1990*	*Smith 1990*	*Smith 1990*
Sedimentation	*Bouteloup et al. 2011*	*Bouteloup et al. 2011*	*Bouteloup et al. 2011*
Orographic gravity wave drag	*Catry et al. 2008*	*Catry et al. 2008*	*Catry et al. 2008*
Surface scheme	*SURFEX Masson et al.2013*	*SURFEX Masson et al.2013*	*SURFEX Masson et al.2013*
Shallow Convection	*Bechtold et al. 2001, Bazile et al. 2001*	*Bechtold et al. 2014*	*Bechtold et al. 2014*
Deep Convection	*Bougeault 1985*	*Bechtold et al. 2014*	*Becker et al. 2021*

during a summer day: 28 August 2019, over two regions: Sahel (5N-20N,10E-30E) and Ocean (5N-20N, 35W-20W). The results are presented in figure 1. On one hand, the afternoon precipitation peak over land is better simulated in both B14 and B21 when compared to Oper. On the other hand, the B21 experiment shows an improved diurnal cycle in comparison to B14 over land. Moreover, the B21 is closer to GPM observations especially during the afternoon over the ocean region.

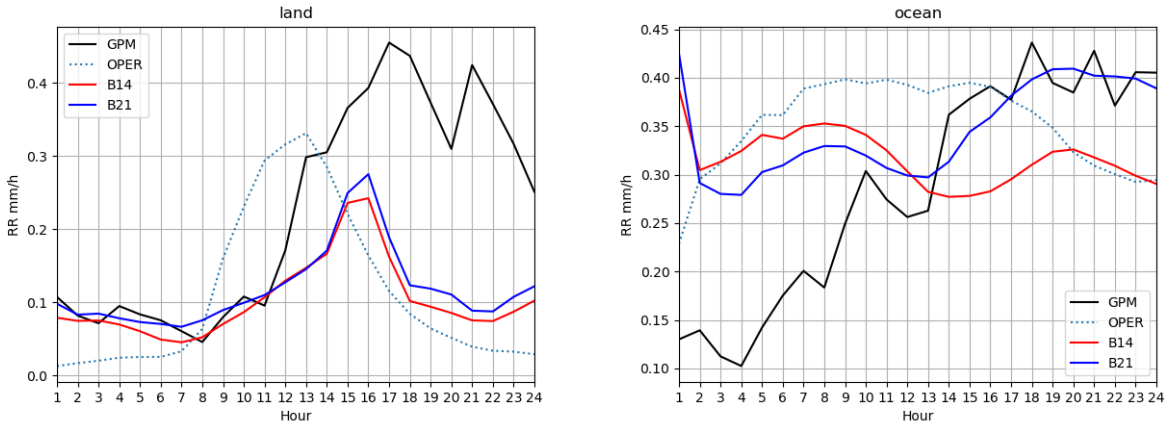

Figure 1: Hourly cumulated precipitation over land (left) and over ocean (right) during a day: 28-08-2019

In order to assess the behaviour of B14 and B21 experiments in terms of the localisation and vertical extension of the convective cells associated with the simulated rainfall, we produced the simulated brigthness temperatures in the infrared chanel $10.8\mu m$. Those simulated quantities in B14 and B21 are compared to the METEOSAT equivalent images. The figure 2 represents those products for 16h, 18h and 22h, and shows that both B14 and B21 are generally similar and are underestimating the vertical extension of some cells.

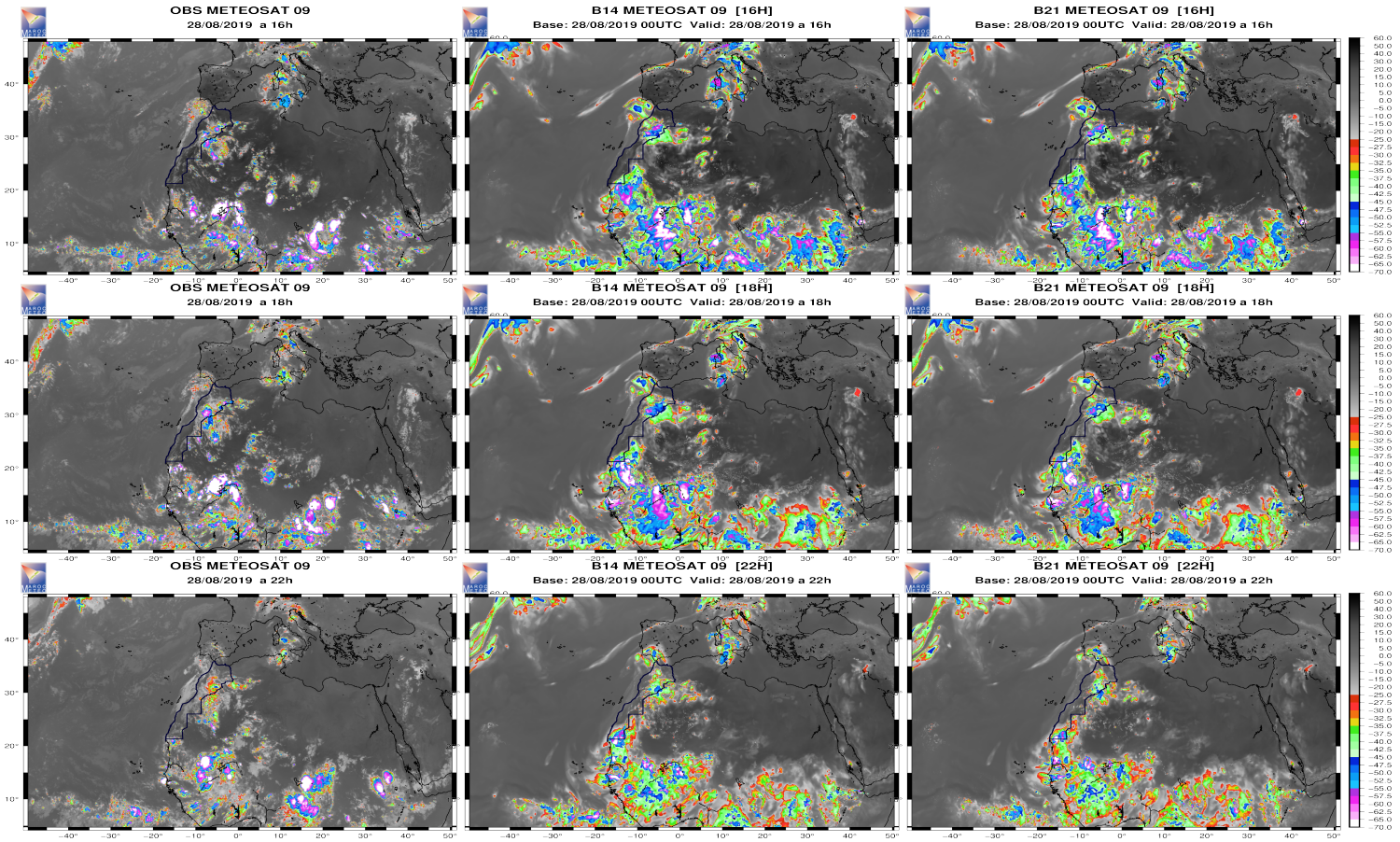

Figure 2: Meteosat Infrared ($10.8\mu m$) *observed (left) and simulated brigthness temperatures by B14 (middle) and B21 (right) for the 28th of august 2019 at 16h, 18h and 22h (resp. from the top to the bottom).*

4 Discussion and future work

In this study, we implemented deep and shallow convection schemes based on Tiedtke 1989 and modified by Bechtold et al. 2008, 2014 in ALADIN-NORAF framework. We have also implemented a modified version of the Bechtold et al. 2014 scheme by incorporating a total advective moisture tendency as done in Becker et al. 2021. The results during one summer day over the north Africa and the Atlantic ocean have shown an improvment in the precipitation diurnal cycle in comparison to Global Precipitation Measurments. More tests are ongoing to cover a longer period.

5 References

Bechtold, P., Köhler, M., Jung, T., Leutbecher, M., Rodwell, M., Vitart, F. and Balsamo, G. 2008. Advances in predicting atmospheric variability with the ECMWF model, 2008: From synoptic to decadal time-scales. Q. J. R. Meteorol. Soc., 134, 1337–1351.

Bechtold, P., N. Semane, P. Lopez, J.-P. Chaboureau, A. Beljaars, and N.Bormann, 2014: Representing equilibrium and nonequilibrium convection in large-scale models. J. Atmos, 71, 734-753.

Becker, T., Bechtold, P. and Sandu, I., 2021: Characteristics of convective precipitation over tropical africain storm-resolving global simulations. Q. J. R. Meteorol. Soc., 147, 4388-4407.

Bougeault, P., 1985: A simple parameterization of the largescale effects of cumulus convection, Mon. Weather Rev., 113, 2108–2121.

Termonia, P. and Fischer, C. and Bazile, E. and Bouyssel, F. and Brožková, R. and Bénard, P. and Bochenek, B. and Degrauwe, D. and Derková, M. and El Khatib, R. and Hamdi, R. and Mašek, J. and Pottier, P. and Pristov, N. and Seity, Y. and Smolíková, P. and Španiel, O. and Tudor, M. and Wang, Y. and Wittmann, C. and Joly, A., 2018: The ALADIN System and its canonical model configurations AROME CY41T1 and ALARO CY40T1, Geosci. Model Dev., 11, 257-281.

Tiedtke, M., 1989: A comprehensive mass flux scheme for cumulus parametrization in large-scale models. Mon. Wea. Rev., 117, 1779–1800.

June 2022 harp working week

Carl Fortelius, James Fannon, Carlos Peralta, Daniel Yazgi, Florian Weidle, Guðrún Nina Petersen

1 Introduction

The Hirlam-Aladin R Package for verification (harp) is being increasingly used within ACCORD for computing and displaying in different ways a large variety of deterministic and probabilistic measures of forecast quality. Exploiting to the full the capabilities of any system as complex as harp takes quite a bit of learning, and many users have developed their own scripts for controlling the work flow. The advantage of having a common interface providing simple, albeit limited control of harp functionalities has been recognized in the community, and consequently the development of such an interface was included in the rolling work plan for meteorological quality assurance. An ACCORD working week was held in Helsinki on 7-10 June 2022, with the purpose to set up a first version of such a common set of verification scripts. We believe that the result, although far from complete, can still be useful for evaluating and comparing forecasts. We hope to attract users who are willing to try using the scripts, and take part in their further development.

2 The working week

The working week was realized as a hybrid event on the premises of the Finnish Meteorological Institute, and attracted 5 participants on site (Daniel Yazgi, Florian Weidle, Andrew Singleton, Carlos Peralta, Carl Fortelius) and 7 participating remotely (Fabiola Silva, Rahma Ben Romdhane, Guðrún Nína Petersen, Gema Morales, Ahto Mets, Emily Gleeson, James Fannon) representing, in all, 11 Member institutes.

The first day was reserved for presentations illuminating the way harp is being used in various institutes and groupings. The remaining days were then spent on working together on coding and problem solving, with a review and status update taking place on the last day. Further details, including the presentations given, are provided on the ACCORD wiki:ă https://opensource.umr-cnrm.fr/projects/accord/wiki/MQAWW202206

3 The ACCORD verification scripts

The first version of he ACCORD verification scripts is an adaptation of software developed for routine verification within UWC-West. They provide a user-friendly interface to harp verification functions. The scripts are available on github in the repository harphub/accord-verif-scripts, and currently support deterministic point verification based on station data. The repository currently includes scripts to:

1. convert into sqlite the ascii files of surface and upper-air observations and corresponding forecasts produced by Harmonie-Arome (i.e. the vobs and vfld files),
2. compute the standard point verification statistics and save to harp .rds files which can be visualized in the harp shiny app,

3. derive additional diagnostics, such as forecast frequency distributions, which are not included in the default harp .rds files,
4. display individual figures from the .rds files, and
5. plot a range of standard verification statistics as png files.

Examples of configuration files, sample observations and forecasts, as well as instructions for easy installation are also included in the repository.

The scope and content of the verification are controlled by editing a small number of configuration files. Currently available metrics and diagnostics are:

- Stored in rds-files:
  - deterministic summary scores and threshold scores
- As graphics files (png):
  - time-mean bias and rmse errors at individual stations displayed as charts
  - bias and stde errors as function of valid time averaged over stations
  - observations and forecasts averaged over stations as function of valid time
  - scatter (density) plots of observations vs. forecast
  - frequency distributions of observations and forecasts
  - observed and predicted diurnal cycles averaged over stations and time
  - vertical profiles of bias and stde error averaged over stations and time
  - score cards

Examples of such plots are shown in Figures 1, 2, and 3.

The set of scripts can be extended to utilize any observations or measures supported by harp (at present or in the future), such as probabilistic verification of an ensemble.

4 Ongoing developments

The common user-friendly interface to harp still needs to be consolidated, enhanced and improved. Capabilities developed Identified topics for improvement include:

- documentation and guidance for first-time users
- generalizing the scripts for ensemble verification. Such capabilities are in use within MetCoOp and under development within UWC-West
- catering for spatial verification methods, under development within UWC-West
- wrapper scripts to extract point forecasts from grib and FA format to be used by harp and/or written to sql database are developed at ZAMG
- optimizing performance and ensuring full functionality of scorecard generation is under development within UWC-West.
- ability to submit verification jobs via ecflow is in use within MetCoOp andă under development within UWC-West

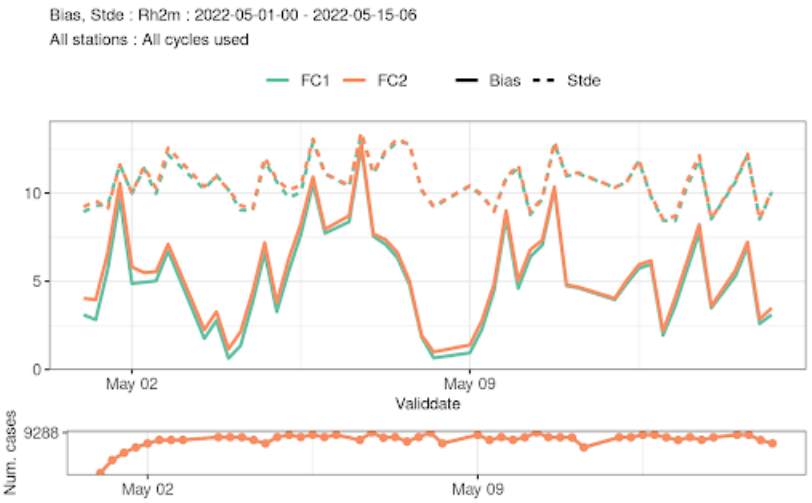

Figure 1: Sample bias and stde error of screen level relative humidity as a function of valid time in two forecasting systems averaged over all stations.

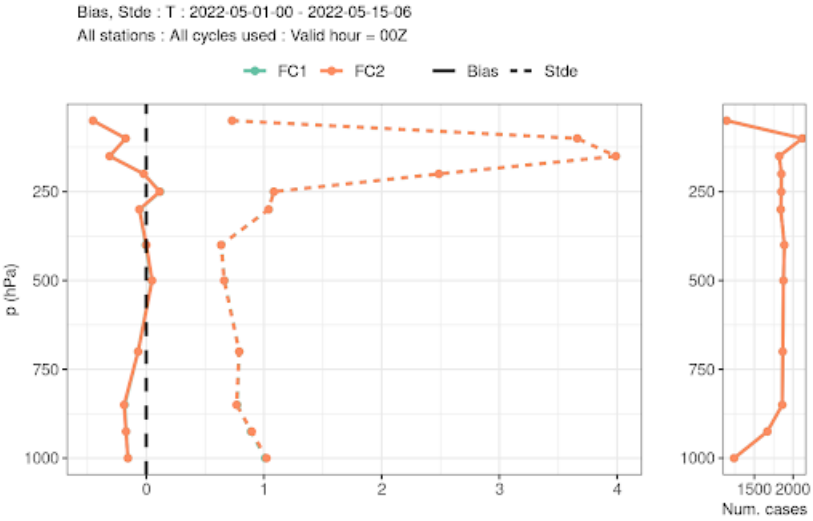

Figure 2: Sample vertical profiles of temperature bias and standard deviation in two forecasting systems at a given valid hour (00Z in this case), averaged over all stations and over time.

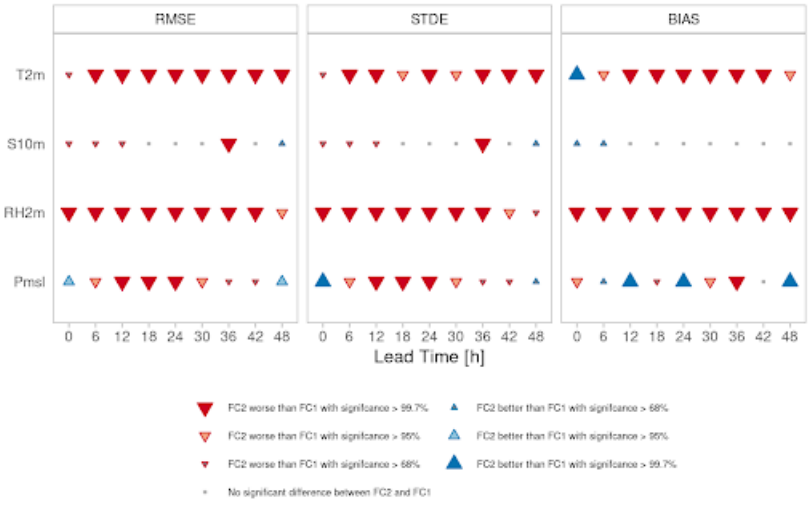

Figure 3: Sample score card for the period 2022-05-01 00 UTC - 2022-05-16 00 UTC.

Monitoring spatial and temporal aspects of precipitation maxima in Limited Area NWP Systems.

Bent H. Sass, Danish Meteorological Institute

1 Introduction

In this note two examples are presented of statistics from post-processing of output from a scheme verifying precipitation maxima in daily runs of the HARMONIE-AROME weather prediction system in DMI. Forecast inaccuracies occur both as a result of spatial and temporal aspects of the forecast. This is illustrated by the provided data.

In the operational Met-Services there is a significant focus on predicting extreme weather because of its large potential impacts on society. Precipitation is among the prioritized weather parameters, e.g. due to the risk of destructive flooding events that may occur as a consequence of extreme precipitation.

Traditional verification schemes used in NWP do not verify extreme precipitation explicitly as part of routine verification. However it seems logical to develop such schemes with explicit focus on verifying the largest values of precipitation, analysed or forecasted. For example, one may ask how well does forecasted precipitation maxima in some geographical area compare with observed (analysed) precipitation in the same area and time period ?

In order to carry out such verification it is a prerequisite that precipitation can be analysed and forecasted as full fields in order to compare the details of the fields spatially. A precipitation analysis based on combining information from calibrated radars in Denmark with measurements from rain gauges on the ground is available and may be compared with fields from HARMONIE-AROME run at DMI. Having this development available a verification scheme was developed and documented (Sass 2021a, Sass 2020) for this type of verification. The scheme is able to assess the ability of an NWP model to forecast maxima and minima correctly in a certain model area over a given accumulation period. The scheme named SLX (**S**tructure of **L**ocal **E**xtremes) has been summarized briefly in the first ACCORD newsletter (Sass 2021b).

In section 2 the data used for this short study is summarized. In section 3 some results are presented and discussed: A focus is on discussing results of a frequency bias computation as a function of accumulated 3h-precipitation thresholds. Also data is discussed that shows the impact of allowing a larger forecast time window to reproduce analysed precipitation accumulation above some threshold. Some conclusions and recommendations are provided in section 4.

2 Data

Data stored from HARMONIE-AROME (“NEA” model domain) at 2.5 km grid size has been compared with corresponding data from the DMI radar based analysed precipitation. Data are verified over 3-hour periods up to 48 hours. Data cover a year, from May 2021 – April 2022. Later data have not yet been included in order to limit the results to be valid to model Cycle 40.of HARMONIE-AROME.

The verification area is covering Denmark with the exception of some islands in the Baltic Sea. The total domain is divided into 4 sub-domains. The size of each is approximately 150 times 190 km. The analysis- and forecast data that are used in the verification are applied and stored with a delay of two days required to secure quality of the precipitation analysis.

In order to save storage only data of maximum forecasted and analysed 3 hour precipitation is stored for the sub-area containing the highest value which may be forecasted or analysed precipitation. These values may be compared in subsequent statistics. Data have been stored monthly in SQLite data files. These have been combined into one file representing data of the whole year. However, data are missing or incomplete for some days due to irregular operations, in July 2021 (11 days) and in August 2021 (9 days) and on few other days.

The statistics from the SLX related computations are currently done from simple postprocessing scripts as suggested in Sass (2021a). By comparing the stored information on initial time and forecast length of the forecasts it is also possible to study the impact of comparing not only the same analysis and forecast periods of 3 hours, but also the impact of accepting information from neighbouring time periods (forecast lengths) as a prediction of the event. This increases the likelihood that e.g. analysed 3 hour values are in better agreement with a forecasted 3 hour precipitation. This implies that credit is given to good agreement between forecast and analysis when forecast- and analysis time periods are different by one or two neighbouring periods. This will be commented on in section 3.

3 Results

In this study the statistics of the verification are averaged over different forecast lengths. This is done in order to increase the number of comparisons used when computing a score. Two examples are provided to illustrate that useful information can be extracted from the data stored.

The first example concerns the computation of frequency bias. It is possible, for the chosen precipitation intervals of the table below, to count the number of analysed and forecasted occurrences respectively in each interval of the table, and from that the associated frequency bias. The observed data counts are also written in the table.

The results of the table indicate that relatively small precipitation accumulations below 5 kg/m^2 in 3 hours are forecasted less frequently than observed. At higher accumulations up to ~35 kg/m^2 in 3 hours an overprediction in frequency occurs. At even higher accumulations, mainly above 50 kg/m^2, an under-prediction occurs. The dry conditions (151 %) represented by the first column may be somewhat uncertain since one may expect that both rain gauges and radar data are somewhat uncertain under these conditions (e.g. Sass 2021a). Interestingly the underestimation up to ~ 5 kg/m^2 in 3 hours is consistent with claims by forecasters that showers of small to moderate intensity are under-forecasted by HARMONIE-AROME. The over-forecasting of frequencies up to ~35 kg/m^2 in 3 hours seems to be less mentioned by forecasters. The under-forecasting of the highest class above 50 kg/m^2 is less surprising: Such extremes are normally associated with very small scale phenomena not resolved by the model.

It should be noted that comparing analysis values with forecast values in all 3 hour intervals leads to a bias of 0.197 kg/m^2 which is only about 5 % of the total average value of 3.89 kg/m^2 analysed. This is re-assuring regarding the values of maxima computed by the scheme, since deviations of this size are to be expected.

The second example is illustrated in the Figure below the table. It shows three curves displaying the percentage of correct forecasts that occur above the values shown on the abscissa. The blue curve shows the average of correct forecasts of 3-hour accumulations that are compared with the corresponding observed accumulation in the same period. The solid and dashed black lines

respectively, show the corresponding percentage of correct forecasts (above threshold on the abscissa), obtained when the forecast period is allowed to be extended by +/- one and +/- two periods respectively. The impact of an extended forecast interval around the observed period is perhaps less mentioned than spatial aspects of the forecast accuracy, but it is a relevant aspect. The two black curves apply to effective forecast intervals of 9 hours and 15 hours respectively, instead of 3 hours. The impact is significant and increases somewhat with increasing accumulation threshold. It is clearly seen that the curves are decreasing with increasing threshold. This is to be expected since higher precipitation amounts are expected to be more difficult to predict than low values. The number of the blue curve, below 30 % at 20 kg/m^2, might appear to be low. However, some of the realized values in the sub-area with observed maximum could be just below 20 kg/m^2. Alternatively a forecast value above 20 kg/m^2 might occur in a neighbouring sub-area. This is possible as long as the highest (observed) value occurs in the current sub-area. A possible occurrence of a larger value in a neighbouring area could be investigated by choosing a larger sub-area size. A special choice would be to choose the entire verification domain, which is 4 times as big as the current choice. One may also note that predicting values above, say 20 kg/m^2, at a given time is difficult considering its small statistical occurrence estimated from the table, indicating a frequency of about 4 %.

TABLE

Precipitation interval (3-hour period)	**< 0.2 kg/m^2**	**[0.2, 1 [kg/m^2**	**[1, 2 [kg/m^2**	**[2,5 [kg/m^2**	**[5,10 [kg/m^2**	**[10,20 [kg/m^2**	**[20,35 [kg/m^2**	**[35, 50 [kg/m^2**	**> 50 kg/m^2**
Frequency Bias (%)	151	61	70	84	114	125	112	96	20
Data counts	7487	8524	6002	10179	5300	2561	1044	278	430

Frequency bias and data counts applying to the precipitation intervals shown in the table.

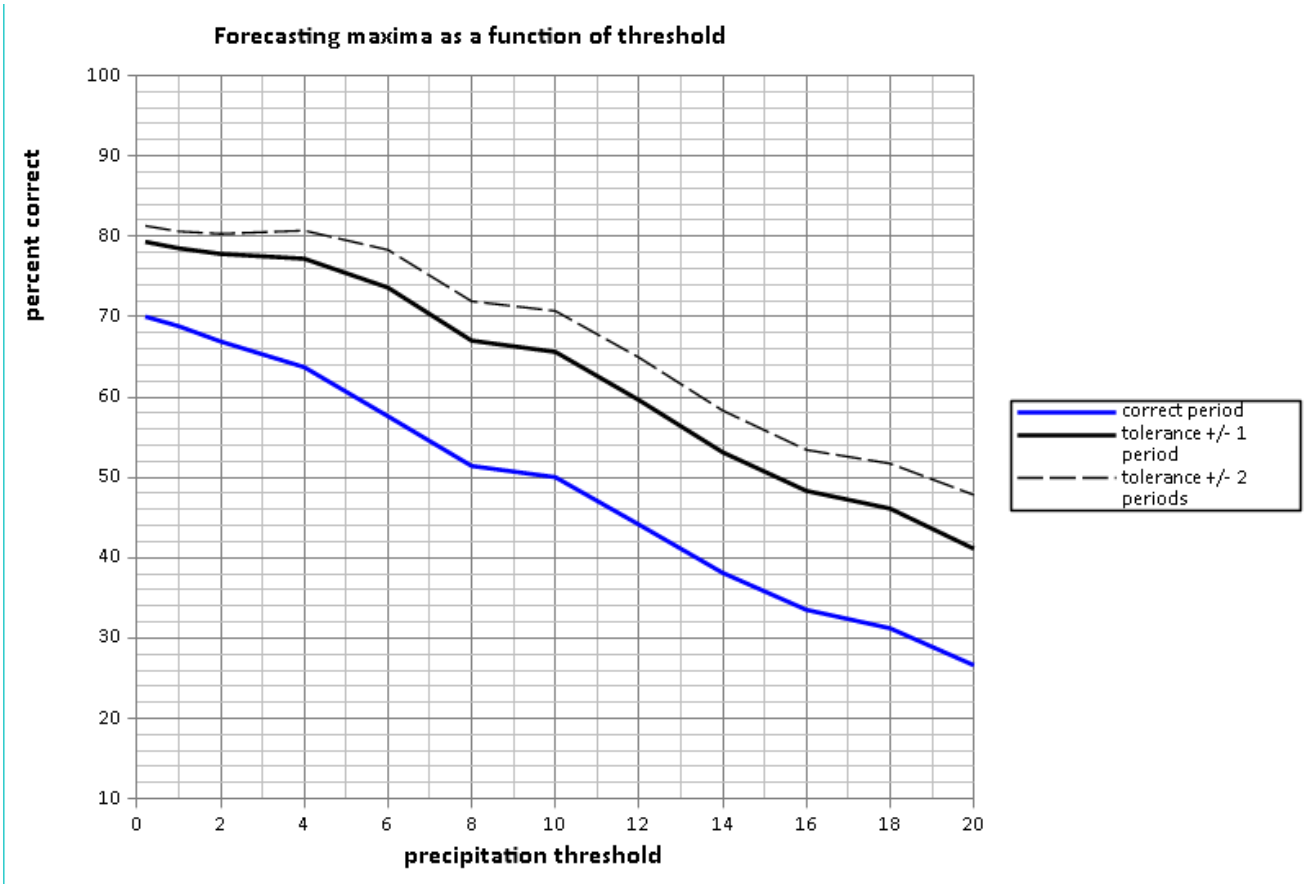

4 Conclusions and recommendations

A short extract from a preliminary study has been presented to illustrate the potential of postprocessing from schemes computing statistics from analyzing and forecasting spatial and temporal aspects of precipitation in a limited area NWP system. The post-processed results indicate that HARMONIE-AROME (CY40) under-predicts the occurrence of precipitation accumulations in the interval up to about 5 kg/m^2. At higher thresholds up to about 35 kg/m^2 a statistical over-prediction occurs. At even higher thresholds an underprediction occurs. These results may depend somewhat on the LAM domain considered. The impact of accepting too early and too late forecasting of precipitation events compared to the true observed period has been seen to be significant when studying the percentage of 'correct' forecasts.

When developing improved NWP an obvious goal is to demonstrate that new model versions are able to improve on the prediction of high precipitation amounts. This aspect of NWP could be investigated in parallel setups of verifying two model versions producing comparable verification statistics. It is preferable to deduce statistics over one or several past years forecasted with the two model versions, in order to produce reliable estimates of statistics as a function of precipitation thresholds, especially when considering NWP for domains with long periods of dry weather patterns.

Studying the sensitivity of the spatial verification to domain/sub-domain size used in the computations is desirable. Emphasis could be paid to the most important spatial- and temporal aspects of the current NWP applications. Considering ensemble model systems will allow developments of probabilistic aspects of the verification (Sass 2021 a).

A prerequisite for a continuous availability of high quality precipitation analyses, needed in a spatial- and temporal verification, is that measurements from rain gauges and from radar systems can be monitored and maintained. This requires that competent staff resources are continuously available.

5 References

Sass, Bent H., DMI (2021 b): Precipitation extremes in NWP, ACCORD NL 1 , 9 pp, October 2021

Sass, Bent H. (2021 a): A scheme for verifying the spatial structure of extremes in numerical weather prediction: exemplified for precipitation, Meteorological Applications , http://dx.doi.org/10.1002/met.2015

Sass, B.H. 2020: Forecasting spatial structure of local precipitation extremes : International Verification Methods Workshop Online (2020-IVMW-O), Nov.2020, https:// jwgfvr.univie.ac.at

GAM models for post-processing the ALARO wind speed

Alexandra Crăciun (Meteo-Romania)

1. Introduction

This study presents some results regarding the evaluation of a statistical calibration method applied to ALARO model output, with the purpose to investigate if such models can be applied to obtain more realistic wind speed in specific areas, such as mountain stations.

2. Experiments and results

Previous verification studies showed that the wind speed is more difficult to be accurately estimated for some complex topography regions in Romania. The general landscape is characterised by the central placement of mountains, followed by the surrounding hilly regions, as well as some other regional features that influence the wind flow locally, such as the position of the Black Sea. Nowadays, many statistical methods have been designed and implemented in order to improve the forecast of different meteorological parameters, by means of post-processing the direct model output. One of these methods was implemented and evaluated for the wind speed forecast of ALARO in Romania. This method consists of applying GAM (Generalized Additive Models) models (Hastie and Tibshirani, 1986; Wood, 2006) to estimate wind speed. These are regression models that allow for more complex relations (than a single predictor simple regression model) between the response variable and the predictors. Several GAM models were defined in a progressive manner, going from one predictor to several predictors considered to be of interest for the wind speed forecast.

The first GAM model presented in this study (m1) is practically a simple regression model (one single predictor which is the wind speed simulated by ALARO). Model m2 takes into consideration the coordinates (latitude and longitude) of the point where it is applied; model m3 includes the altitude of the station; m4 includes the simulated wind direction; m5 adds the 24 hours lagged simulated wind speed; m6 takes into consideration two local characteristics: the distance to the Black Sea and the number of urban pixels within 3 km radius for the point considered. More detailed description for the definition of the models may be found in (Brabec et al, 2021). Technical implementation was done using the R package *mgcv* (Wood, 2011). To summarise briefly, the predictors each model involves are the following:

- m1 – simulated wind speed
- m2 – station latitude and longitude
- m3 – station altitude
- m4 – simulated wind direction
- m5 - 24 hours lagged simulated wind speed
- m6 - the distance to the Black Sea and the number of urban pixels within 3 km radius

The choice of these predictors is a way in which the effect of some local characteristics is taken into account. Typically, this type of regression model requires a training or fit period. In this study, these

models were applied for a one year training period (the year 2021), and then they were used to estimate the wind speed for a five-month period: January – May 2022. The GAM models are applied for hourly 10 m wind speed and pointwise for 157 meteorological stations in Romania. ALARO model data is extracted for the nearest grid-point to each meteorological station. The forecasts are obtained from the operational model version, from the 00 UTC run. This is characterised by the following setup: 6.5 km horizontal resolution, 60 vertical levels, ALARO 0 physical package and cy43. Statistical scores were computed in order to evaluate the wind speed obtained with these models. Figure 1 shows the bias and RMSE values for the ALARO forecast and each proposed GAM model, computed for the whole period and all stations. While the bias values for all models are very small, ranging between -0.15 to 0.1 m/s, it seems that in the RMSE score, we can observe some gradual decrease in the values coming with each model m1 to m6.

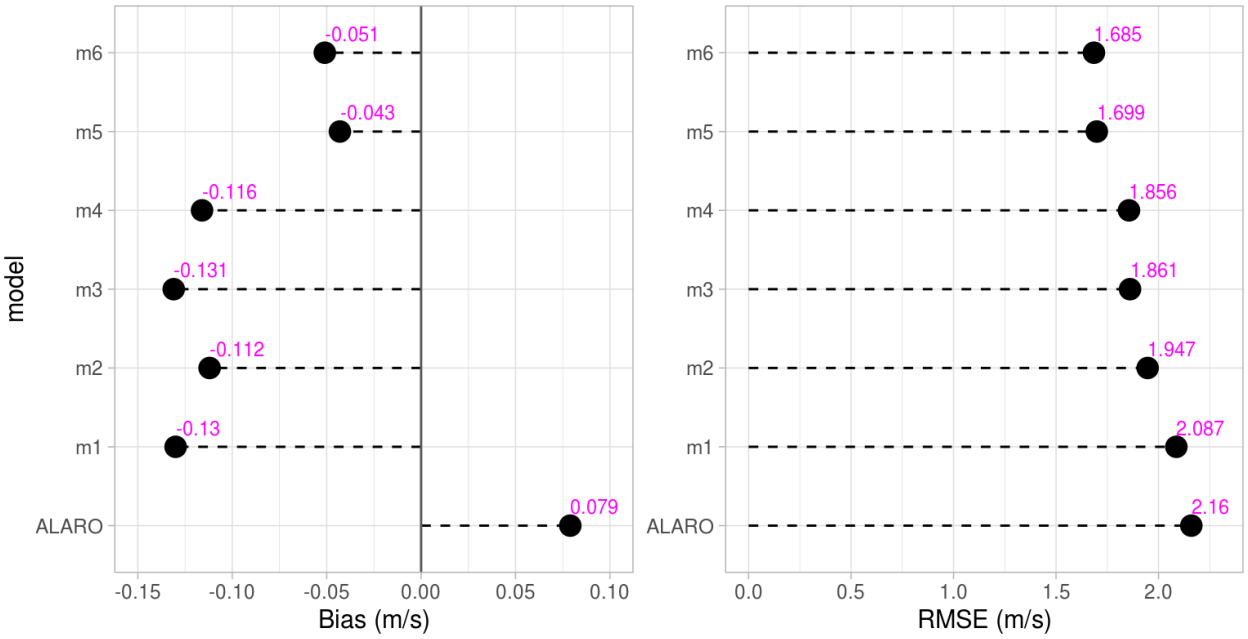

Figure 1. Bias and RMSE for all considered models for the period January – May 2022.

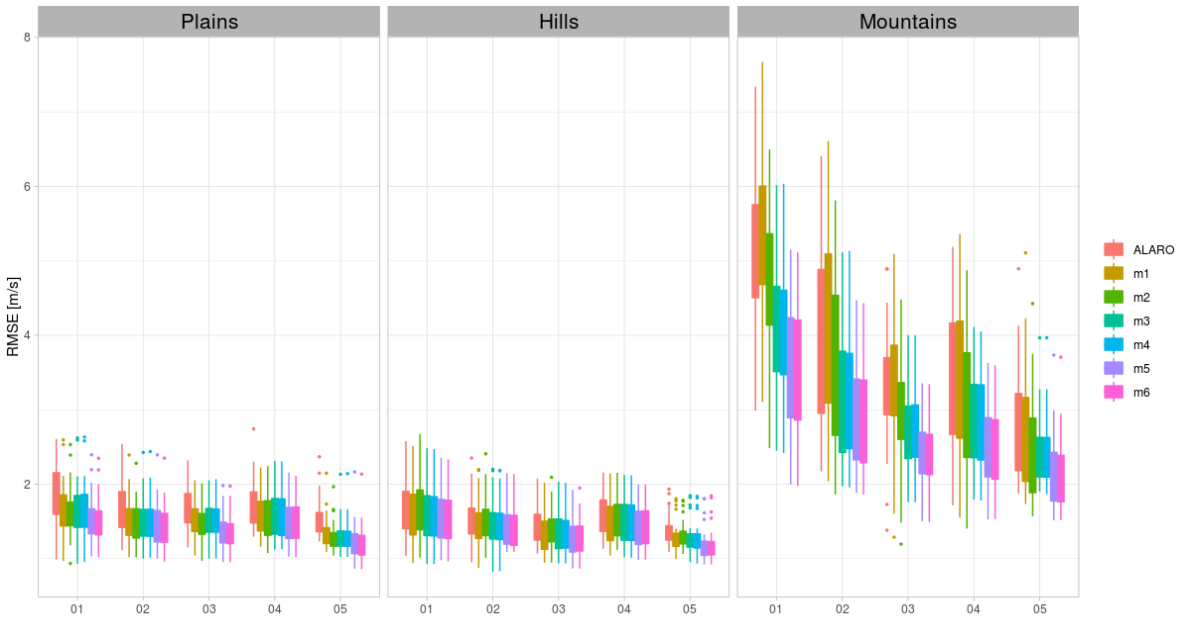

Figure 2. Boxplots of daily RMSE values for each month, model and altitude type (plains – stations

located between 0 and 300 m, hills – between 300 and 800 m and mountains - over 800 m).

In order to further analyse the indication of improvement seen in the RMSE values, daily RMSE score was computed for each month. In addition, since the GAM models are defined as to consider some local features, the score was also computed for three major relief categories: plains, hills and mountains.

It was observed from the RMSE scores (figure 2) that the models indeed show different results, depending on the month or altitude of the station. For the plains category, there is a slight decrease of the RMSE values for each GAM model compared to the ALARO forecast. For stations located in hilly regions, it seems that there are only very slight differences between the forecasts. Improvements are more visible for mountain stations, where the ALARO forecast leads to larger values of the score. Lowest values for the daily RMSE in this case are found for models m5 and m6. These results show that in this case having a more complex defined GAM model leads to more significant improvement.

It can be noticed that models m5 and m6 seem to be more similar in performance. Model m6, in addition to model m5 introduces two new elements: the distance to the Black Sea and number of urban pixels within a 3 km radius. The idea came when larger wind speed errors for the ALARO forecast were observed in points that represented stations located close to the Black Sea, since weather conditions might be more difficult to simulate in such areas. Also, forecast was found to be more problematic for stations that with time became more and more surrounded with urban areas and landscape. Typically, this kind of vicinity may lead to some forecasting issues.

An example that illustrates the behaviour of these models can be seen at two stations that are relatively close to each other and in the same altitude range: stations 15421 (București – Afumați) and 15422 (București – Filaret). The first one is outside Bucharest, while the second is located inside the city. Figure 3 shows the daily bias of wind speed from models ALARO in comparison with model m5 and model m6. It can be seen that while real wind speed is overestimated (the bias is computed as the difference between the forecasted and observed values) by the ALARO model, models m5 and m6 lead to better scores. Model m6 adds some slight improvement to the values.

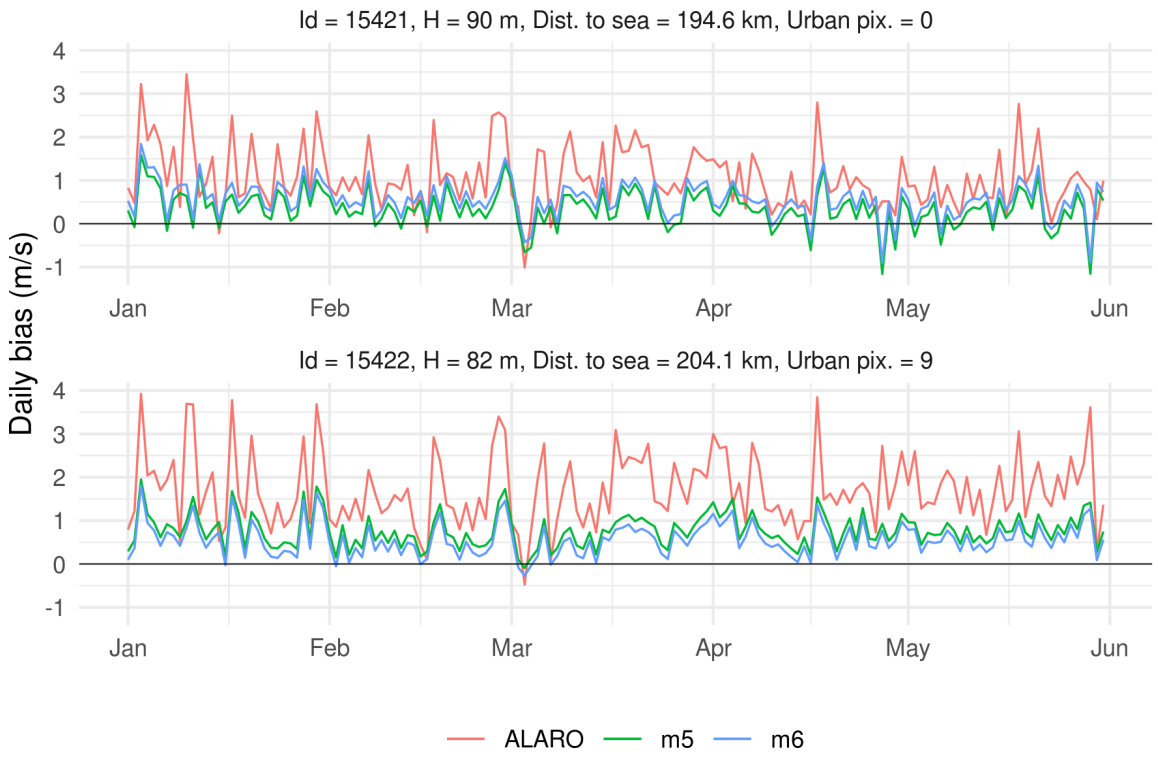

Figure 3. Daily bias of wind speed from ALARO (red), model m5 (green) and model m6 (blue).

Taking into consideration the indication that more benefit may be found in applying the GAM models in mountain stations, the forecast for the station Varful Omu (located at 2506 m altitude) is analysed. Daily mean wind speeds are shown for models m1 (figure 4) and m6 (figure 5) compared to ALARO and the observed wind values. It can be seen that while model m1 shows very slight differences compared to ALARO in this case and both underestimate the real wind speed, model m6 leads to wind speeds closer to registered values. However, it can be seen that some peak values are overestimated by model m6.

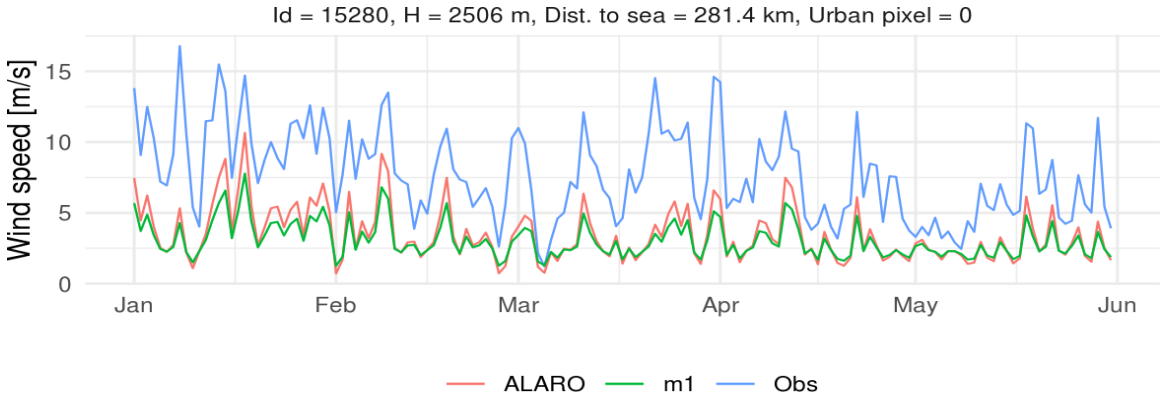

Figure 4. Daily mean wind speed from ALARO (red), model m1 (green) and observations (blue).

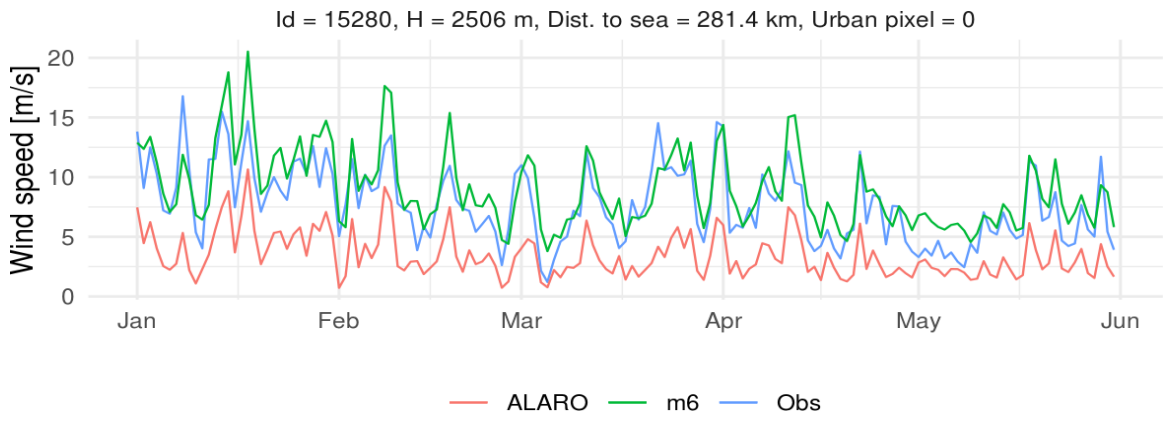

Figure 5. Daily mean wind speed from ALARO (red), model m6 (green) and observations (blue).

Further analysis was done for model m6. Daily differences of the RMSE values between model m6 and model ALARO are shown in figure 6. The results are shown for each month and relief category. Larger negative values mean that model m6 leads to better values of the score. It seems that with very few exceptions, model m6 improves the score values. Most improvements are visible in winter months, January and February, for mountain stations, as was concluded from results in figure 2.

In cases where these differences are very small, it should be decided if the post-processing of the ALARO model output is necessary. For example, it may be found that a post-processing technique proves beneficial for specific cases, where the NWP forecast shows to be problematic. From the results obtained it is visible that for example, mountain stations can be a possible candidate for this purpose. These stations were selected for a more detailed evaluation for a specific winter case, the 30th of January 2022, when strong winds have occurred. The mean registered wind speed is represented in figure 7. Figure 8 shows the mean bias and RMSE for models ALARO and m6 for the considered date. These scores show that in almost all stations, the simulated values from m6 lead to smaller errors. To go into more detail and see if an hourly forecast can be feasible using model m6, hourly biases were computed for models ALARO (figure 9) and model m6 (figure 10). It can be observed that for many stations and forecast hours, the biases are smaller for model m6 compared to model ALARO, for example stations 15317, 15088 or 15108. On the other hand, some stations can be found where for night hours, the GAM models have smaller bias, while for daytime, ALARO performs better (station 15280). This leads to the overall small error observed for the daily score in this case. Hence, careful evaluation must be made before choosing the appropriate situations where the post-processing can be successfully applied.

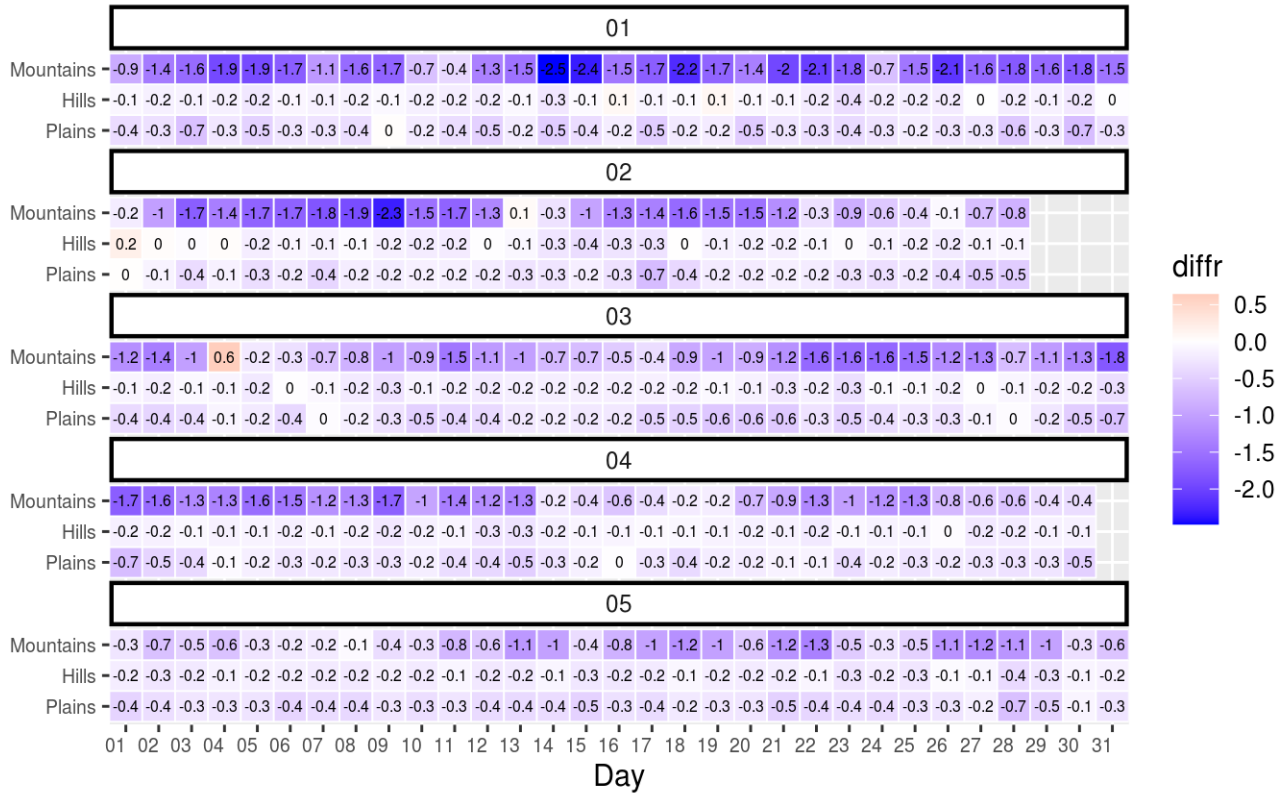

Figure 6. Differences of daily RMSE values between model m6 and ALARO, for each month and relief unit.

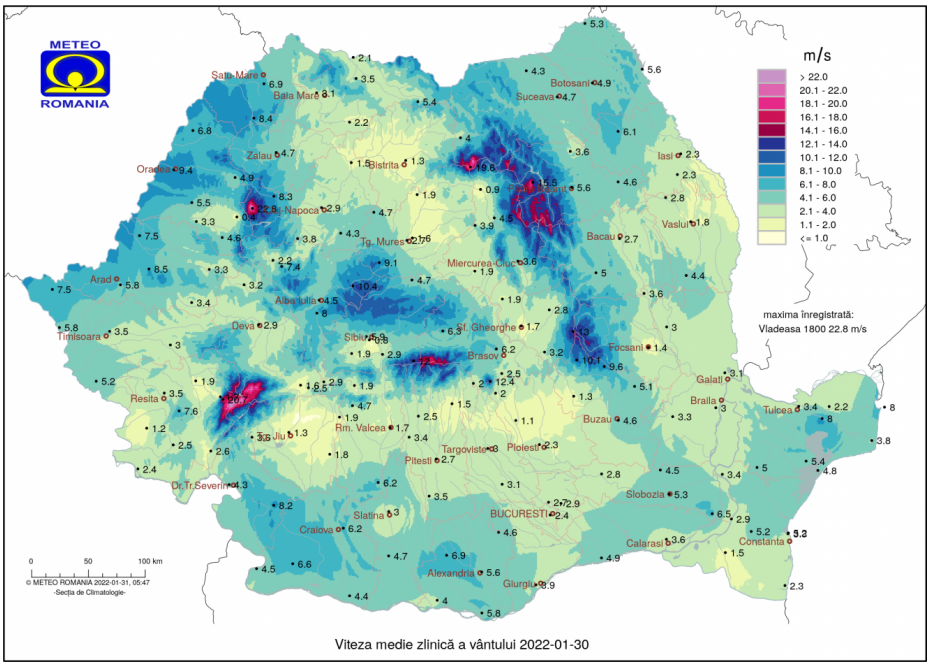

Figure 7. Daily mean wind speed for the case of 30.01.2022. Figure source: internal webpage of the Romanian National Meteorological Administration, Department of Climatology.

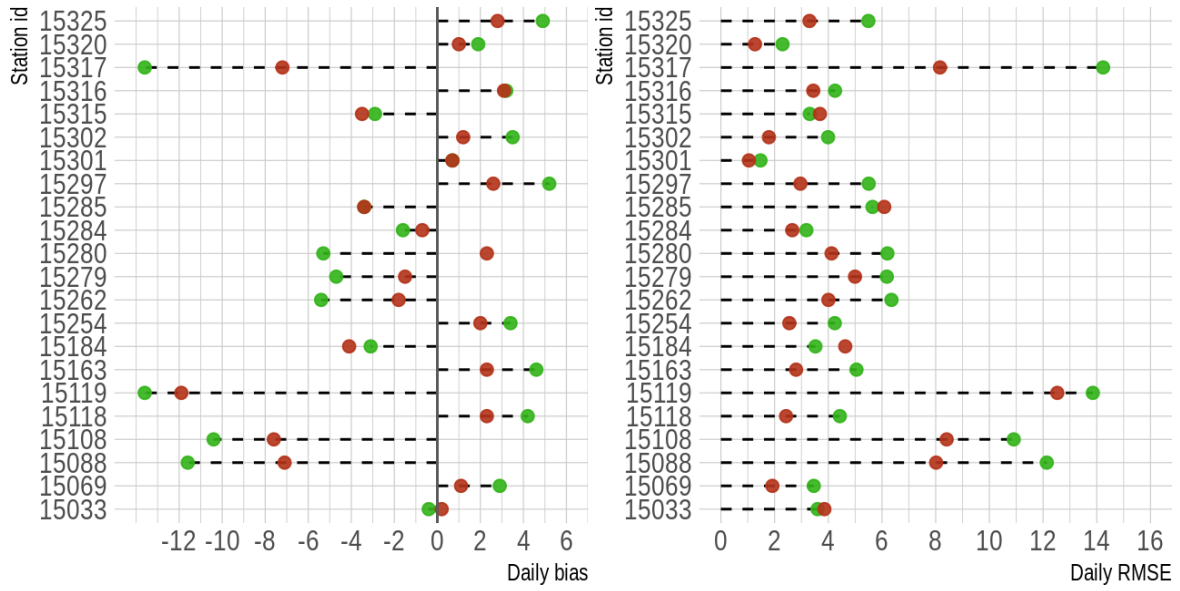

Figure 8. Daily bias and RMSE for the forecast of ALARO (green dots) and m6 (red dots), for each mountain station, for the case of 30.01.2022.

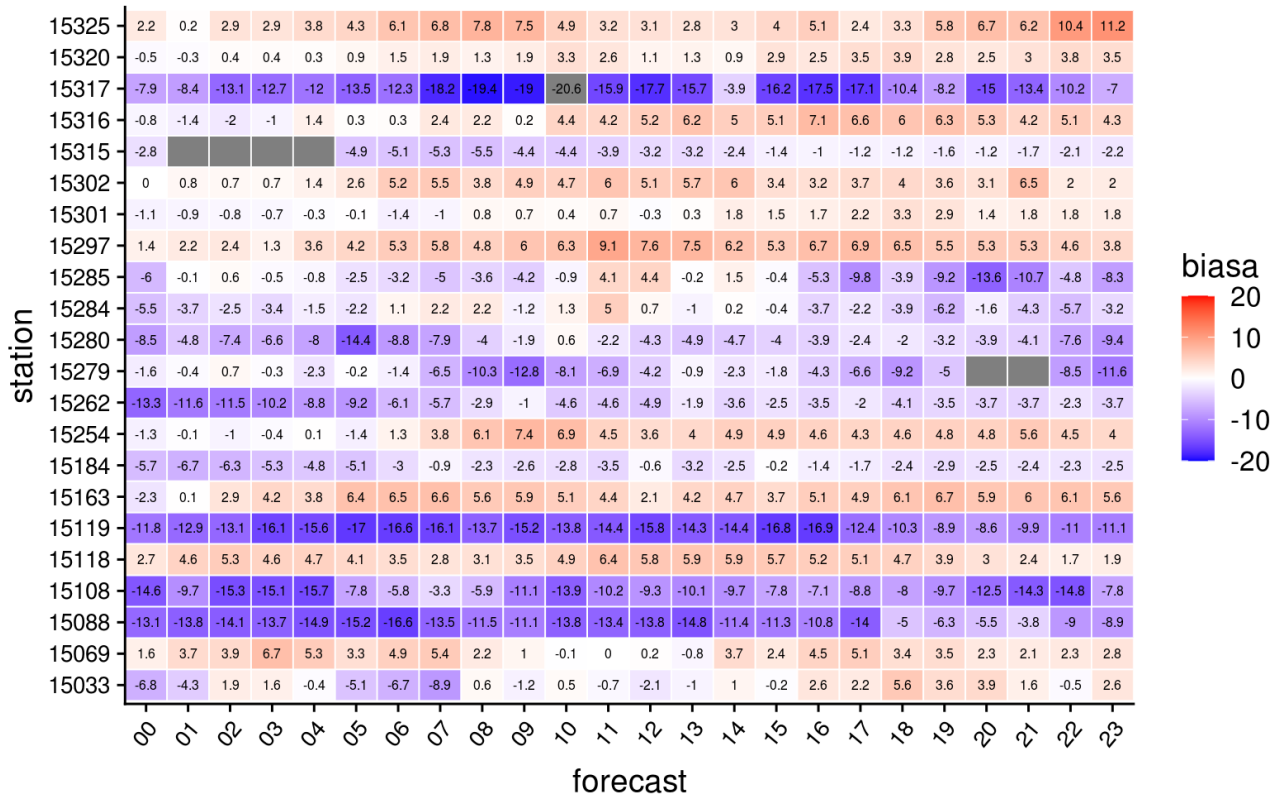

Figure 9. Hourly biases of model ALARO, for each mountain station, for the case of 30.01.2022.

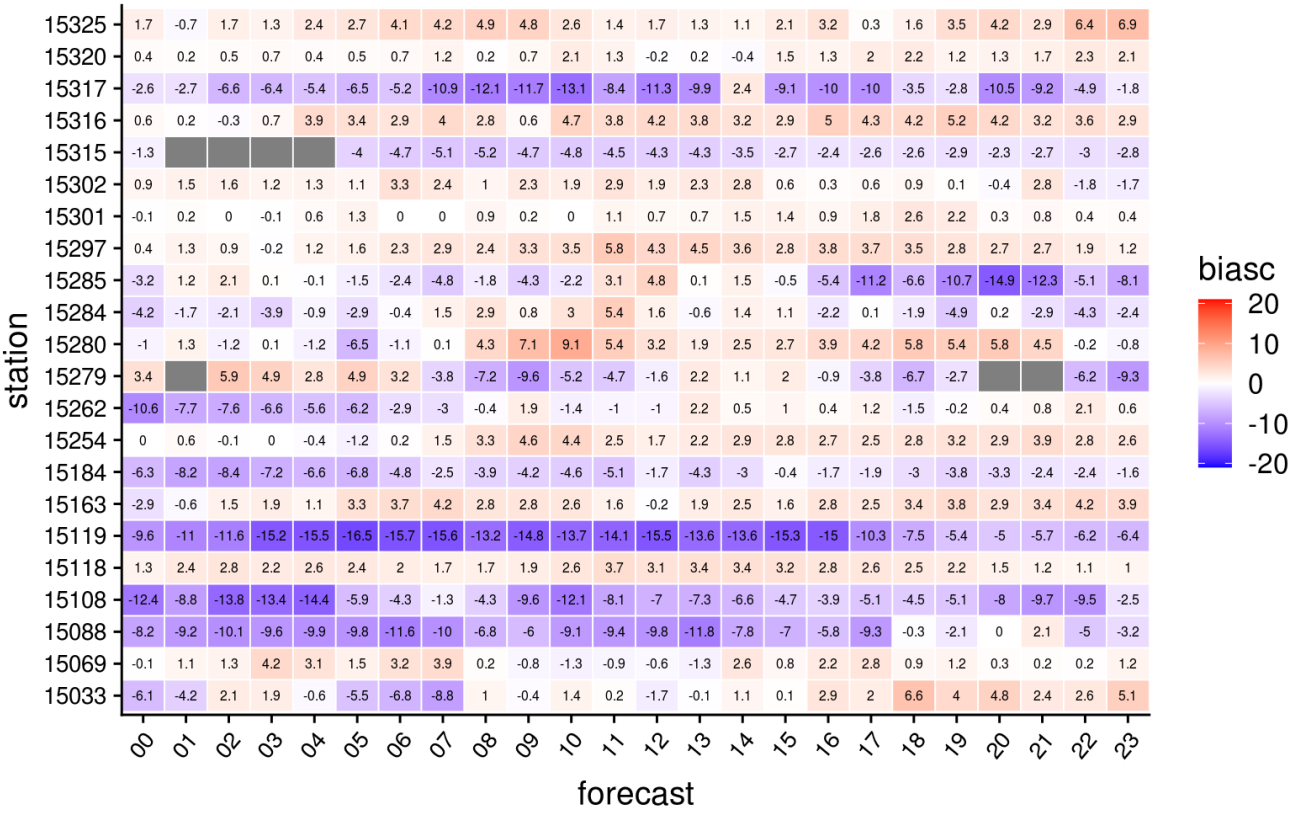

Figure 10. Hourly biases of model m6, for each mountain station, for the case of 30.01.2022.

3. Conclusion

These results show that this type of post processing method (which is quite easy to implement using R tools and relatively computationally cheap) can be found useful for specific cases where the model forecast proves problematic. Such local characteristics that have a significant influence on wind speed are more difficult to tackle for coarser resolution models and it should be expected that some would be better taken into consideration with higher resolution models. Limitations of the statistical validation should be also kept in mind, in the sense that, for example – when the scores are computed, nearest model grid points are considered in comparison to the observation point values. Other averaged values of scores may also lead to overlooking some more detailed information.

Acknowledgments

Special thanks to all my colleagues in the Romanian ACCORD group for their valuable help, feedback and suggestions with this work.

References

[1] Brabec, M., Craciun, A. and Dumitrescu, A., 2021. Hybrid numerical models for wind speed forecasting. Journal of Atmospheric and Solar-Terrestrial Physics, 220, p.105669.

[2] Hastie, T.J., Tibshirani, R., 1986. Generalized Additive Models. Stat. Sci., 1, 297-310. https://doi.org/10.1214/ss/1177013604.

[3] Wood, S.N., 2006. Generalized additive models: an introduction with R. Chapman and hall/CRC.

[4] Wood SN, 2011. Fast stable restricted maximum likelihood and marginal likelihood estimation of semiparametric generalized linear models. Vol. 73, Journal of the Royal Statistical Society (B). 2011. p. 3–36.

Some news on operational validation work at ARSO

Jure Cedilnik, Neva Pristov, Benedikt Strajnar, Neža Lokošek, Eva Bezek, Matic Šavli

1 Introduction

The current operational model resolutions at ARSO in Slovenia are 4.4 km (up to 72 hours ahead) and 1.3 km RUC (forecast length of up to 36 hours – mostly intended for nowcasting), ALARO physics is used in both cases (see Table 1 for details).

This newsletter contribution describes the 4.4 km short wave radiation verification compared to in-situ data, the initial convection related subjective validation of the 1.3 km RUC model with some rather innovative visualisations and the preliminary results of high-resolution wind climatology generation using the 1.3 km model.

Table 1: Description of operational suites running at ARSO[1].

	4.4 km	1.3 km RUC
Code version	cy43t2_bf10, ALARO-v1B physics	cy43t2_bf10, ALARO-v1B physics
Resolution	4.4 km, 87l , 450x450 points	1.3 km, 87l, 600x600 points
Time step	180 s	60 s
Coupling	ECMWF, space consistent, every hour	ECMWF, space consistent, every hour
Cut-off times	45 min	35 mins after nominal time, (double for assimilation cycle)
Production frequency	Every 3 hours (00, 06, 12, 18 up to +72 h, 03, 09, 15, 21 up to +36 hours)	Every hour, up to +36h
Radar reflectivity assimilation	no	yes
Output	Hourly	Hourly, Some fields every 5 minutes

2 Shortwave radiation verification in 4.4 km

A verification of shortwave radiation in the 4.4 km operational model using the ACRANEB2 scheme has been performed against in-situ measurements.
The consistent underestimation of about 50 W/m2 solar radiation flux during daily maxima in clear sky conditions has been observed. The reason for this significant discrepancy is probably due to use of climatological aerosol values (Tegen).
During this study some very low values of model solar radiation have been observed in the mid of the day in June - many below 200 W/m2 and a few even below 20 W/m2. Initially met with scepticism, it

1 SEEMHEWS suite running operationally at ECMWF not listed here.

has been eventually understood that these model grid points are related to thick optical depth associated to 100% cloud coverage due to convection and heavy precipitation. A deeper insight into station data revealed that this is indeed also occurring in nature, of course generally not at the same time and location. See histograms in Figure 2 for an illustration.

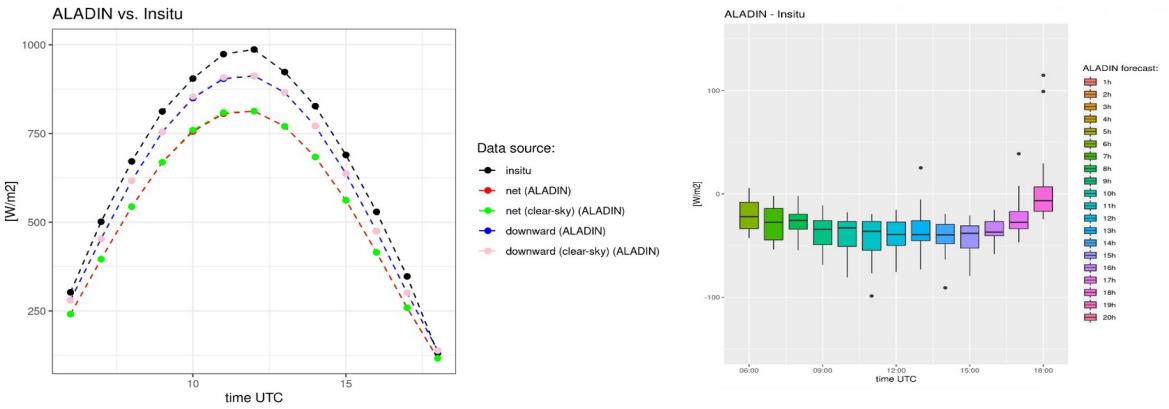

Figure 1: *Comparison of averaged daily distribution of shortwave radiation insitu vs. model (left) and the corresponding error distribution (right) for 13 selected stations in Slovenia for 10 clear days of summer 2021.*

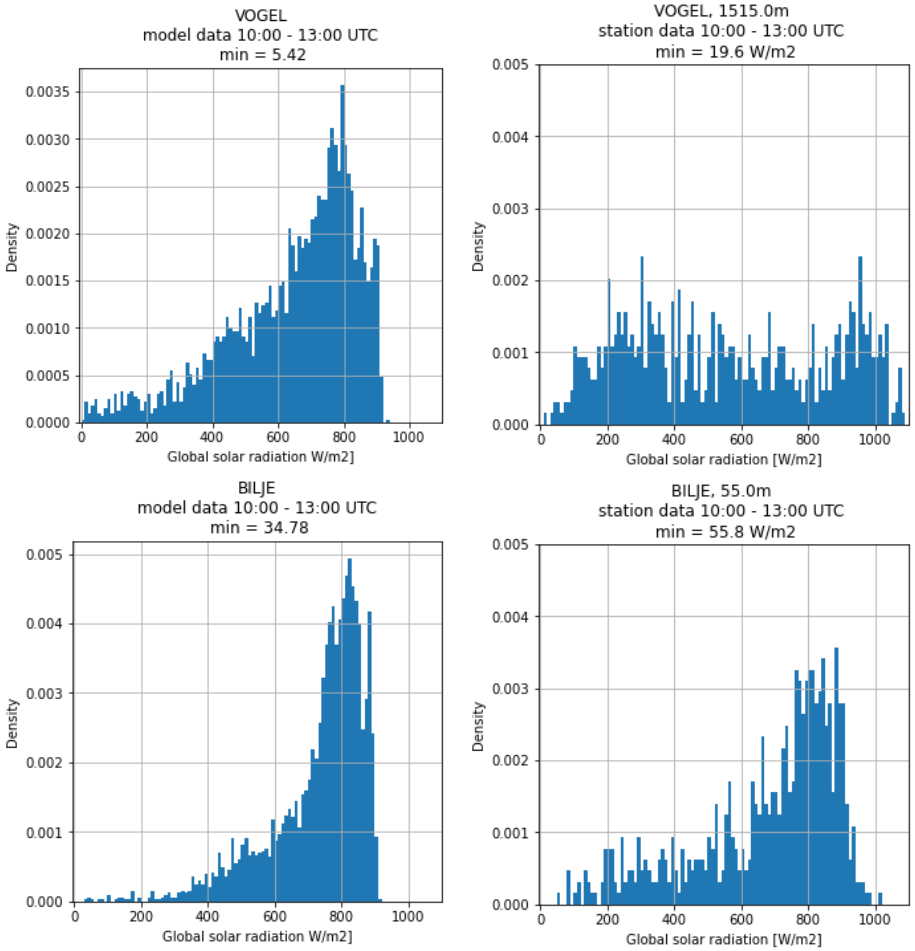

***Figure 2**: Hourly global solar radiation distribution (relative number of cases in the interval of 10 W/m2) for one mountain (top) and flat land station (bottom); model in the left column and measurements in the right for the period of JJA 2021 between 10 and 13 UTC (centred around local noon).*

3 A convection focused subjective validation of 1.3 km RUC

The RUC system was put in operations in spring 2022 and has been since then mainly used by the forecasters during the convective season. In general, three desired qualities of such a high-resolution RUC model are pursued:

1) *Actuality*: The ability to simulate the convection as it is in progress; to capture the convection cells as they pop-up and while they grow, as they are assimilated through radar measurements. Ideally, the latest model run would simulate the convection exactly where it occurs.
2) *Consistency:* The desired monotonous shift of the model from run to run towards reality; is the model able to gradually shift convection cells or the centrepoint of convection activity towards where it happens in reality and adjust its timeliness. Ideally consistent, all model runs would simulate the convection activity in the same location and at the same time.
3) *Nature*: The ability of the model to capture the nature of the convection process or the convection mode; is it slow or fast moving, what is the longevity of the cells, backbuilding or not, is the nature of cells supercellular...

Several new visualisations were implemented in order to address this goals. The points 1) and 2) were tackled by plotting a huge multi run matrix of reflectivities of a lagged ensemble compared to the observed radar reflectivity. This is a so-called “post-stamp radar plot”, see Figure 1. To examine the actuality, top right triangle in the first two rows is studied: the information from the radar in the previous hour has entered the model run and ideally should manifest itself in the second row one cell to the right at forecast of +1 hour. Secondly, to observe the consistency, each single column of the model is compared: how different are the images of +1h to the older ones of up to +10h. The case in Figure 3 is presented as an example, but further comprehensive analysis shall be carried out in the future to encompass the entire convective season.

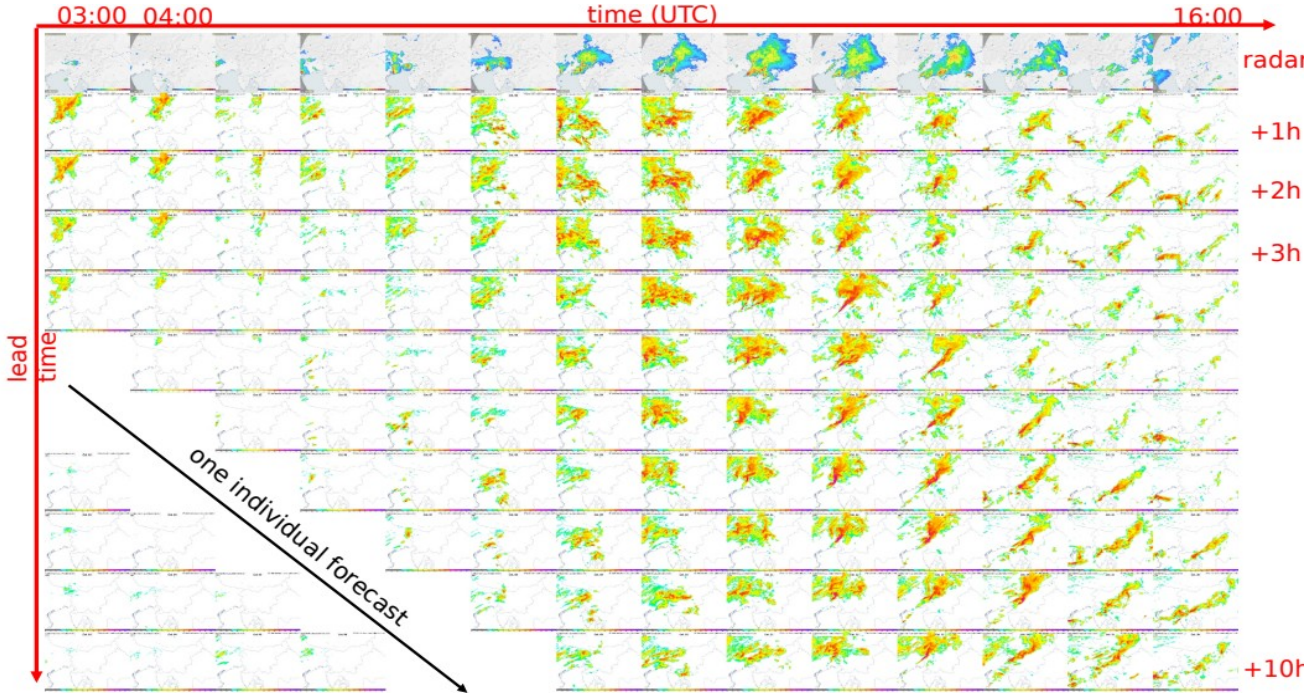

***Figure 3**: RUC validation: the so-called poststamp radar plot: top row is the time axis with radar reflectivity at every hour, every column below consists of all available model results for corresponding validity time: 1st row are +1 hour forecasts and 10th row +10 hour forecasts. In this view, an individual forecast lies on a diagonal line. The case presented is for September 8, 2022, an intensive convection associated with a cold front passage.*

To further evaluate the RUC system's consistency, a contour plot of different highest model reflectivities (only 45 dBZ and above) of a lagged ensemble is produced. The lead time of each forecast is depicted using the rainbow colour legend (older runs in red, newest in violet). See an example in Figure 4, where an advancing upper level through led to deep convection in N-Adriatic basin. The conclusion is that in this case the system was able to gradually, from run to run, shift the location of convection towards where it later occurred in reality.

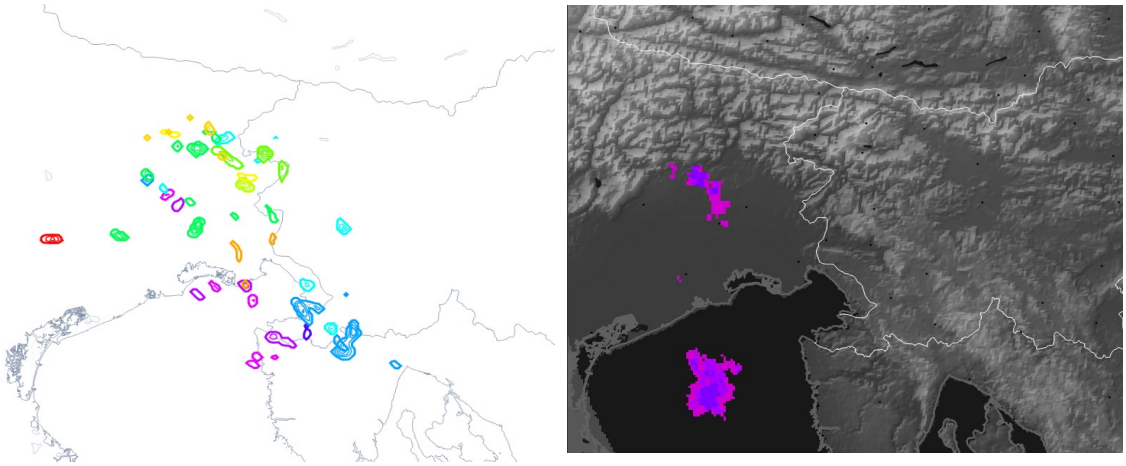

***Figure 4**: 15 August, 2022 23 UTC, contour plot of simulated radar reflectivities (thick line is 45 dBz with thin lines inside for greater values) of a lagged ensemble with colour rainbow legend corresponding to lead time (violet for +1h, red for +12) (left), observed radar reflectivity at the same time (45 dBz and above) (right).*

Lastly, one of the most welcomed features by the forecasters was the very high frequency output for some of the fields, namely simulated radar reflectivity or wind fields. By providing images every 5 minutes, one is able to produce and ad-hoc movie and thereby deduce the nature or the mode of the convection process as it is simulated in the model.

4 Climatology oriented 10m wind verification

With the aim of exploring options for high-resolution wind climatology production, the 1.3 km model wind was verified for a 7 month period (from September 21 to March 22). +1h hour model integration and the lowest model level at 10m was used for comparison against hourly averaged wind from automatic stations.
The preliminary results show a strong underestimation of wind on mountain ridges, see Figure 5 with average relative error for individual stations. On the average, the wind on mountain tops and ridges can be up to 50% underestimated (in some cases even much more) and the opposite is true for valley floors. However, the representativity of station data can be questionable in many cases. As this is still work in progress, a more thorough analysis will be carried out with a longer set of data and further focus on additional measurements from masts and profilers.

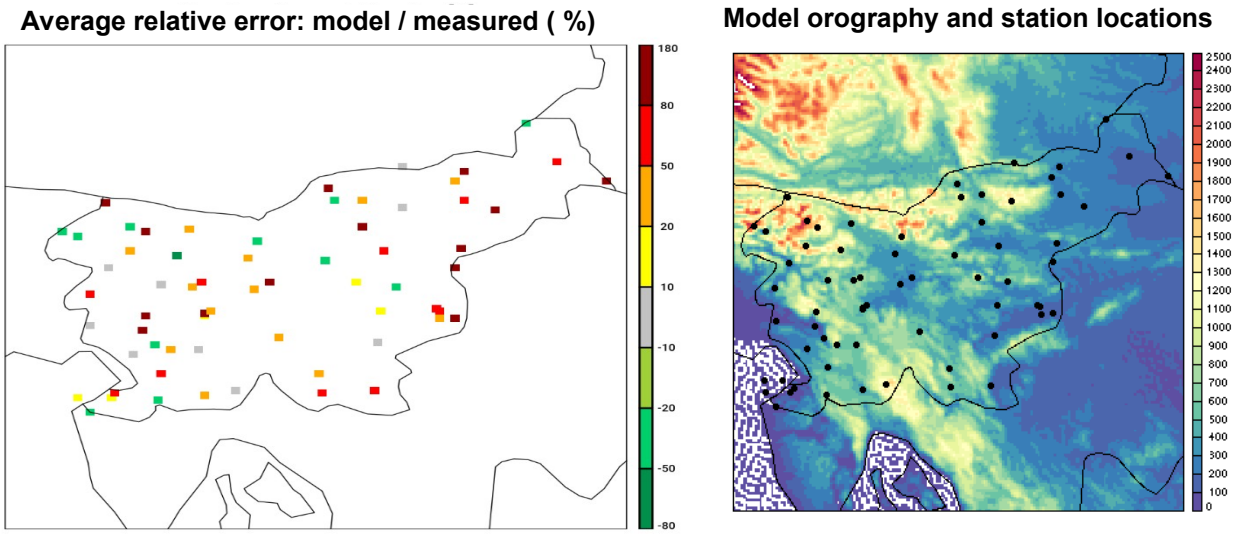

***Figure 5**: Stations with wind measurements used in verification of 10 m wind, with colours corresponding to the average ratio of model over measurement data (left), locations of the same stations plotted on top of model orography (right).*

Recent activities in NWP-Algeria : Compilation of cy46 locally and first use of Harp

Walid CHIKHI [(1)] *,Nour El Isslam KERROUMI* [(1)] *, Zakaria BENGHABRIT* [(1)] , AMBAR Abdenour [(1,2)]

[(1)] Numerical weather prediction department, Office National de la Météorologie ,Algiers, ALGERIA.
[(2)] University of sciences and technology Houari Boumediene, Algiers, ALGERIA

1 Introduction

This report summarizes the first results obtained from the update of our operationnal numerical weather prediction system. Curently, our operationnal suite is based on Cy43t2.bf.10 and we aim to update the system toward the export version made available by Météo France (Cy46T1.bf.07). We mentionned also in this report that we have recently used the HARP [4,5] verification tool, and the validation results presented here are made with this tool.

The different steps made for the preparation of the new operationnal suite on our HPC are discribed in this report. The verification has been made against the operationnal suite (Cy43T2.bf.10) and compared to the ARPEGE analysis and ground stations observations. This update will allow Meteo-Algeria services to better exploit some new diagnostics such as visibility and to improve its products and services .

2 Compilation and installation of Cycle 46 :

In this work, we have used the export version «CY46T1_bf.07 » released on November 2021 and available on «Belenos» under the path tree : ***Belenos:/home/gmap/mrpe/faure/public/export_cy46*** .
For the gmkpack, the last version also was used « gmkpack.6.8.2 ».

The transition from Cy43 to Cy46 on local HPC [1] required an update of certain libraries in order to meet the needs of the latter. Compared to libraries used in Cy43, we have used «eccodes-2.22.0» instead of «grib_api» and we have used the last version of dummies libraries instead of the oldest ones used on Cy43. The compilation of the libraries and the code is done with INTEL compilers (icc,ifort).

At the end of the compilation, only the routines linked to the two projects "**cope**" and "**oopsifs**" were not compiled, and 69 binaries were generated (Tab.01).

Tab.01: Generated binaries after the compilation of Cy46T1.bf.07

ADD_CLOUD_FIELDS	FEDIACOV	**PGD**
ADDPEARP	FESTAT	**PINUTS**
ADDSURF	fscheduler.x	PREGPSSOL
adjust_seqnos.x	GOBPTOUT	PREP
BATOR	hcat	PROCADRE
BLEND	ioassign	**PROGRID**
BLENDSUR	LECBDAP	QSCAT_25TO50
bufr2odb.x	lfitools	QSCAT_BUFR
CHECK_LIMITS	MANDALAY	QSCAT_DCONEQC
CLUST	MASTER911	QSCAT_FILTER
COMBI	**MASTERODB**	revert_seqnos.x
CONVERT_ECOCLIMAP	MRGVARBC	RGRID
create_odb.x	MSE_SURFEX	RTTOV_ASCII2BIN_SCATTCOEF
CTPINI	mysort.x	**RTTOV_CONV_COEF**
dcagen.x	OBSCONVERT	**SFXTOOLS**
DDHC	odbdiff.x	simulobs2odb.x
DDHR	odbmd5sum.x	SODA
DDHT	**odbsql.x**	split_bufr_data.x
EATSTPRO	**odbtools.x**	split_timeslot_bufr_data.x
ETESTADJ	**OI_MAIN**	SURFEX
FCQODB	PERTSURF	SXPOST
TESTADJ	TEST_BIPER	TESTER_GPCOU
TEST_EZONES	TEST_TWOTRUNC	UNHOLO

3 Comparison between 43T2.bf.10 and 46T1_bf.07 export version :

Only the canonical configuration AROME was tested for this report (Tab.02).

Tab.02: Characteristics of the AROME configuration tested with Cy46T1.bf.07

Characteristics	**AROME Configuration**
Initial Conditions	Dynamic adaptation (Coupled with ALADIN-Algeria 6Km)
Coupling range	1h
Time step	180s
Horizontal resolution	3 km x 3 km
Vertical resolution	41 Levels
Lead_Time	48 Hours

A visual comparison can already show a slight difference between the two cycles with AROME. As shown in figure 01 (yellow circle) and the figure 02, we can easily see that AROME-Cy46 gives lower values for the 2 meter temperature than the operational Cy43.T2.bf10.

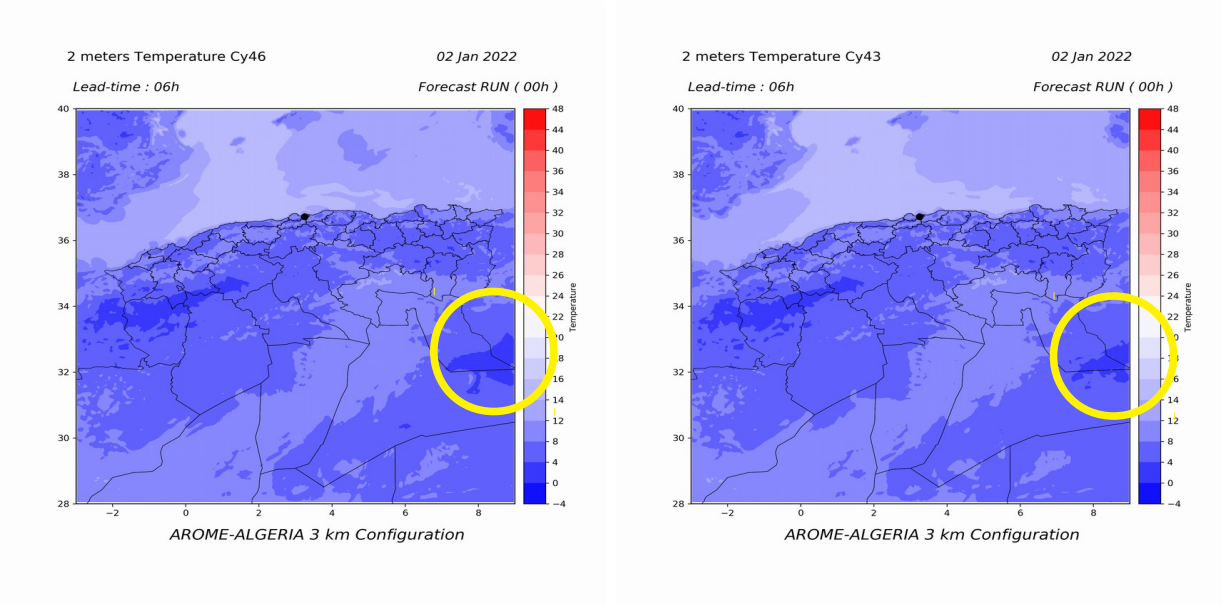

Fig 01 : plots of 2 meters temperature for AROME Cy46 export version (left map) and AROME Cy43_T2_bf.10 (right map).

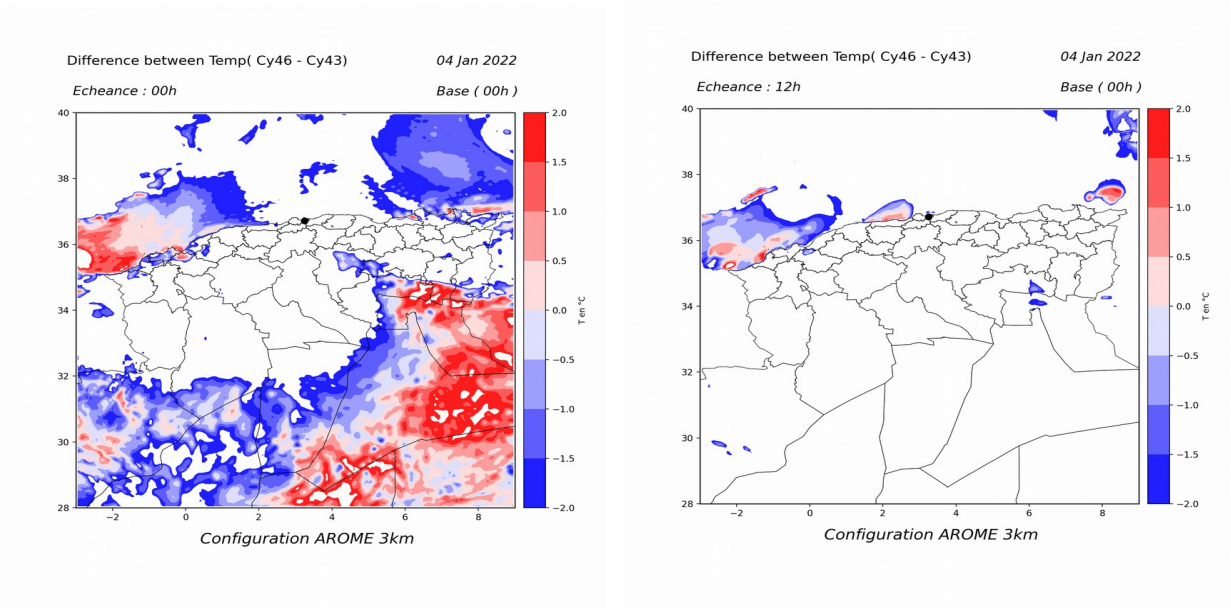

Fig 02 : plots of 2 meters temperature differences between AROME Cy46 export version and AROME Cy43_T2_bf.10.

4 Scores

In this section, we present the scores for AROME-Cy46 and AROME-Cy43 compared first to the ARPEGE analysis for whole month of January 2022 then compared to the observations extracted from synops of the Algerian Observation System. The scores were calculated using the ***Harp*** tool.

4-1 What is Harp ?

Harp (**H**irlam-**A**ladin **R** **P**ackage) is a meta-package developed within the ACCORD-Consortium under the topic of Meteorological Quality Assurance. Developed with R language and attaches functionalities from the *harpIO* , *harpPoint, harpVis* and *harpSpatial* packages.
Harp is a full tool , it takes into account multiple data formats (sqlite , NetcDF , GRIB , fa , lfi…) and provides multiple set of functions to read ,write , interpolate , plot ,analyse and verify numerical weather prediction (NWP) data.
With all the advantages that Harp offers. We took the opportunity of this compilation of cycle 46 to install and discover this tool in-doors for the first time at Meteo-Algeria and hoping to reach operational status in the future.

In order to give more illustration to the scores obtained, we have represented in figures below the variation of the bias and the root mean square error (RMSE) for four (04) parameters (2 meters relative humidity ***"Rh2m"*** *;* 2 meters temperature ***"T2m"*** *;* 10meters wind speed***"S10m"***, temperature at 500 hPa ***"T500"***) :

4-2 Scores compared to ARPEGE analysis

Plots presented in figure 3 show the verification scores of 2 meters temperature, 2 meters humidity, 10 meters wind speed and temperature at 500hpa. From these plots, we can see that the two Cycles present an almost similar behavior on all the scales with a very small difference between the two in favor of the cycle 46 on some parameters, as we see :

- For Humidity, The biases obtained with the two cycles are always negative for all the month. which means that the two cycles underestimate the humidity ,noticing that the RMSE curves are overlaid.

- For T2m, AROME-Cy46 presents better results than AROME-Cy43 for the entire leadtimes.
- For 10m Wind , AROME-Cy46 shows lower values than AROME-Cy43 with all the leadtimes
- For temperature at 500 hPa no change was observed and both bias and rmse curves of the two cycles are overlaid.

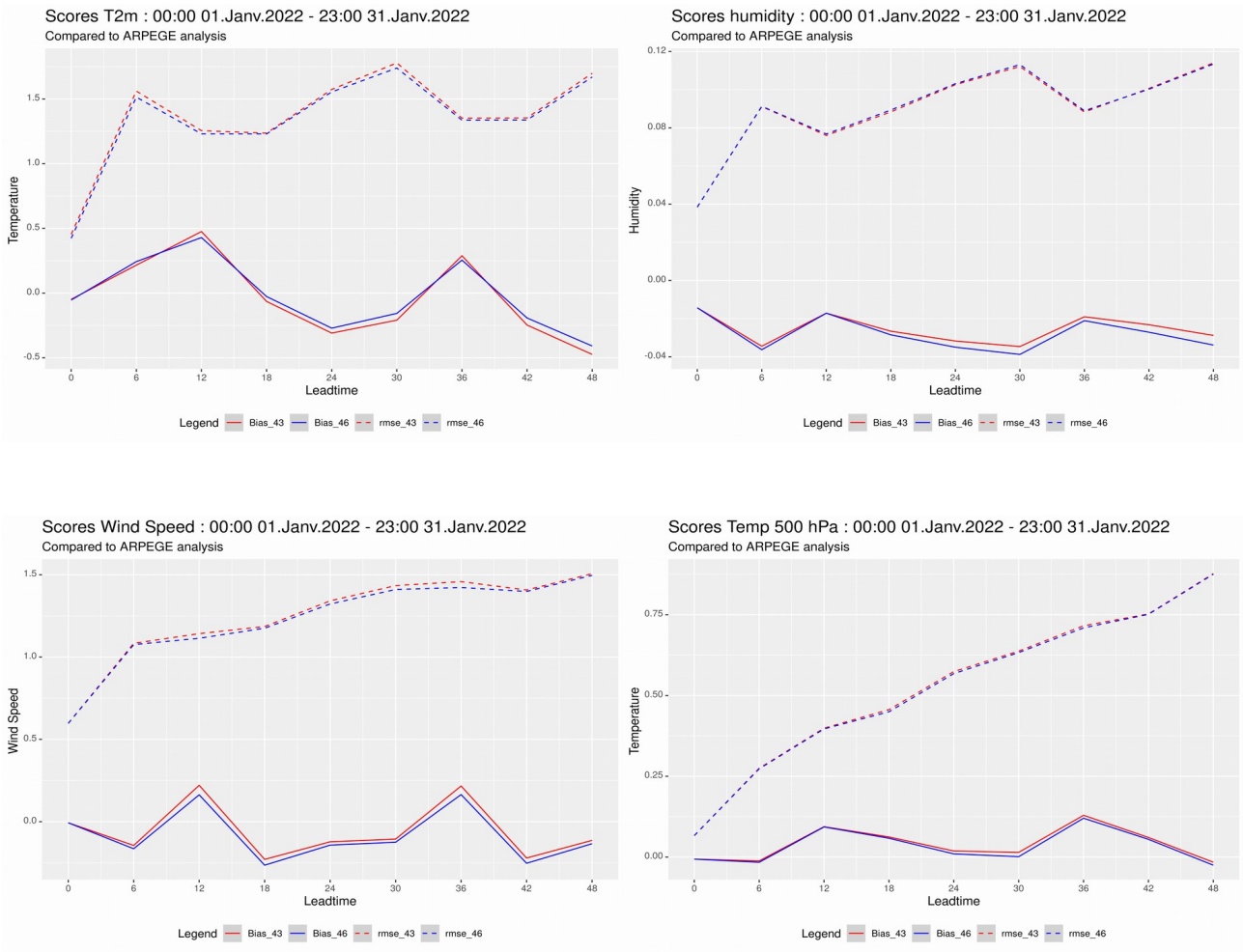

Fig 03 : Scores of the T2m , Rh2m , S10m and T850 for the two cycles compared with ARPEGE analysis; (Red : Cy43_T2_bf.10 ; Blue : Cy46 Export version).

4-3 Scores compared to observations (SYNOPs)

For this evaluation, we used 59 ground stations well distributed over the Algerian Observation network (fig 03).

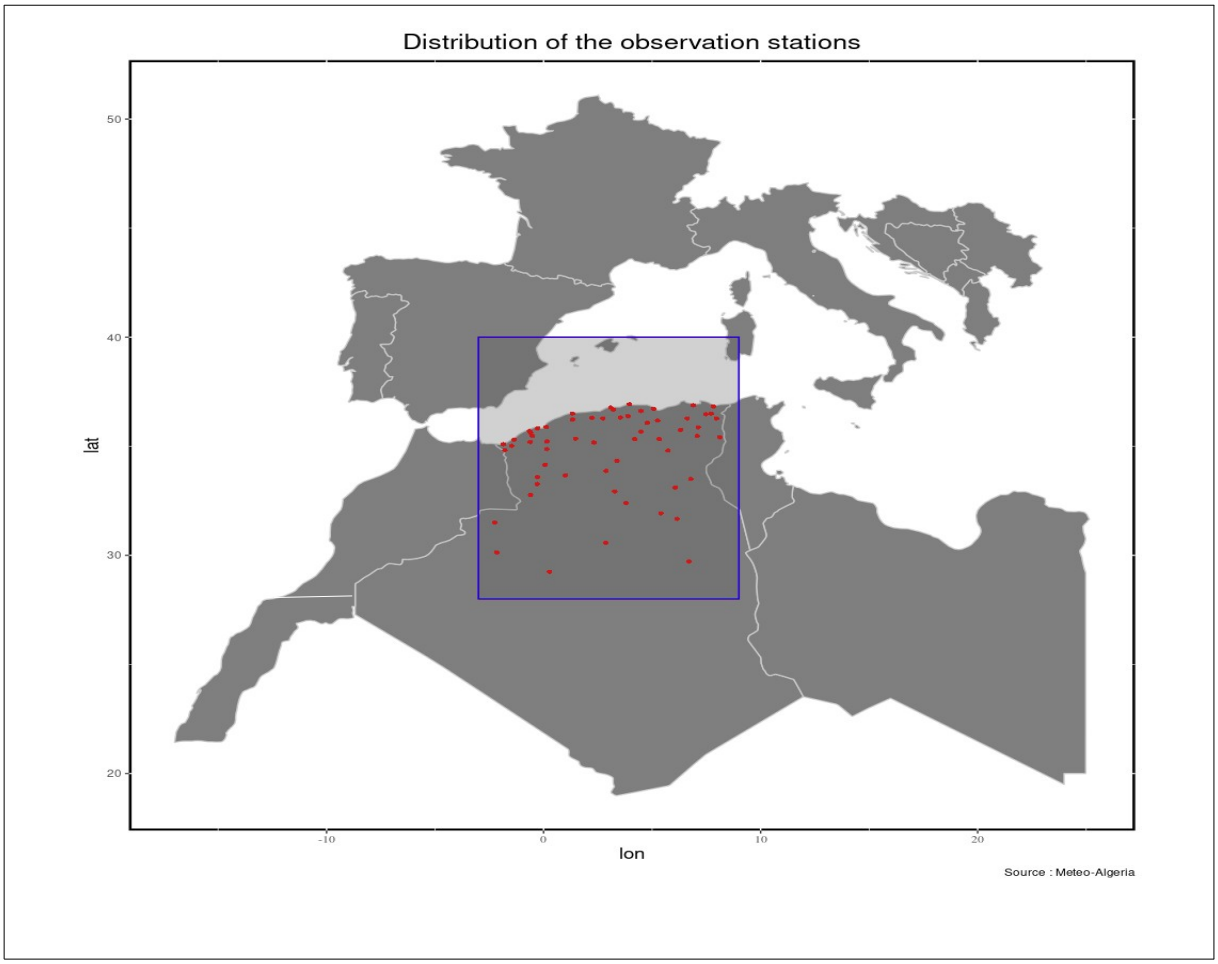

Fig 04 : Distribution of the 59 Stations chosen for the evaluation (Blue Box = AROME Domain)

Compared to the observations, the new cycle 46 export version, presents globally better results, where the scores are improved for two parameters T2m and Rh2m while there was a very slight deterioration in bias for the 10 meters wind speed.

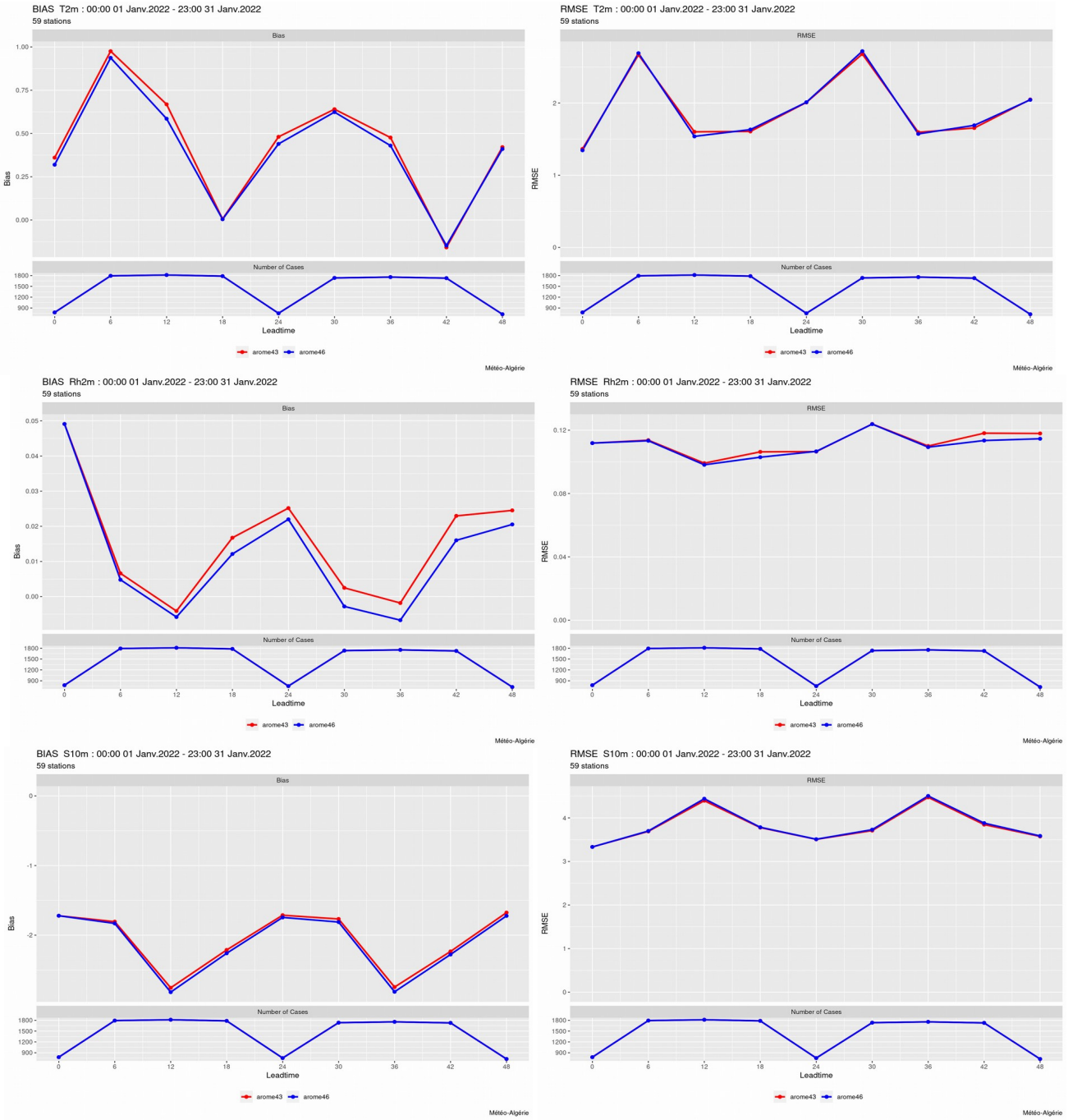

Fig 05 : Scores of the T2m , Rh2m and S10m for the two cycles compared to the Observations (synops) ; (Red : Cy43_T2_bf.10 ; Blue : Cy46 Export version).

5 Conclusion :

The main objective of this report is to summarize all the tasks done to implement the export version of Cy46 locally [1] then compare it within the operational cycle 43_T2_bf.10 with the canonical configuration arome. The comparison were performed over the month of January 2022 using both ARPEGE analysis and observations. The results shows that both

cycles have a similar behaviour with generally better results for the new export version compared to operational cycle.

With these results, Meteo-Algeria plans an update of the operational chain, starting with a migration from 43_T2_bf.10 to the Cy46 , with an increase of both vertical and horizontal resolution for AROME in order take advantage of the characteristics of this non-hydrostatic model and the new features and diagnostics added in cycle 46.

6 References :

[1] - Walid CHIKHI , Nour El Isslam KERROUMI, Zakaria BENGHABRIT, Mohamed MOKHTARI, Abdenour AMBAR, « Recent NWP activities at Météo Algérie : Report on the new HPC and the newcomers training» . ACCORD NL 2, pages 63-68 , February 2022 .

[2] - Sara Chikhi , Mohamed Mokhtari , Abdenour Ambar,Islam Bousri , Mohamed Arab Benamara ,« Operational Numerical Weather Prediction Models Verification at Météo Algérie ». ACCORD NL 1 , pages 25-35, October 2021.

[3] - Joël Stein ; Jean Pailleux ; Fabien Stoop ; Marielle Amodei ; Olivier Dupont ; Mireille Mayoka ; Francis Pouponneau ; Isabelle Sanchez. La vérification des prévisions météorologiques à Météo-France.La Météorologie,2015,N°90; p. 40-49. DOI : 10.4267/2042/56837

[4] - HARP v2: Documentation, (www.hirlam.org), by Andrew Singleton (Met.Norway) and Alex Deckmyn (RMI).

[5] - Harp Training 2022 , Meterological Quality Assurance, https://harphub.github.io/harp-training-2022/

Météo-France Research report 2021

Marc Pontaud, Director of Research and Higher Education

1 Introduction

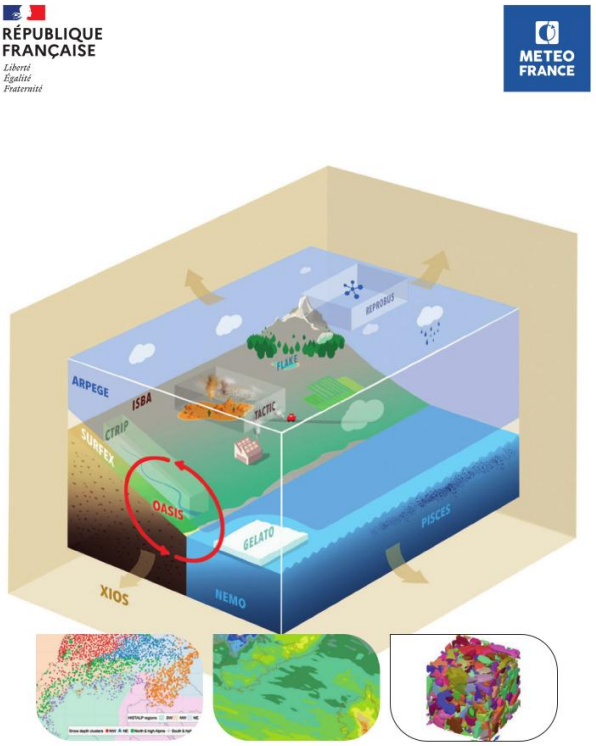

In 2021, Météo-France finalised a new Contract of Objectives and Performance (COP) with the French State for the period 2022 to 2026. Research occupies a privileged place in it, as it supports all the institution's missions.

In 2021, the two new supercomputers became operational in February, bringing an increase in power by a factor of 5.5. The operational numerical weather prediction suite has been installed identically, but above all the first major evolutions of this suite have been tested since mid-2021. For the first time, the ensemble forecasting systems AROME-France and ARPEGE have the same resolution as the deterministic versions. ARPEGE also benefits from a major evolution of its physics with a new deep convection scheme. The resolution of the AROME overseas systems is reduced from 2.5 km to 1.3 km, which particularly benefits the realism of precipitation. This new suit was installed in operation on 29 June 2022 and brings significant progress in both global and regional forecasts. The details of this new operational suit are the subject of one of the three main topics highlighted in the Research Report 2021.

This report highlights two other major topics this year: several contributions from Météo-France to the 6th IPCC report, and future satellite instruments, which herald "a new revolution for meteorology and climate".
Other works and results are presented by main themes in relation to the priority research areas of Météo-France: process studies, measurement campaigns, overseas territories, hectometric resolution, cities and their heat islands, climate, seasonal forecasting, atmospheric composition, snow and mountains.
All this work contributes to the continuous improvement of knowledge and forecasting of phenomena, which are the task of the Institute to monitor and forecast. In order to pursue these advances, the research entities of Météo-France are involved in numerous national and international (especially

European) research projects. 2021 was the start-up year for the ACCORD consortium, which brings together the regional NWP activities of 26 European and North African countries around the AROME system. The work plan is now defined and aims to address all the issues of tomorrow, including dynamic cores, the adaptation of codes to different hpc architectures and high-resolution physics with its 3D effets.

2 Content

- Météo-France's contribution to the IPCC 6th assessment report
- Preparation of a new version of the operational numerical weather prediction systems
- Future satellite instruments, a new revolution for meteorology and climate
- A collection of results illustrating research advances in 2021
    - Numerical weather prediction and data assimilation
    - Process studies and modelling
    - Climate
    - Chemistry, aerosols and air quality
    - Snow and mountain
    - Engineering, campaigns and observation products

3 Documents

The Research Report 2021 document can be downloaded from Météo-France website: here are the links to the English version and to the French version, or consult the page with Research Reports.

Review of summary notes, published papers, PhD

Patricia Pottier, ACCORD Consortium Scientific Secretary

On proposal by their authors or readers, we advertise summary notes or published papers in peer-reviewed journals, and some PhD.

1 On proposal by Wim de Rooy

de Rooy et al. .: Model development in practice: a comprehensive update to the boundary layer schemes in HARMONIE-AROME cycle 40, Geosci. Model Dev., 15, 1513–1543, https://doi.org/10.5194/gmd-15-1513-2022, 20

2 On proposal by Maria Derkova

Belluš M., M. Tudor, X. Abellan, 2022: "The mesoscale ensemble prediction system A-LAEF", ECMWF Newsletter, No. 172 - Summer 2022, p27-34, DOI: 10.21957/xa927ug5k0, https://www.ecmwf.int/node/20453

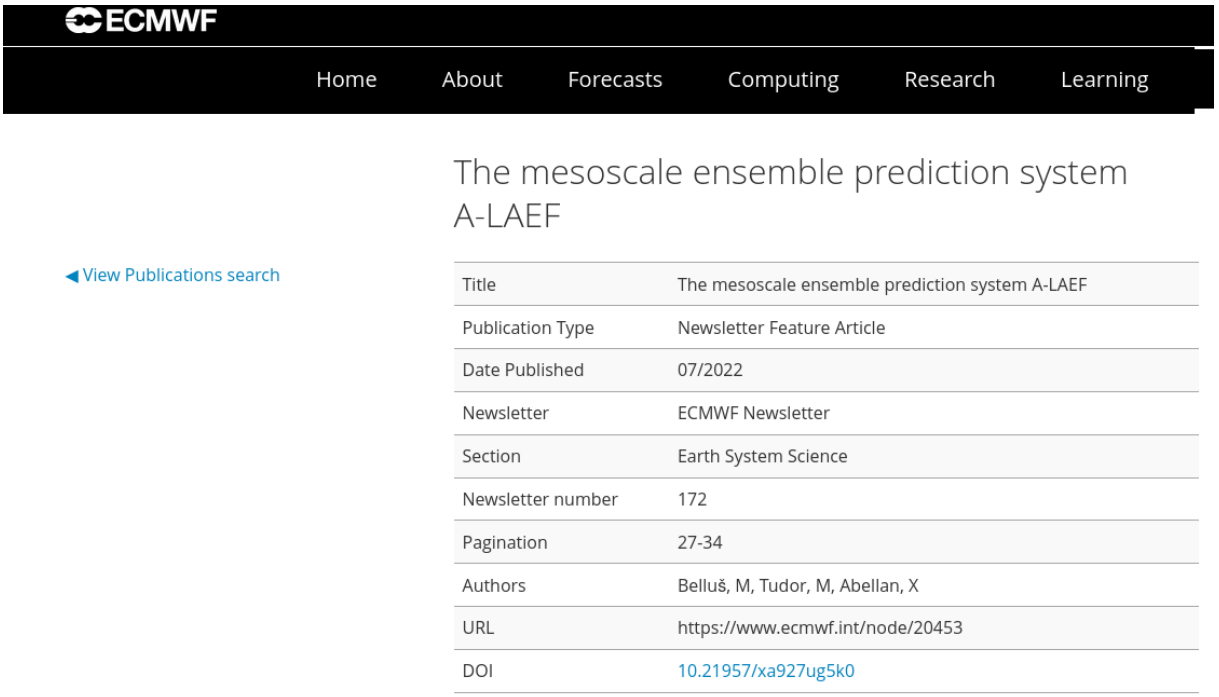

3 On proposal by Kurzeneva Ekaterina

MSc Yurii Batrak defended his doctoral dissertation entitled "Parameterisation of sea ice cover in short-range regional numerical weather prediction" on Wednesday 24 August 2022 at 13:00 in the Physicum auditorium E204, Helsinki.
Opponent: Senior Scientist Steffen Tietsche, ECMWF
Kustos: Professor Heikki Järvinen
The dissertation is available here: https://helda.helsinki.fi/handle/10138/346384

ACCORD Musical adventure

Maria Monteiro and Patricia Pottier

In the spirit of the ACCORD logo, the choir of the Portuguese meteorological service, known as "O TEMPO CANTA" and its conductor Sérgio Peixoto invites all ACCORD colleagues to take part in a little musical adventure.
They would like to record a video-clip with an ensemble of voices from the ACCORD community performing the piece "What a Wonderful World", which was immortalized by Louis Amstrong.

To help ACCORD colleagues on this task, are provided on this shared folder :

- the individual record of each voice on piano (BASS/ALTO/SOP/TENOR+piano .wav files),
- the musical arrangement for four voices (pdf file).

To participate:

1. learn the melody suitable for your voice (by reading the lyrics and listen the records, for instance) until you become confident; and then
2. record your voice and image, while listening simultaneously with headphones, the record suitable for your voice.
3. once you are happy with your record, just upload it to this shared directory that already contains the material provided for you to participate.
4. if you have further ideas for instrument arrangements, please contact Maria Monteiro (maria.monteiro@ipma.pt) or provide your proposal.

Your record is welcome up to the end of October 2022, in order to release the video-clip before Christmas.

Previous editions of the ACCORD Newsletter

1st ACCORD Newsletter,
published on 5 October 2021

2nd ACCORD Newsletter,
published on 28 February 2022

The joint ALADIN-HIRLAM Newsletter (2013-2021, 16 editions) can be found on the ALADIN dedicated webpage.